UNIVERSITÀ DELLA CALABRIA

UNIVERSITY OF CALABRIA

Department of Computer Engineering, Modeling, Electronics and Systems

PhD in

INFORMATION AND COMMUNICATION TECHNOLOGY

CYCLE

XXXII

THESIS TITLE

A multi-scale theoretical paradigm to model the complex interactions between macromolecules and polymeric membranes

Disciplinary Scientific Sector ING-IND/24

Coordinator: Prof. Felice Crupi

Sign [redacted] Firma oscurata in base alle linee guida del Garante della privacy

Supervisors/Tutors: Prof. Stefano Curcio

Sign [redacted] Firma oscurata in base alle linee guida del Garante della privacy

Prof. Felice Crupi

Sign [redacted] Firma oscurata in base alle linee guida del Garante della privacy

Dott. Giorgio De Luca

Sign [redacted] Firma oscurata in base alle linee guida del Garante della privacy

PhD student: Dott. Francesco Petrosino

Sign [redacted]

Firma oscurata in base alle linee guida del Garante della privacy

Francesco Petrosino
PhD Thesis

A multi-scale theoretical paradigm to model the complex interactions between macromolecules and polymeric membranes

Tutors:
Prof. Felice Crupi felice.crupi@unical.it
Prof.Stefano Curcio stefano.curcio@unical.it
Dott. Giorgio De Luca g.deluca@itm.cnr.it

Department of Computer Engineering, Modeling, Electronics and Systems (D.I.M.E.S.), Laboratory of Transport Phenomena and Biotechnology, University of Calabria, Ponte P. Bucci, cubo 42/a, 87036 Rende (CS), Italy;
f.petrosino@dimes.unical.it

Alla mia famiglia

To my family

ABSTRACT

The overall aim of the work was to provide a complete Multiscale Model of macromolecules interactions to simulate different processes and bioprocesses where such interactions, among different macromolecules and between macromolecules and polymeric surface, strongly determine the system behaviour.

The adsorption of proteins on material surfaces is an essential biological phenomenon in nature, which shows a wide application prospect in many fields, such as membrane based processes, biosensors, biofuel cells, biocatalysis, biomaterials, and protein chromatography. Therefore, it is of great theoretical and practical significance to study the interfacial adsorption behaviour of proteins and their structuration and aggregation in order to describe concentration polarization phenomena in separation processes. It is worthwhile remarking that *ab-initio* simulations allow the estimation of parameters without exploiting any empirical or experimental methodology.

In the present work, an improved multiscale model aimed at describing membrane fouling in the UltraFiltration (UF) process was proposed. The proteins-surface interactions were accurately computed by first-principle-based calculations. Both the effective surface of polysulfone (PSU) and the first layer of proteins adsorbed on the membrane surface were accurately modelled. At

macroscopic scale, an unsteady-state mass transfer model was formulated to describe the behaviour of a typical dead-end UF process.

The adsorption of an enzyme, i.e. the phosphotriesterase (PTE), on polysulfone (PSU) membrane surface was investigated as well through a double-scale computational approach. The results of such a formulated model were useful to obtain a detailed knowledge about enzyme adhesion and to give precise indications about the orientations of its binding site.

One of the most important challenges is to use the stochastic approach adding an improved nano- and micro-scale step to the well-established multiscale procedure. The implementation of a Monte Carlo algorithm was performed with the aim of investigating the fouling structure during membrane operation like different micro-equilibrium states. The final aim of the work was to carry out the calculation of both Osmotic Pressure and Diffusion Coefficient in the fouling cake by the already-performed Monte Carlo simulations. Furthermore, the so-obtained parameters were exploited in macroscopic CFD simulations so as to calculate the overall resistance of the deposit accumulated on membrane surface during filtration.

Contents

Chapter1

1 Introduction 5

1.1 Multiscale modelling in chemical engineering 5

1.2 Ab-initio models in Multi Scale simulations 8

1.3 Monte Carlo models in Multi Scale simulations 9

1.4 Ultrafiltration processes 11

1.5 Multidisciplinary aspects 12

1.6 Aim of the thesis 13

1.7 Methodology and outline of the thesis 15

Chapter 2

2 Theoretical background 21

2.1 Introduction 21

2.2 Introduction to Density Functional Theory 22

2.3 Introduction to Molecular Dynamics 25

2.4 Monte Carlo methods 27

2.5 A short introduction to Physics of Colloidal Soft Matter 30

2.6 Computational-Fluid-Dynamic 33

2.7 Conclusions 36

Chapter 3

3 Interactions between proteins and membrane surface in multiscale modeling of organic fouling 41

3.1 Introduction 42

3.2 Multi scale approach and experimental setup 45

3.2.1 Protein contact surface 45

3.2.2 Polysulfone surface model 47

3.2.3 Interaction potential energy 49

3.2.4 Proteins-surface interaction 51

3.2.5 Microscopic and Macroscopic models 54

3.2.6 Experimental setup 57

3.3 Results and Discussion 59

3.3.1 Surface Charge Density 59

3.3.2 Protein packing on polysulfone surface 60

3.3.3 Macro results of multi-scale modeling 63

3.4 Conclusions 70

Chapter 4

4 Enzyme Immobilization on Polymer Membranes: A Quantum and Molecular Mechanics Study 77

4.1 Introduction 78

4.2 Computational approach 80

4.2.1 Quantum calculations....80
4.2.2 Molecular mechanics optimizations....82
4.3 Results and Discussion....83
4.4 Conclusions....89

Chapter 5

5 Osmotic pressure and transport coefficient in ultrafiltration: a Monte Carlo study using quantum surface charges....94
5.1 Introduction....95
5.2 Theoretical....97
5.2.1 Quantum mechanics calculations....97
5.2.2 Colloid interaction potential energy....98
5.2.3 Monte Carlo simulation method....100
5.2.4 Theoretical approaches....102
5.3 Numerical implementation....103
5.4 Results and discussions....104
5.4.1 Ab-initio total protein charge and minimum distance....105
5.4.2 MC simulation sets and code validation....105
5.4.3 Osmotic Pressure and Diffusion Coefficient....109
5.5 Conclusions....112

Chapter 6

6 Theoretical modeling of UF fouling at micro-CFD scale: the case of BSA 120

6.1 Introduction 121

6.2 Computational framework and preliminary results 123

6.3 Conclusions 129

Conclusions and future perspectives

7 132

Figures index

8 134

Appendix

Appendix A 138

Appendix B 143

Appendix C 150

Acknowledgments

I 155

Chapter 1

Introduction

1.1 Multiscale modelling in chemical engineering

Multiscale approaches are receiving more and more interest in different scientific and technological areas. "Multiscale simulation can be defined as the enabling technology of science and engineering that links phenomena, models, and information between various scales of complex systems. The idea of multiscale modeling is straightforward: one computes information at a smaller (finer) scale and passes it to a model at a larger (coarser) scale by leaving out, i.e., coarse-graining, degrees of freedom." [1] Multiscale modeling is becoming of fundamental importance, for instance, in drug design and is having a very high impact on human health; drugs do indeed act at the molecular scale but, obviously, have macroscopic effects, so their behavior has to be analysed considering the impact they may have at different time- and space- scales.

Nowadays, one of the major challenges in chemical engineering resides in the description of complex phenomena, which are essentially multiscale in nature. Chemical engineering is increasingly trying to describe these complex phenomena by formulating (and solving) multiscale models. Generally speaking, it is possible to distinguish three kinds of multiscale methodologies: *descriptive, correlative and variational.* A *descriptive* approach describes the phenomenological differences of structure at different scales. The *correlative* approach allows explaining a certain phenomenon at larger time- and space- scales by analyzing some of the mechanisms characterizing its behavior at smaller scales. The *variational* approach, instead, is used for revealing the dominant mechanisms of the structure and the mutual relationships existing among different scales [2].

A possible scheme of these relationships (and the corresponding transitions) that are to be considered to develop a complete description of a chemical engineering phenomenon according to mutiscale approach is shown in Fig. 1.

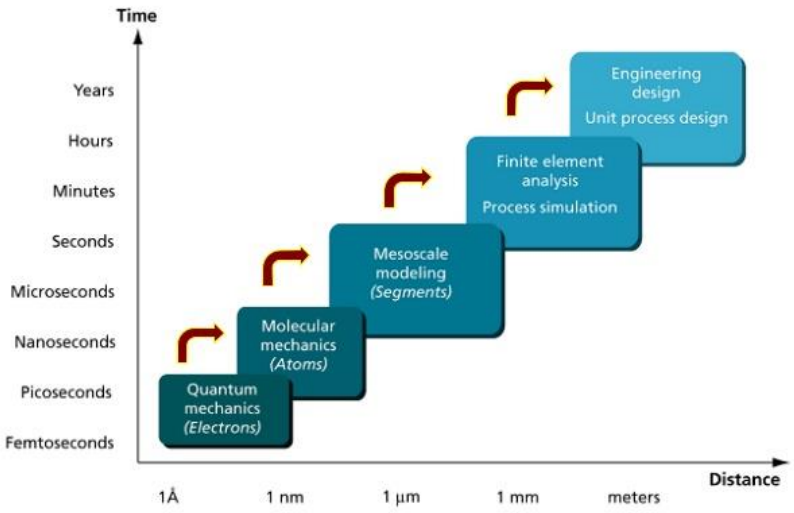

Figure 1 Characteristics lengths and times of a multiscale methodologies

A multiscale approach, therefore, requires both a detailed study at each of the scales, which characterize the system behavior, and the identification of some linking parameters allowing a proper transition (coarse-graining) between different scales. No single simulation method does exist to attain a detailed insight about real processes performance considering their actual multiscale nature; in addition, no general and comprehensive methodology can be defined to suggest how to link and couple the phenomena occurring at different scales. Multiscale simulations, instead, allow properly modeling and analyzing the connections between the different scales so to determine how a change or even a perturbation at one scale may influence the results at a different scale of detail. Nowadays, a challenge is still represented by the proper integration of data and simulations across different space scales and timescales [3].

Seminal contributions to multiscale approach have been given by Karplus, Levitt and Warshel (2013 Nobel Prize in Chemistry) with the development of multiscale methods for modelling complex

biochemical systems[4]. Today, 50 years after their pioneering studies, these methods offer the possibility of analyzing very complex and sophisticated systems. For example, multiscale modelling provides an understanding of how a chemical reaction occurring at an enzyme active site can affect other proteins and extend through the hierarchy of biological complexity from subcellular neighborhoods to cells and tissues. The power of multiscale methods lies in the possibility to create a fluid knowledge landscape that can encompass disparate modeling and experimental data at different spatiotemporal scales. A practical outcome of this methodology relies on the proper combination of diverse approaches, thus linking chemistry at the atomic scale with biological function at the cellular and higher levels to elucidate the mechanisms of emergent phenomena, and doing so in a way that circles back to drive drug design and development [5].

Incorporating the transition from one to another scale in a multiscale approach is a real challenge concerning same material mechanics applications. Localized properties at the microscale have to be incorporated directly in the macroscale description without any averaging due to their model key role. Different simplified approaches have been proposed to make a direct volumetric coupling between the size of a finite element (at the macroscale) and the localizing representative volume elements (RVE) at the microscale. In contrast to the previously explained methods (coarse graining or homogenization techniques), this solution, called localization technique, is not really of the homogenization type anymore and rather resembles a domain decomposition approach in which the fine scale is embedded as a local refinement.

However, multiscale approaches are not restricted to chemical engineering problems: environmental, biological, medical, astrophysical situations would equally benefit from such approaches.

Given the importance of these modeling techniques and given the different studies carried out by our research group in this area from over 5 years ago[6,7], the present work appears to be a fundamental element in the study of macromolecule interactions, which in turn is important in various fields

ranging from bioengineering up to process engineering, passing through Information and Communication Technology (ICT) areas of neural networks and artificial intelligence. Machine learning and artificial intelligence increasingly recognized as a promising technology in the biological, biomedical, and behavioral sciences. In the biomedical sciences machine learning and multiscale modeling can mutually benefit from one another. Machine learning methods have recently permeated into composites research and materials design for example to enable the homogenization of representative volume elements with neural networks or the solution of high-dimensional partial differential equations with deep learning methods.

1.2 Ab-initio models in Multi Scale simulations

During the last decades, numerical ab initio calculations have become possible as a tool for investigating the structural, dynamic and electronic properties of complex molecules, clusters, polymers, and solids. Chemical and physical atomic processes nowadays may be simulated on a computer. A visible sign of these developments can be seen in the 1998 Nobel prize of Chemistry awarded to the quantum chemist J.A. Pople and to the theoretical physicist W. Kohn[8].

Ab-initio simulations have become increasingly important in the fields of physics and chemistry during the past decade, especially for the advent of easily accessible high-performance computers[9].

A quantum computational approach allows answering two fundamental questions:

- What is the electronic structure of the material formed by specified atoms?
- What is its atomic structure?

The ultimate goal of *ab-initio* calculations in materials science is to virtually “design” materials having predefined properties by changing their specific atomic bonding and electronic structure. However, a lot of theoretical methods were developed to address the above questions. The numerical methods for computing structural properties of materials may be divided into two classes:

1. Methods that use empirically, i.e. experimentally determined, parameters;
2. Methods that do not make use of any empirical quantity.

The former methods are often called “empirical” or “semi-empirical”, whereas the latter are called “*ab-initio*” or “first-principles methods”. *Ab-initio* methods are often useful for predicting the electronic properties of new materials, clusters or surfaces, and for predicting trends across a wide range of materials [10].

In *ab-initio* quantum mechanics methods, the potential energy between atoms is calculated by solving the Schrodinger equation for electrons in the field of many atom cores. Due to the very high number of degrees of freedom, different theories aimed at obtaining an approximate solution of Schrodinger equation have been formulated. Some of these theories are the Self-Consistent Field Theory (SCF) and the Density Functional Theory (DFT) [10] that they will be treated hereafter in the dedicated theoretical chapter.

The present work is founded on an *ab-initio* approach to have a complete description of the analyzed process. By such a multiscale approach based on the aforementioned *ab-initio* simulations, all the parameters used in at macroscopic level, such as the mass transport coefficient, can be derived from lower and lower scales regardless of any empirical or adjustable parameters. In the case of macromolecules, characterized by very complex chemical structures composed by thousands of atoms, the overall behavior can be traced back to the single electrostatic interactions, as calculated at smaller time- and space- scales.

1.3 Monte Carlo models in Multi Scale simulations

To make the *ab-initio* knowledge robust, thus allowing the transition to nano and microscopic scale, it is necessary to exploit complex and well-assessed models, such as the Monte Carlo methods.

The term Monte Carlo generally applies to all simulations that use stochastic methods to generate new configurations of a system to be analyzed. In the context of molecular simulation, specifically, the simulation of proteins, Monte Carlo refers to the importance of configuration sampling at equilibrium. In general, a Monte Carlo simulation proceeds as follows: starting from an initial configuration of particles in a system, a Monte Carlo move is attempted to change the particles configuration and their arrangement. This move is accepted or rejected based on an acceptance criterion that guarantees that all the configurations are sampled during the simulation from a statistical mechanics ensemble distribution, and that the configurations are sampled by a correct weight. After the acceptance or rejection of a move, one calculates the value of a property of interest, and, after many such moves, an accurate average value of this property is obtained. The application of statistical mechanics allows calculating a variety of equilibrium thermodynamic properties of the system[11].

Unlike molecular dynamics simulations, Monte Carlo simulations are free from the restrictions of solving the Newton's equations of motion. This independence upon the Newton's equations allows for randomness in the proposal of moves that generate trial configurations within the statistical mechanics ensemble of choice. Although these moves might be nontrivial, they can lead to huge speedups of computational times, which, in some cases, are in the order of magnitude of 10^{10} or more in the sampling of equilibrium properties. Specific Monte Carlo moves can also be combined in a simulation allowing the modeler great flexibility in the approach to a specific problem. In addition, Monte Carlo methods are generally easily parallelizable, with some techniques being ideal for use with large CPU clusters.

In this work approaches based on Monte Carlo methods have been used with the aim of removing various limitations related to the imposition of fixed structures in a model for the ultrafiltration of proteins developed in previous works available in the literature[6,7].

1.4 Ultrafiltration processes

On an industrial scale, membrane processes have been proved to be effective and economically attractive in a variety of processes, e.g. protein recovery, pharmaceutical or oil-water separations, alcohol or latex recovery[12,13]. The separation and purification of bio-products such as proteins, protein hydrolysates, polysaccharides, vitamins and amino acids are important steps in the food industry due to the large number of possible applications[14,15]. In particular, UltraFiltration (UF) is widely used in colloidal dispersions treatment and has become a standard method in protein recovery due to its good performance in terms of cost and selectivity[16].

However, UF has a number of downsides, the major one being the flux reduction during permeation. Such a problem is due both to concentration polarization (CP), a reversible phenomenon referred to the development of concentration gradients at a membrane/solution interface, and to membrane fouling, an irreversible phenomenon, which is due either to solute deposition on the membrane surface forming a gel layer or to solute adsorption inside the pore structure and over the membrane[17].

The interplay between osmotic pressure and applied transmembrane pressure (TMP) is responsible for CP and fouling formation and strongly affects membrane performance. Four classes of models have been proposed in the literature to describe membrane fouling; each of these models takes into account the actual characteristics of both the membrane and the solute(s) dispersed in the solution to be filtered. The *complete blocking* model assumes that the particles of solute(s) seal off the pore entrances; the *intermediate blocking* model is similar to *complete blocking* but assumes that some of the particles do actually seal off the pores, whilst some others accumulate on membrane surface. The *cake filtration* model presupposes that particles may accumulate on the membrane surface, thus forming a permeable cake of increasing thickness, which is responsible for an additional resistance to permeate flow; finally, the *standard blocking* assumes that solute(s) particles or colloids may accumulate inside the walls of membrane pores, considered as straight cylinders[18].

In particular, with reference to the cake filtration model, it is necessary to emphasize on the fact that the concentrated layer of solute particles developing on the membrane is much lesser permeable to the solvent (usually water) as compared to a solution with bulk concentration. Therefore, in order to properly predict the behavior of UF process, it is necessary to precisely calculate both the additional resistance, R_{add}, to permeate flow and the osmotic pressure $\Delta\pi$, related to the solute concentration, which, evaluated at the membrane surface, leads to a decrease in the driving pressure that is equal to $-\Delta\pi$.

1.5 Multidisciplinary aspects

Multiscale modeling is characterized by the use of many tools and in-depth knowledge of different complex approaches. For these reasons, it is necessary to underline the multidisciplinary aspect of a work that aims at the implementation of an entire multiscale model.

Even though multiscale problems have long been studied in mathematics, the current efforts are actually dedicated to the use of complex mathematical models in applied sciences and technology: in particular, material science, chemistry, fluid dynamics, biology and engineering. Problems in these areas are often multiphysics in nature; namely, the processes at different scales are governed by physical laws of different nature: for instance, quantum mechanics at one scale and classical mechanics at another.

Emerging from this intense activity, an increasing interest for novel mathematical models and new ways of interacting with mathematics is observed. Research areas belonging to mathematical physics or stochastic processes, which so far have exploited rather “traditional” models and computational techniques, are moving faster and faster towards new scenarios opened, for instance, by multiscale modeling. New questions and new challenges are, however, arising, new priorities are to be properly evaluated as a result of the rapid evolution in computational procedures.

From past few years the field of life science has seen a rapid change in genomics, DNA sequences, gene expression, proteomics and metabolomics etc. There are two main brisk vicissitudes going in the field of life science one is the capability of computers and software tools to manage Zettabytes (and beyond) of data; the other is represented by the progression in molecular biology experiments, which produce huge amount of data related to genome and RNA sequence, protein and metabolism, protein-protein and protein-DNA interaction, gene expression, 3D structure of protein molecules and more. Life science and computers have become a balancing bridge to each other to form different branches of science like the combination of versatile knowledge that caused the dawn of big data in computational biology, bioinformatics, biostatistics and chemical engineering [19].

The present work, aimed at proposing the use of innovative computer techniques to analyze the complex phenomena occurring in chemical engineering problems, is perfectly inserted in ICT (Information and Communication Technologies) field. The study of the complex interactions among macromolecules, as analyzed in this work, relies on the development of home-made codes based on complex approaches such as Quantum Mechanics and Monte Carlo techniques. Furthermore, the amount of data processed in the analysis of interactions of cluster molecules reveals the existence of strong analogies with Big Data structures, typical in Computer Science. The interactions between N macromolecules constituting a real aqueous solution of proteins to be filtered through a membrane can indeed be studied using advanced techniques used in the "big data analysis" domain.

1.6 Aim of the thesis

The formulation of a multiscale model to simulate useful macroscopic quantities related to ultrafiltration processes, was the final aim of this thesis. This modelling provides useful information for different processes and bioprocesses where the intermolecular (noncovalent) interactions drives the entire phenomena. Proteins adsorption on material surfaces is a basic biological phenomenon in

nature, which shows a wide application prospect in many fields, such as membrane based processes, biosensors, biofuel cells, biocatalysis, biomaterials, and protein chromatography [20–22]. Therefore, it is of great theoretical and practical significance to study the interfacial adsorption behavior of proteins. It is worthwhile remarking that *ab-initio* simulation allows the estimation of parameters without the use of any empirical or experimental methodology.

Compared to the papers available in the literature[23,24], the present project contains a major peculiarity. This multiscale analysis was in fact performed on the entire range of possible physical details. It starts from the quantum mechanics scale and reaches the macroscopic scale through a series of coarse graining techniques allowing the transition between the considered time- and space- scales.

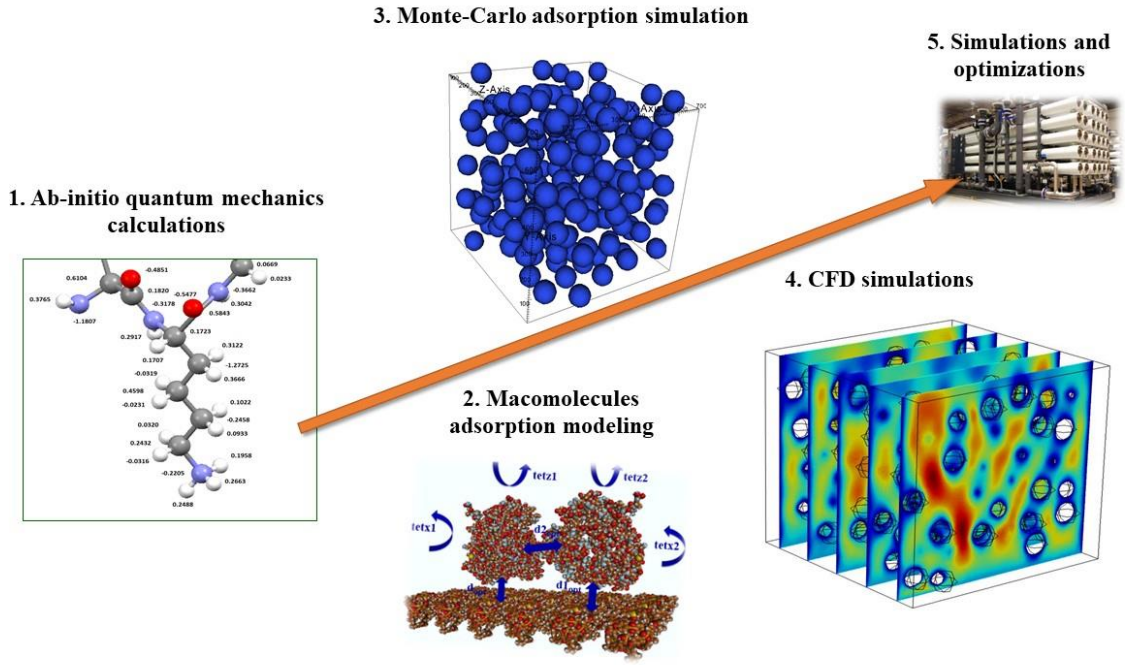

Figure 2 Multiscale framework of the present work

The main objective of this work was to merge and integrate several complex theories in the same multiscale framework and to provide a strong and versatile approach that can be exploited to investigate different areas of interest for science and technology. One of the most relevant challenges is the use of a stochastic approach, which definitely represents a significant breakthrough since

introduces an improvement in the prediction of the phenomena occurring at nanoscopic and microscopic scale and, therefore, to the overall multiscale procedure. The implementation of Monte Carlo algorithm was performed with the goal of investigating the fouling structure during membrane operation in terms of different micro-equilibrium states. One of the final aims of the work was to achieve the calculation of both the Osmotic Pressure and the Diffusion Coefficient in the fouling cake by Monte Carlo simulations. These quantities were then exploited in macroscopic CFD simulations to calculate the additional resistance to permeation as provided by the deposit of proteins (cake) accumulated on the membrane surface during the ultrafiltration process.

1.7 Methodology and outline of the thesis

Summarizing, in this thesis four specific problems based on different works were investigated.

Firstly, based on different works[7,25–29], an improved multiscale modeling aimed at describing membrane fouling in the UltraFiltration (UF) process was proposed. Some of the authors of this work previously published a multiscale approach to simulate the ultrafiltration of Bovine Serum Albumin (BSA) aqueous solutions[29]. However, the noncovalent interactions between proteins and the membrane surface were not taken into account in the previous model. Herein, the proteins-surface interactions were accurately computed by first-principle-based calculations considering also the effect of pH. Both the effective surface of polysulfone (PSU) and the first layer of proteins adsorbed on the membrane surface were accurately modeled. The equilibrium distance between adsorbed proteins was calculated and imposed as lower bound to the protein−protein distances in the compact deposit accumulated on the membrane surface. The computed BSA surface charges were then used to estimate the protein potential and the charge density, both necessary to formulate a force balance at microscopic scale. The protein surface potential was compared to some Z-potential measurements of BSA aqueous solution, and a remarkable agreement was found. Finally, the overall additional

resistance, as due to both the compact and loose layers of the deposit, was computed, thus allowing the final transition to a macroscopic scale, where an unsteady-state mass transfer model was formulated to describe the behavior of a typical dead-end UF process. A good agreement between simulated and experimental permeate flux decays was observed as well.

Secondly, as another important application of the same modeling approach, the adsorption of phosphotriesterase (PTE) enzyme on polysulfone (PSU) membrane surface was also investigated through a double-scale computational approach. The surface charges of both the enzyme and the membrane were calculated at sub-nanoscopic and nanoscopic scales, whereas protein adsorption was simulated at a bigger scale. The adsorption energies were calculated as a function of the enzyme-surface distance and, for each distance, several protein rotations were tested in order to find the most stable macromolecule orientations. The results of this modeling approach were useful to obtain a detailed insight about the enzyme adhesion and to give indications on the orientations of its binding site. The calculated adsorption energies agreed with the literature data, in addition the work showed that the binding site of immobilized PTE was less accessible with respect to native (in solution) enzyme due to the steric hindrance of the polymer surface; thus, a reduction of its efficiency should be expected.

Thirdly, a computational study aimed at estimating the Osmotic Pressure and the Diffusion Coefficient characterizing the cake layer accumulated on the membrane surface, i.e. the loose layers of the deposit, was performed. Using *ab-initio* results obtained at sub-nanoscopic and nanoscopic scales[6], the surface potential of BSA and the minimum equilibrium distance between two proteins were theoretically calculated. A home-made Metropolis Monte Carlo (MC) algorithm aimed at the simulation of the layers formation during membrane operations was implemented. For the use of the aforementioned Monte Carlo methods a Yukawa based energy calculation methodology of the system was also developed[30]. After a complete validation of Monte Carlo methodologies by the Hypernetted-

Chain (HNC) theory[31] and through the calculation of radial distribution function (RDF), different MC simulations were performed. Finally, in accord to the approach proposed by Chun and Bowen[32] the Osmotic Pressure and Diffusion Coefficient characterizing the concentration-polarization profile developing in membrane filtration process were computed. These results were finally validated both experimentally and by the HNC theory[31] and could be used at macroscopic scale during a ultrafiltration process simulation.

Finally, different fluid-dynamics simulations through Monte Carlo boxes of molecules were carried out. Thanks to the results of the Monte Carlo simulations, various 3D structures were created. These structures represent the deposit layer at different distances from the membrane. With the help of computer aided tools these geometries were imported in a computational tool and the corresponding meshes allowed performing micro-fluid dynamics calculations. From these simulations, a series of macroscopic parameters, such as the flow resistance of the deposit layers generally obtained as a result of experiments, were devised.

It is important to underline that the above-described works, three of which have been already published or submitted for publication[6,33], although different in their subjects, are linked by a fundamental unifying basic strand, which is represented by the multiscale approach for the analysis of protein-protein and protein-surface interactions, carrying out useful macroscopic quantities. Moreover, as already discussed, this unifying strand has fallen into a very broad and promising multidisciplinary field.

The thesis is divided in **7** chapters as follows: After an overview in the introductive chapter, in chapter 2 a short prologue about theoretical background of the performed calculations is provided. In chapter 3 to 6 the aforementioned works are reported. In chapter 7 conclusions are provided and, finally, in two appendices, both the main developed codes and some important extra results are showed.

References

(1) Fermeglia, M.; Pricl, S. Multiscale Modeling for Polymer Systems of Industrial Interest. *Prog. Org. Coatings* **2007**, *58* (2–3), 187–199.

(2) Li, J.; Kwauk, M. Exploring Complex Systems in Chemical Engineering - The Multi-Scale Methodology. *Chem. Eng. Sci.* **2003**, *58* (3–6), 521–535.

(3) Amaro, R. E.; Mulholland, A. J. Biomolecular Simulations Are Essential Tools for Drug Design and Development, and for Our Understanding of the Molecular Basis of Disease.

(4) Hodak, H. The Nobel Prize in Chemistry 2013 for the Development of Multiscale Models of Complex Chemical Systems: A Tribute to Martin Karplus, Michael Levitt and Arieh Warshel. *J. Mol. Biol.* **2014**, *426* (1), 1–3.

(5) The Royal Swedish Academy of Science. Development of Multiscale Models for Complex Chemical Systems. *Sci. Backgr. Nobel Prize Chem. 2013* **2013**, *50005*.

(6) Curcio, S.; Petrosino, F.; Morrone, M.; De Luca, G. Interactions between Proteins and the Membrane Surface in Multiscale Modeling of Organic Fouling. *J. Chem. Inf. Model.* **2018**, *58* (9), 1815–1827.

(7) F. Petrosino; S. Curcio; G. De Luca. Modellazione Multiscala Dei Processi Di Separazione Di Proteine Mediante Tecnologie a Membrana, University of Calabria, 2015.

(8) Walter Kohn. Electronic Structure of Matter - Wave Functions and Density Functionals. 1999.

(9) M. O. Steinhauser. *Computational Multiscale Modeling of Fluids and Solids*; Springer-Verlag Berlin Heidelberg, 2008; Vol. 111.

(10) Mikael P. Johansson, Ville R.I. Kaila, and D. S. Ab Initio, Density Functional Theory, and Semi-Empirical Calculations. **2013**, *924* (August 2013), 2–27.

(11) Kukol, A. *Molecular Modeling of Proteins: Second Edition*; 2014.

(12) Cheng, T. W.; Yeh, H. M.; Gau, C. T. Flux Analysis by Modified Osmotic-Pressure Model for Laminar Ultrafiltration of Macromolecular Solutions. *Sep. Purif. Technol.* **1998**, *13*, 1–8.

(13) Chakraborty, S.; Loutatidou, S.; Palmisano, G.; Kujawa, J.; Mavukkandy, M. O.; Al-Gharabli, S.; Curcio, E.; Arafat, H. A. Photocatalytic Hollow Fiber Membranes for the Degradation of Pharmaceutical Compounds in Wastewater. *J. Environ. Chem. Eng.* **2017**, *5*, 5014–5024.

(14) Zin, G.; Penha, F. M.; Rezzadori, K.; Silva, F. L.; Guizoni, K.; Petrus, J. C. C.; Oliveira, J. V.; Di Luccio, M. Fouling Control in Ultrafiltration of Bovine Serum Albumin and Milk by the Use of Permanent Magnetic Field. *J. Food Eng.* **2016**, *168*, 154–159.

(15) Nath, A.; Mondal, S.; Chakraborty, S.; Bhattacharjee, C.; Chowdhury, R. Production, Purification, Characterization, Immobilization, and Application of β-Galactosidase: A Review. *Asia-Pacific J. Chem. Eng.* **2014**, *9*, 330–348.

(16) Saha, K.; R, U. M.; Sikder, J.; Chakraborty, S.; da Silva, S. S.; dos Santos, J. C. Membranes as a Tool to Support Biorefineries: Applications in Enzymatic Hydrolysis, Fermentation and Dehydration for Bioethanol Production. *Renew. Sustain. Energy Rev.* **2017**, *74*, 873–890.

(17) Suki, A.; Fane, A. G.; Fell, C. J. D. Flux Decline in Protein Ultrafiltration. *J. Memb. Sci.* **1984**, *21*, 269–283.

(18) Bolton, G.; LaCasse, D.; Kuriyel, R. Combined Models of Membrane Fouling: Development and Application to Microfiltration and Ultrafiltration of Biological Fluids. *J. Memb. Sci.* **2006**, *277*, 75–84.

(19) Martiz, R. Application of Big Data Bioinformatics – a Survey. **2016**, 206–212.

(20) Quan, X.; Liu, J.; Zhou, J. Multiscale Modeling and Simulations of Protein Adsorption: Progresses and Perspectives. *Curr. Opin. Colloid Interface Sci.* **2019**, *41*, 74–85.

(21) Bhakta, S. A.; Evans, E.; Benavidez, T. E.; Garcia, C. D. Protein Adsorption onto Nanomaterials for the Development of Biosensors and Analytical Devices: A Review. *Anal. Chim. Acta* **2015**, *872*, 7–25.

(22) Yu, L.; Zhang, L.; Sun, Y. Protein Behavior at Surfaces: Orientation, Conformational Transitions and Transport. *J. Chromatogr. A* **2015**, *1382*, 118–134.

(23) Rabe, M.; Verdes, D.; Seeger, S. Understanding Protein Adsorption Phenomena at Solid Surfaces. *Adv. Colloid Interface Sci.* **2011**, *162* (1–2), 87–106.

(24) Zhang, L.; Sun, Y. Molecular Simulation of Adsorption and Its Implications to Protein Chromatography: A Review. *Biochem. Eng. J.* **2010**, *48* (3), 408–415.

(25) Harmant, P.; Aimar, P. Coagulation of Colloids Retained by Porous Wall. *AIChE J.* **1996**.

(26) Rohani, M. M.; Mehta, A.; Zydney, A. L. Development of High Performance Charged Ligands to Control Protein Transport through Charge-Modified Ultrafiltration Membranes. *J. Memb. Sci.* **2010**, *362* (1–2), 434–443.

(27) Polyakov, Y. S.; Zydney, A. L. Ultrafiltration Membrane Performance: Effects of Pore Blockage/Constriction. *J. Memb. Sci.* **2013**, *434*, 106–120.

(28) S. Curcio; G. De Luca; F. Paone; V. Calabrò. MODELLAZIONE MULTISCALA DEI PROCESSI DI SEPARAZIONE DI PROTEINE MEDIANTE TECNOLOGIE A MEMBRANA, 2011.

(29) De Luca, G.; Bisignano, F.; Paone, F.; Curcio, S. Multi-Scale Modeling of Protein Fouling in Ultrafiltration Process. *J. Memb. Sci.* **2014**, *452*, 400–414.

(30) Edwards, J. P.; Gerber, U.; Schubert, C.; Trejo, M. A.; Weber, A. The Yukawa Potential: Ground State Energy and Critical Screening. *Prog. Theor. Exp. Phys.* **2017**, *2017*, 083A01.

(31) Howard L. Lemberg; Frank H. Stillinger. Application of Hypernetted-Chain Integral Equations to a Central-Force Model of Water. **1976**, *32* (2), 353–362.

(32) Chun, M. S.; Bowen, W. R. Rigorous Calculations of Linearized Poisson-Boltzmann Interaction between Dissimilar Spherical Colloids and Osmotic Pressure in Concentrated Dispersions. *J. Colloid Interface Sci.* **2004**.

(33) Petrosino, F.; Curcio, S.; Chakraborty, S.; Luca, G. De. Enzyme Immobilization on Polymer Membranes : A Quantum and Molecular Mechanics Study. *Comput. Sci. Eng.* **2019**, 1–9.

Chapter 2

Theoretical background

2.1 Introduction

The choice of theoretical and computational procedures strongly depends on the aims of the model to be formulated and solved. Furthermore, the definition of both the model structure and the linking parameters among the considered space- and timescales is another crucial aspect to be considered. Quantum Mechanics (QM) approaches allow for the evaluation of chemical-physical quantities that cannot be estimated by experimental tests. However, when computational procedures are used, particular attention has to be paid to the structural chemical models. For instance, it is worthwhile remarking that QM methods are not applicable to the optimization of macromolecules geometries such as polymers due to the huge computational time, whereas Molecular Dynamics (MD) methodologies or Monte Carlo (MC) methods can be exploited in these cases. MC models are widely used for the simulation of macromolecules adsorption during membrane processes. However, accurate QM approaches, such as correlated Hartree-Fock[1] and Density Functional Theory (DFT)[2], allow the evaluation of different electronic properties, which are worthwhile for the definition of accurate multiscale computational frameworks.

In the present work, DFT calculations were done at sub-nanoscopic scale to obtain point charges on colloidal (protein) structures. On the other hand, MD simulations were very useful to obtain the polymeric surface of PolySulfone membranes by a Simulated Annealing (SA) procedure. At microscopic scale, the stochastic methodologies such as the Monte Carlo (MC) approaches were of particular interest. They indeed allowed optimizing geometries containing several hundreds of interacting units.[3] Moreover, colloidal solutions such as proteins were described by well-assessed

colloid theories that assimilate their behavior to interacting systems of defined particles. A versatile class of liquid state theory methods, which permits the theoretical determination of the microstructural and thermodynamic proprieties starting from the knowledge of particle interactions, was widely exploited both for the validation of some previous simulations and for the calculation of different macroscopic proprieties, like the osmotic pressure or the diffusion coefficient of solute in the cake layer accumulated on the membrane surface. The so-called Orstein-Zernike (OZ) equation schemes were used along with different approximation theories aimed at solving the OZ equation.

Only an appropriate merging and coordination of all the theories formulated at each of the considered scales allow the implementation of a complete multiscale model, which could describe the complex interactions existing among different macromolecules and between the macromolecules and the membrane surface without resorting to empirical information or even to adjustable parameters.

The basics of the different modelling approaches were shortly described in the following. An introduction to Density Functional Theory was reported starting from the very bottom of the length scale of the multiscale model and going to Molecular Dynamics techniques that were briefly analyzed. Monte Carlo methods were also described to provide a complete theoretical background of the present work and a short introduction to Physics of Colloidal Soft Matter is given too. Finally, to "close the loop" Computational-Fluid-Dynamic techniques were introduced.

2.2 Introduction to Density Functional Theory

Density Functional Theory (DFT) is a variational method that is presently one of the most successful approach to compute the electronic structure of matter. Its applicability ranges from atoms, molecules and solids to quantum and classical fluids. Geometric and electronic proprieties of nano-structures can be evaluated faster than Hartree-Fock methods[1].

The wavefunction ψ for an n-electron molecule is a function of $3n$ spatial coordinates and n spin coordinates. From ψ one can produce the molecule's spin-free electron density function, $\rho(1)$, by integrating $\psi*\psi$ over all of the spatial and spin coordinates, except those for one of the electrons:[4]

$$\rho(1) = \int |\psi(1, 2, \ldots, N)|^2 d\omega_1 d\tau_2 \ldots d\tau_n \qquad (\mathbf{2.1})$$

which is a function only depending on the three spatial coordinates. In the early days of quantum chemistry, a major challenge was the evaluation of integrals over the interelectronic-repulsion term in the Hamiltonian, mathematical operator corresponding to the total energy of the system, as well as dealing with the related problem of electron correlation. Several methods were devised attempting to approximate these quantities from the density function $\rho(1)$, with moderate success. However, the ongoing progress in computer performance and the development of sophisticated *ab initio* methods gradually shifted attention away from approaches which use the density function.

In 1964, a proof by Hohenberg and Kohn[5] of a connection between the ground state energy, E_0, for a system and ρ_0, the ground state density function,[6] sparked new interest in finding a rigorous way to move from the knowledge of the attractively simple three-dimensional density function to a value for E_0.

Specifically, for a system having n electrons and N nuclei, the Hamiltonian operator for the electronic energy can be expressed as:

$$H = -\frac{1}{2}\sum_{i=1}^{n}\nabla_i^2 + \sum_{i=1}^{n}\sum_{\alpha=1}^{N}\frac{-Z_\alpha}{r_{i\alpha}} + \sum_{i=1}^{n-1}\sum_{j=i+1}^{n}\frac{1}{r_{ij}} \qquad (\mathbf{2.2})$$

The first and last terms can be written down immediately if we know how many electrons are present, but the middle term depends on $\sum_{\alpha=1}^{N} -Z_\alpha/r_{i\alpha}$, which is a function of nuclear charges and their

locations/coordinates. The latter quantity is called the external potential, symbolized $v_{ext}(\vec{r})$, because it results from the presence of fields produced by particles not included in the group of electrons[7].

Hohenberg and Kohn were able to prove that there is a uniqueness relation between ρ_0 and the external potential. This raises the possibility that one could work backwards from ρ_0 to find $v_{ext}(\vec{r})$ and then E_0.

A relation proved by Hohenberg and Kohn[5] indicated away to proceed. They proved that an approximate density function, $\rho_{0\,approx}$, to which, for the Hohenberg and Kohn I theorem, an E_0 is associated through a function, must lead to an energy higher than the exact E_0: $E_{0_{approx}} \geq E_0$, so a variational bond does exist. The barrier to proceeding is the lack of a way to get E from ρ. Hence, as hereafter explained, only the exchange-correlation part of the total relation between E_0 and ρ_0, is unknown. The development of approximate functional that relate the energy to the electron density is an extremely active area of current research and probably will be for some time to come.

In analogy to wavefunction methods and Hamiltonian, the functional that connects E to ρ, $E[\rho]$, can be separated into an electronic kinetic energy contribution, $T\,[\rho]$, a contribution due to nuclear-electron attractions, $E_{ne}[\rho]$, and the electron-electron repulsions, $E_{ee}[\rho]$. The latter term can be further decomposed into Coulomb and exchange-correlation terms, $J\,[\rho]$ and $E_{xc}[\rho]$. Both the nuclear-electron attraction (corresponding to $v_{ext}\,[\rho_0]$) and the interelectronic Coulomb terms can be easily written in terms of the density using their classical expressions as in wavefunction methods. For the electronic kinetic energy *Kohn and Sham* propose different relations[4].

The final DFT energy expression is then written as the following functional:

$$E_{DFT}[\rho] = T_{S[\rho]} + E_{ne}[\rho] + J[\rho] + E_{xc}[\rho] \qquad (\mathbf{2.3})$$

The exact form of $E_{xc}[\rho]$ is not currently known. However, a rapidly growing list of approximate exchange correlation functionals have appeared in the literature. Current functional nomenclature

often reflects this with two-part acronyms, e.g., the BLYP DFT method that uses an exchange functional from Becke (B)[8] and a correlation functional proposed by Lee, Yang, and Parr (LYP)[9].

The great benefit of DFT methods is the computational cost. With the exchange correlation functional commonly used, the computational effort is similar to a Self-Consistent-Fields[10] (SCF) calculation, but with better accuracy.

Density functional theory provides an efficient and unbiased tool which is useful to compute the ground state energy in realistic models of bulk materials and surfaces. The reliability of such calculations depends on the development of approximations for the exchange-correlation energy functional. Significant advances have been carried out in recent years to improve the quality of exchange correlation functionals as the using of local density gradients, and nonlocal exchange functionals[2].

2.3 Introduction to Molecular Dynamics

Molecular dynamics is the term used to describe the solution of the classical equation of motion (Newton's equations) for a set of atoms or molecules. In MD, the particles move at constant velocity between perfectly elastic collisions, and it is possible to solve the dynamic problem without making any approximation, within the limits imposed by machine accuracy[12].

The total energy of the molecule can be splitted between potential and kinetic energy, and molecules are thus able to overcome barriers separating minima interaction energy, if the barrier height is less than the total energy minus the potential energy (Force Field). Given a high-enough energy, which is closely related to the simulation temperature, the molecular dynamics will sample the whole surface but will also require a huge simulation time.

In Molecular Dynamics simulations, Newton's equations of motion are integrated numerically for typically $N = 100 - 10000$ particles, starting from an initial configuration (representing all particle positions and velocities in the system) on a certain time interval $t_0 \leq t \leq t0 + \tau$ in a phase trajectory[15]. In contrast to the Monte Carlo simulations described hereafter, which only yield thermodynamic ensemble averages, Molecular Dynamics simulations can provide not only equilibrium properties, but also transport properties of the system. A Molecular Dynamics simulation is performed as follows:

1. Start with a configuration Γ_o, i.e., select the initial positions and the velocities for N particles;
2. An input Force Field is defined for all particles and the force is given by:

$$\boldsymbol{F_i(r) = -\frac{\partial U(r)}{\partial r}} \qquad (\mathbf{2.4})$$

with $U(r)$ the pair potential and r is the distance between two particles.

3. Integrate the Newton's equations of motion to obtain a set of updated positions and velocities:

$$\boldsymbol{F_i = m_i \times \frac{dv_i}{dt}} \qquad (\mathbf{2.5})$$

$$\boldsymbol{v_i = \frac{dr_i}{dt}} \qquad (\mathbf{2.6})$$

in which F_i, m_i, v_i and r_i are the total force, mass, velocity and position of particle i respectively. Quite small time steps dt must be used for integrating Newton's equation (femtoseconds), obtaining the trajectories of the molecules. In a Molecular Dynamics simulation, thermodynamic properties, e.g., temperature, pressure, radial distribution functions, etc., can be evaluated during the simulation. In addition to the static equilibrium properties, in a Molecular Dynamics simulation, one can also calculate dynamic equilibrium properties[16,17].

At sufficiently high temperatures and long running times, all the conformational space (conformers) is sampled. For this reason, in a Simulated Annealing (SA) techniques, the initial temperature is

chosen to be very low and then is increased instantaneously until a fixed value (usually from 20K to 500K). After that, an MD run is then initiated, during which the temperature is slowly reduced. Initially, each of the molecules composing the system is allowed to move over a large area, due to the high temperature, but as the temperature is decreased, it becomes trapped in a minimum. If the cooling is infinitely slow (implying an infinite run time), the resulting minimum is the global minimum (OK). In practice, however, an MD run is so short that only the local area is sampled. The name, simulated annealing, comes from the analogy of growing crystals. If a melt is cooled slowly, large single crystals can be formed. Such a single crystal represents the global energy minimum for a solid state. A rapid cooling produces a glass (local minimum), i.e. a disordered solid[18].

2.4 Monte Carlo methods

The importance of computer simulation from the standpoint of liquid-state theory relies on the fact that it provides essentially exact, quasi-experimental data on well-defined models and, in particular, on prototypical models of simple liquids[22].

Given a set of initial conditions, a conventional molecular-dynamics simulation is, in principle, entirely deterministic in nature. By contrast, as the name suggests, a stochastic element is an essential part of any Monte Carlo calculation. In Monte Carlo simulation a system of N particles, subject to the same boundary conditions used in molecular-dynamics calculations and interacting through some known potentials, is again assigned a set of arbitrarily chosen, initial coordinates. A sequence of configurations is then generated by successive random displacements of the particles, usually of one particle at a time. Not all of the configurations that are generated are added to the sequence. The decision whether to “accept” or “reject” a trial configuration is made in such a way that asymptotically configuration space is sampled according to the probability density corresponding to a particular statistical mechanical ensemble. The ensemble average of any function of the particle coordinates,

such as the total potential energy, is then obtained as an unweighted average over the resulting set of configurations[23].

The Monte Carlo method can be considered as a solution to the thermodynamic limitations, which affect the calculation of system total energy for a very large number of particles as the total number of states is too large. A possible way to compute thermodynamic averages such as $\langle E \rangle$ would generate random system states and use the Boltzmann factor as the *statistical weight* for these configurations. After all, the average energy $\langle E \rangle$ can be expressed as:

$$\langle \mathrm{E} \rangle = \frac{\sum_{\mathrm{spins}} \mathrm{E}(\mathrm{s}_1 \cdots \mathrm{s}_{\mathrm{N2}}) \exp[-\beta \mathrm{E}(\mathrm{s}_1 \cdots \mathrm{s}_{\mathrm{N2}})]}{\sum_{\mathrm{spins}} \exp[-\beta \mathrm{E}(\mathrm{s}_1 \cdots \mathrm{s}_{\mathrm{N}^2})]} \qquad (\mathbf{2.7})$$

in which Σ_{spins} denotes a summation over all the possible system states of $E(s_1 \cdots s_{N^2})$. As for large N it is not possible to generate all system states, we can simply choose random states. The relative "importance" or *statistical weight* of such a randomly chosen configuration is the Boltzmann factor. Supposing to generate *K* random system states $s_1 \cdots s_K$ in which the vector $s = \{s_1 \cdots s_{N^2}\}$ denotes the value of all spins in the system, the ensemble average of the energy can be approximated as:

$$\langle \mathrm{E} \rangle \approx \frac{\sum_{\mathrm{j}=1}^{\mathrm{K}} \mathrm{E}(\mathbf{s}_{\mathrm{j}}) \exp[-\beta \mathrm{E}(\mathbf{s}_{\mathrm{j}})]}{\sum_{\mathrm{j}=1}^{\mathrm{K}} \exp[-\beta \mathrm{E}(\mathbf{s}_j)]} \qquad (\mathbf{2.8})$$

For a sufficiently large number of samples (K), it was proved that this expression represents a good approximation[24].

Summing up, the MC scheme is as follows[24]:

1. Generate an initial configuration;
2. Start with an old configuration o, and calculate its energy $E(o)$;
3. Select a particle at random;

4. Give the selected particle a random displacement $x(n) = x(o) + \Delta$ in which Δ is a uniformly distributed random number from $[-\Delta x, \Delta x]$. Periodic boundary conditions are used, so if a particle moves out of the central box, it enters in the adjacent box;
5. Calculate the energy $E(n)$ of the new configuration n;
6. Accept the trial move with a probability given by:

$$\begin{aligned} \boldsymbol{acc(o \rightarrow n)} &= \mathbf{min}\big(\mathbf{1}, \boldsymbol{exp}\big[-\boldsymbol{\beta} \times \big(\boldsymbol{E(n)} - \boldsymbol{E(o)}\big)\big]\big) \\ &= \mathbf{min}(\mathbf{1}, \mathbf{exp}[-\boldsymbol{\beta}\, \Delta \boldsymbol{E}]) \end{aligned} \qquad (\mathbf{2.9})$$

7. Update the ensemble averages, also after a rejected trial move.

Regarding the above-defined acceptance criteria (# 6), if a decrease of total energy is observed, the proposed move is downhill and so accepted. If total energy increases, the proposed move is uphill and for the acceptance the probability has to be evaluated. To accept the move with a probability of $\rho_n/\rho_o = \exp(-\beta\, \Delta E)$ with $\beta = 1/K_B T$, K_B is the Boltzmann constant, a random number ξ is generated uniformly in the range $(0,1)$. ξ is then compared to ρ_n/ρ_o and in the case it is lower than ρ_n/ρ_o, the move is accepted; otherwise, it is rejected[20]. Basically, the sampling of Monte Carlo algorithm ensures that system states with a very low Boltzmann factor are rarely explored.

In conclusion, Monte Carlo simulations have been very valuable in understanding the structure and properties of liquids. For example, MC with accurate energy potentials (Force Fields) can estimate liquid densities and heats of vaporization with a remarkable accuracy. Monte Carlo simulations can provide also indications about the structure of hydration shells around solutes and allow estimating how different solvents may alter the energy profiles in chemical reactions.

2.5 A short introduction to Physics of Colloidal Soft Matter

The liquid state of matter is intuitively perceived as being intermediate in nature between a gas and a solid. Thus, a natural starting point for discussing the properties of any given substance is the relationship between pressure P , density ρ and temperature T in the different phases, summarised in the "classical" equation of state $f\ (P, \rho, T\ ) = 0$ [25].

The use of conventional liquids theory leads to an important simplification, namely that the contributions to thermodynamic properties arising from thermal motion can be separated from those ones which are due to the interactions among the particles composing the system under study. The separation of kinetic and potential terms suggests a simple means of characterising the liquid state. Let V_N be the total potential energy of a system, where N is the number of particles, and let K_N be the total kinetic energy. Then, in the liquid state, it is found that $K_N/|V_N| \approx 1$. Liquids and dense fluids are also distinguished from dilute gases by the greater importance of collisional processes and short-range, positional correlations, and from solids by the lack of long-range order; their structure is in many cases dominated by the "excluded-volume" effect, associated with the packing together of particles with hard cores[23].

In statistical thermodynamics a basic quantity is represented by particle distribution function. It measures the extent to which the structure of a fluid deviates from complete randomness. If the system is also isotropic, the pair distribution function $g_N\ (r1, r2)$ is a function only of the separation $r_{12} = |r2 - r1|$ between the two observed macromolecules; it is then usually called the radial distribution function (RDF) expressed as g(r). When r is much larger than the range of inter-particle potential, the RDF approaches the ideal-gas limit identified as $(1 - 1/N) \approx 1$ [26].

The radial distribution function plays a key role in the physics of monatomic liquids and, by similarity, in the physics of all types of molecules approximated by rigid particles. There are several

reasons for this. First, g(r) is measurable by radiation-scattering experiments. The characteristic RDF of such an experiment performed on liquid argon is represented in Fig.3:

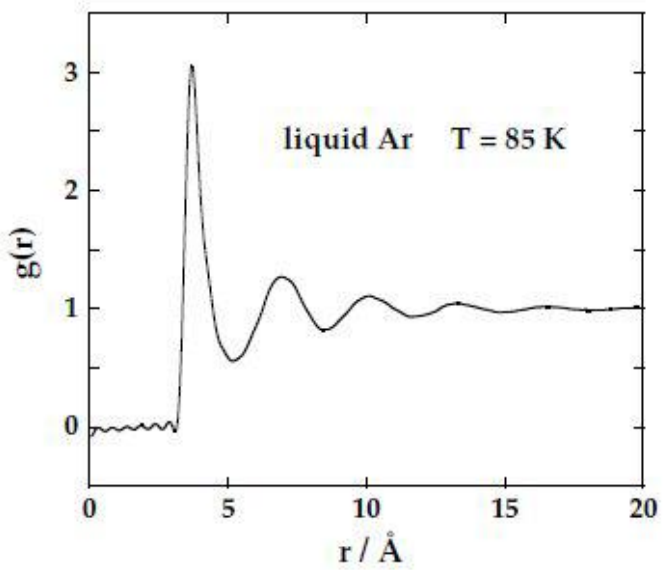

Figure 3. Results of radiation-scattering experiments for the radial distribution function of liquid argon near the triple point [27].

$g(r)$ exhibits a pattern of peaks and troughs that is characteristic of all monatomic liquids, tends to unity at large r, and vanishes as $r \rightarrow 0$ as a consequence of the strongly repulsive forces that act at small particle separation distances. Secondly, the shape of $g(r)$ provides a considerable insight about the structure of a liquid, at least at the level of pair correlations. The definition of $g(r)$ implies that, on average, the number of particles lying within the range r to $r + dr$ from a reference particle is $4\,\pi\,r^2\,\rho\,g(r)\,dr$ and the peaks in $g(r)$ represent "shells" of neighbours around the reference particle. Integration of $4\,\pi\,r^2\,\rho\,g(r)$ up to the position represented by the first minimum of the curve provides an estimate of the nearest-neighbour "coordination number". The concepts of a "shell" of neighbours and a "coordination number" are obviously more appropriate to solids than to liquids, but they give useful measures of the structure of a liquid provided the analogy with solids is not taken too far. Finally, if the atoms interact through pairwise-additive forces, thermodynamic properties can be expressed in terms of integrals over $g(r)$. [28]

Introducing the total correlation function $h(r_{ij}) = g(r_{ij}) - 1$, between two generic particles *i* and *j*, and defining RDF as $g(r) = e^{-\beta W(r)}$ were W is the total interaction potential, the influence of particle *i* on particle *j* can be split into two contributions: direct, defined by the direct correlation function $c(r_{ij})$ and indirect. The indirect influence can be described by a direct influence of particle *i* on particle *n*, which, in turn, directly and indirectly influences the particle *j*.

This arrangement is described by the *Ornstein-Zernike* (OZ) equation:

$$\boldsymbol{h(r_{ij}) = c(r_{ij}) + \sum_{n=1}^{N} \rho_n \int_{-\infty}^{+\infty} c(r_{in})\, h(r_{nj})\, dr_{in}} \qquad (\mathbf{2.10})$$

Where the sum goes over all the components present and ρ is the number density of a given component[29].

After different mathematical rearrangements with the Fourier-transformed correlation functions, $\hat{h}(k_{ij})$, and passing through the definition of convolution integral, the OZ equation can be rewritten as:

$$\boldsymbol{\hat{h}(k_{ij}) = \hat{c}(k_{ij}) + \sum_{n=1}^{N} \rho_n\, \hat{c}(k_{in})\, \hat{h}(k_{nj})} \qquad (\mathbf{2.11})$$

The equation in Fourier space is easier to be solved (at least numerically). In order to be really able to solve this problem, however, one more equation, the so called closure relation, is needed. The most used closure relations, which express $c(r)$ approximately in terms of $h(r)$ and a given pair potential $u(r)$, are the Mean-spherical approximation (MSA), the Rescaled MSA (RMSA), the Percus-Yewick (PY) closure, the Hypernetted Chain (HNC) closure and the Random phase approximation (RPA)[30,31]. In combination with the OZ equation, the closures lead to closed integral equations for $g(r)$. These integral equations have been found, in comparison with computer simulation results and scattering

data, to be most useful in calculating the full r-dependence of $g(r)$ and the thermodynamic proprieties of dense liquids[32].

Two important thermodynamic properties deriving from the RDF are represented by the osmotic pressure and the diffusion coefficient of colloidal solutions. In the present work, starting from the aforementioned $g(r)$, different theories were used for the calculation of these parameters. As explained hereafter in the dedicated chapter, the total suspension pressure can be determined from the generalized virial pressure equation; the diffusion coefficient calculations were based on the *Donnan* equilibrium[33] and on the *Kirkwood and Buff* theory[34].

2.6 Computational-Fluid-Dynamic

The derivation and the understanding of structure-property relationships at the meso- and macroscale represent one the toughest challenge in modeling the complex phenomena typical of either chemical engineering or materials science. Particle simulations, based on truly atomistic models, are not possible at this scale and classical coarse-grained models generally fail since the number of particles whose behavior is to be simulated is too large[35]. Therefore, at meso-/macroscopic scale one has to either further coarsen the description by introducing well-assessed particle models or make use of purely phenomenological models, which are based on the continuum theory. When averaging over many degrees of freedom one finally arrives at the macroscopic scale, where continuum models describe the behavior of solids and the properties of fluids based on the Navier-Stokes Equation.

Most of the engineering problems do not admit an analytical solution of the Navier-Stokes equations[36]; The numerical solution of the governing equations for fluid applications on Eulerian grids is well-established in the engineering community and different commercial software are currently available on the market. Most of these computational environments exploit numerical

methods that discretize the corresponding Partial Differential Equations (PDEs) on grids and are fundamentally based on a mesh-connectivity of grid elements[36]. This is the subject matter of Computational Fluid Dynamics (CFD). The PDEs approximation is typically based upon different types of discretization. The Finite Element Method (FEM) is very commonly used to compute such approximations[38].

Applying the fundamental laws of mechanics to a compressible Newtonian fluid, the governing equations can be devised. These are: the conservation of mass[37]:

$$\frac{\partial \rho}{\partial t} + \nabla \cdot (\rho \mathbf{u}) = 0 \qquad (\mathbf{2.12})$$

and the conservation of momentum[37]:

$$\underbrace{\rho\left(\frac{\partial \mathbf{u}}{\partial t} + \mathbf{u} \cdot \nabla \mathbf{u}\right)}_{1} = \underbrace{-\nabla p}_{2} + \underbrace{\nabla \cdot \left(\mu\left(\nabla \mathbf{u} + (\nabla \mathbf{u})^T\right) - \frac{2}{3}\mu(\nabla \cdot \mathbf{u})\mathbf{I}\right)}_{3} + \underbrace{\mathbf{F}}_{4} \qquad (\mathbf{2.13})$$

Where ρ is the fluid density, $\boldsymbol{u}$ the velocity vector, p the pressure and μ the dynamic viscosity of the considered fluid. The different terms in Eq. 2.13 correspond to the inertial forces (1), the pressure forces (2), the viscous forces (3), and the external forces applied to the fluid (4).

These equations along with the conservation of energy equation form a set of coupled, nonlinear PDEs and are at the heart of fluid flow modelling. The solution of these equations, for a particular set of boundary conditions (e.g. at inlet, outlet, and walls) and initial conditions, allows predicting the fluid velocity and its pressure for a given geometry of the system at hand.

In chemical engineering problems a variety of coupled physical phenomena involving mass transfer take place. The subject of transport phenomena describes the transport of momentum, energy, and mass in the form of mathematical relations[41]. The basis for these descriptions is found in the laws for

conservation of momentum, energy, and mass in combination with the constitutive relations that describe the fluxes of the conserved quantities.

In these cases, the mass balance (particle conservation) is described by:

$$\frac{\partial n}{\partial t} + \nabla \cdot \mathbf{J} = 0 \qquad (\mathbf{2.14})$$

where $n(r,t)$ and $J(r,t)$ are the coarse-grained local particle number concentration and advective-diffusive particle flux, respectively. The latter is the sum of two different contributions:

$$\boldsymbol{J = J^{ad} + J^{D} = n\,v - D(\phi)\,\nabla n} \qquad (\mathbf{2.15})$$

of advection and Brownian diffusion fluxes. Here, $D(\phi)$ is the concentration-dependent long-time collective or gradient diffusion coefficient. For non-zero particle concentration and dominantly repulsive interactions, $D(\phi)$ is, in general, larger than the single-particle translational diffusion coefficient, D_0, measured at infinite dilution[39]. It is worthwhile noting that:

$$\boldsymbol{J^{D} = -D(\phi)\,\nabla n = -\frac{D_0\,K(\phi)}{k_B\,T}\,\nabla \Pi} \qquad (\mathbf{2.16})$$

is valid for a monodisperse solution of electroneutral particles at temperature T, with k_B denoting the Boltzmann's constant. Thus, the diffusion flux is driven by the gradient in the osmotic pressure $\Pi(\phi)$, which in turn is proportional to the gradient of the particles chemical potential[40]. The transport property $K(\phi)$ is the long-time macroscopic sedimentation coefficient.

Substituting the Eq.2.15 into Eq.2.14 and using the local volume fraction $\phi = nV_c$, (V_c is the colloid volume) rather than $n(r,t)$, the macroscopic advection-diffusion equation is obtained:

$$\frac{\partial \boldsymbol{\phi}}{\partial \boldsymbol{t}} + \boldsymbol{v}\,\boldsymbol{\nabla}\boldsymbol{\phi} = \boldsymbol{\nabla}\cdot(\boldsymbol{D}\,\boldsymbol{\nabla}\boldsymbol{\phi}) \qquad (\mathbf{2.17})$$

The determination of the collective diffusion coefficient $D = D(\phi)$ will be explained more in detail hereafter in this thesis. The advection-diffusion equation is the relevant equation from witch volume fraction profile could be calculated if the velocity field is known. The latter could arise from Darcy like equation and iteratively calculated through Eq.2.17.

2.7 Conclusions

In agreement with the multi-scale framework order, a brief theoretical overview was presented in this chapter. The density functional theory, used as the *first-brick* of the entire work, allowed the fundamental atomic proprieties calculations without resorting to any empirical or experimental parameter. The Molecular Dynamics and Monte Carlo approaches permitted the determination of a minimal energy structure of, respectively, the polymeric membrane at nanoscale level, and the aggregated colloidal particles during ultrafiltration at microscale level. Despite the two approaches are aimed at the same minimization goal, the first one is based on the solution of classical equation of motion, while Monte Carlo is a stochastic-based approach.

To get some fundamental macroscopic properties like the Osmotic pressure and the Diffusion coefficient, the colloidal soft matter theory was illustrated. In this field, different statistical thermodynamics approaches resulted of vital importance for the complete closure of the present multiscale framework and the achievement of the final transition at macroscopic level by a completely ab-initio methodology. Moreover, a micro-Computational-Fluid-Dynamic approach was exploited for the final process simulation based on the previously-defined quantities.

References

(1) Slater, J. C. A Simplification of the Hartree-Fock Method. *Phys. Rev.* **1951**.

(2) Mikael P. Johansson, Ville R.I. Kaila, and D. S. Ab Initio, Density Functional Theory, and Semi-Empirical Calculations. **2013**, *924* (August 2013), 2–27.

(3) Cervantes, M. The Monte Carlo Method. *Math. Sci. Eng.* **1972**.

(4) Kohn, W. W. Kohn and LJ Sham, Phys. Rev. 140, A1133 (1965). *Phys. Rev.* **1965**.

(5) Hohenberg, P.; Kohn, W. P. Hohenberg and W. Kohn, Phys. Rev. 136, B864 (1964). *Phys. Rev.* **1964**.

(6) Miehlich, B.; Savin, A.; Stoll, H.; Preuss, H. Results Obtained with the Correlation Energy Density Functionals of Becke and Lee, Yang and Parr. *Chem. Phys. Lett.* **1989**.

(7) Lowe, J. P.; Peterson, K. Quantum Chemistry, Third Edition. *J. Chem. Educ.* **2005**.

(8) Becke, A. D. Current-Density Dependent Exchange-Correlation Functionals. *Can. J. Chem.* **1996**.

(9) Xu, X.; Goddard, W. A. The X3LYP Extended Density Functional for Accurate Descriptions of Nonbond Interactions, Spin States, and Thermochemical Properties. *Proc. Natl. Acad. Sci. U. S. A.* **2004**.

(10) Kohn, W.; Sham, L. J. Self-Consistent Equations Including Exchange and Correlation Effects. *Phys. Rev.* **1965**.

(11) Bartolotti, L. J.; Flurchick, K. An Introduction to Density Functional Theory. In *Reviews in Computational Chemistry*; 2007.

(12) Perdew, J. P.; Burke, K.; Ernzerhof, M. Generalized Gradient Approximation Made Simple. *Phys. Rev. Lett.* **1996**.

(13) Rapaport, D. C.; Blumberg, R. L.; McKay, S. R.; Christian, W. The Art of Molecular Dynamics Simulation. *Comput. Phys.* **1996**.

(14) Lewars, E. G. *Computational Chemistry: Introduction to the Theory and Applications of*

Molecular and Quantum Mechanics: Third Edition 2016; 2016.

(15) Fredrickson, G. H. The Theory of Polymer Dynamics. *Curr. Opin. Solid State Mater. Sci.* **1996**.

(16) Leary, R. H. Global Optimization on Funneling Landscapes. *J. Glob. Optim.* **2000**.

(17) Straatsma, T. P.; Berendsen, H. J. C. Free Energy of Ionic Hydration: Analysis of a Thermodynamic Integration Technique to Evaluate Free Energy Differences by Molecular Dynamics Simulations. *J. Chem. Phys.* **1988**.

(18) Thompson, S. M.; Gubbins, K. E.; Walton, J. P. R. B.; Chantry, R. A. R.; Rowlinson, J. S. A Molecular Dynamics Study of Liquid Drops. *J. Chem. Phys.* **1984**.

(19) Kirkpatrick, S.; Gelatt, C. D.; Vecchi, M. P. Optimization by Simulated Annealing. *Science (80-.).* **1983**.

(20) Allen, M. P.; Tildesley, D. J. *Computer Simulation of Liquids: Second Edition*; 2017.

(21) Heinecke, A.; Eckhardt, W.; Horsch, M.; Bungartz, H. J. Molecular Dynamics Simulation. In *SpringerBriefs in Computer Science*; 2015.

(22) Yethiraj, A. Liquid State Theory of Polyelectrolyte Solutions. *J. Phys. Chem. B* **2009**.

(23) Hansen, J. P.; McDonald, I. R. *Theory of Simple Liquids*; 2006.

(24) Vlugt, T. J. H. *Introduction to Molecular Simulation and Statistical Thermodynamics*; 2009.

(25) Gompper, G.; Schick, M. *Soft Matter*; 2007.

(26) Frisch, H. L. Classical Kinetic Theory of Fluids, by R. Resibois and M. de Leener, John Wiley, New York, 1977. 400 Pp. *Int. J. Chem. Kinet.* **1979**.

(27) Kirkwood, J. G.; Boggs, E. M. The Radial Distribution Function in Liquids. *J. Chem. Phys.* **1942**.

(28) Widom, B. Some Topics in the Theory of Fluids. *J. Chem. Phys.* **1963**.

(29) http://pyoz.vrbka.net/theory/oz-equation-closures.

(30) Howard L. Lemberg; Frank H. Stillinger. Application of Hypernetted-Chain Integral Equations to a Central-Force Model of Water. **1976**, *32* (2), 353–362.

(31) Zerah, G.; Hansen, J. Self-consistent Integral Equations for Fluid Pair Distribution Functions: Another Attempt. *J. Chem. Phys.* **1986**.

(32) Nägele, G. The Physics of Colloidal Soft Matter. *Mater. Struct.* **2004**.

(33) Stell, G.; Joslin, C. G. The Donnan Equilibrium: A Theoretical Study of the Effects of Interionic Forces. *Biophys. J.* **1986**.

(34) Braga, C.; Smith, E. R.; Nold, A.; Sibley, D. N.; Kalliadasis, S. The Pressure Tensor across a Liquid-Vapour Interface. *J. Chem. Phys.* **2018**.

(35) Ingólfsson, H. I.; Lopez, C. A.; Uusitalo, J. J.; de Jong, D. H.; Gopal, S. M.; Periole, X.; Marrink, S. J. The Power of Coarse Graining in Biomolecular Simulations. *Wiley Interdisciplinary Reviews: Computational Molecular Science*. 2014.

(36) Doering, C. R. The 3D Navier-Stokes Problem. *Annu. Rev. Fluid Mech.* **2009**.

(37) Chentanez, N.; Müller, M. Mass-Conserving Eulerian Liquid Simulation. *IEEE Trans. Vis. Comput. Graph.* **2014**.

(38) Yetmez, M. Finite Element Analysis. In *Musculoskeletal Research and Basic Science*; 2016.

(39) Roa, R.; Zholkovskiy, E. K.; Nägele, G. Ultrafiltration Modeling of Non-Ionic Microgels. *Soft Matter* **2015**.

(40) Nägele, G. Colloidal Hydrodynamics. In *Proceedings of the International School of Physics "Enrico Fermi";* 2012.

(41) Schoch, R. B.; Han, J.; Renaud, P. Transport Phenomena in Nanofluidics. *Rev. Mod. Phys.* **2008**.

Chapter 3

Interactions between proteins and membrane surface in multiscale modeling of organic fouling

Curcio, S.; Petrosino, F.; Morrone, M.; De Luca, G. Interactions between Proteins and the Membrane Surface in Multiscale Modeling of Organic Fouling. *Journal of Chemical Information and Modeling* **2018**, *58* (9), 1815–1827. https://doi.org/10.1021/acs.jcim.8b00298.

Interactions between proteins and membrane surface in multiscale modeling of organic fouling

S. Curcio[a], F. Petrosino[a], M. Morrone[b] and, G. De Luca[b*]

[a]*Department of Computer Engineering, Modeling, Electronics and Systems (D.I.M.E.S.), Laboratory of Transport Phenomena and Biotechnology, University of Calabria, Ponte P. Bucci, cubo 39/c, 87036 Rende (CS), Italy;*

[b] *Institute on Membrane Technology, ITM-CNR, Ponte P. Bucci, cubo 17/c, 87036 Rende (CS), Italy*

Abstract

In the present paper, an improved multiscale modeling aimed at describing membrane fouling in the UltraFiltration (UF) process was proposed. Some of the authors of this work previously published a multiscale approach to simulate ultrafiltration of Bovine Serum Albumin (BSA) aqueous solutions. However, the noncovalent interactions between proteins and the membrane surface were not taken into account in the previous formulation. Herein, the proteins-surface interactions were accurately computed by first-principle-based calculations considering also the effect of pH. Both the effective surface of polysulfone (PSU) and the first layer of proteins adsorbed on the membrane surface were accurately modeled. Different from the previous work, the equilibrium distance between proteins was calculated and imposed as lower bound to the protein–protein distances in the compact deposit accumulated on the membrane surface. The computed BSA surface charges were used to estimate the protein potential and the charge density, both necessary to formulate a forces balance at microscopic scale. The protein surface potential was compared with Z-potential measurements of BSA aqueous solution, and a remarkable agreement was found. Finally, the overall additional resistance, as due to both the compact and loose layers of the deposit, was computed, thus allowing the final transition to

a macroscopic scale, where an unsteady-state mass transfer model was formulated to describe the behavior of a typical dead-end UF process. A good agreement between simulated and experimental permeate flux decays was observed.

3.1 Introduction

Efficient and innovative modeling methods are nowadays required to describe the complex phenomena involved in membrane separation processes so to predict the effect of process conditions on permeate flux decay. One of the most promising computational techniques is definitely multiscale modeling, which accommodates a variety of models, ranging from the atomic level to the macroscopic scale. The idea of multiscale modeling is straightforward: one computes information at a smaller (finer) scale and passes it to a model at a larger (coarser) scale by leaving out degrees of freedom[1]. In this way, phenomena and information between various scales are strongly interrelated and a more comprehensive knowledge about complex systems behavior is achieved.

Multiscale modeling is a relatively new technique in membrane science and technology. Chen et al.[2] proposed a multi-scale modeling framework combining a finite volume and lattice Boltzmann methods to predict electrochemical transport reaction in proton exchange membrane fuel cell cathode. Shi et al.[3] formulated a multiscale approach to model forward osmosis (FO) processes; the model was obtained by coupling a micro-scale model for the intrinsic permeability and effective diffusivity of digitally reconstructed membrane, to a macro-scale model, for the fluid flow in FO unit. Oliveira *et* al. proposed a multiscale model to describe a polymer electrolyte membrane water electrolyzer aimed at hydrogen production[4,5]. De Morais *et al.* developed a multiscale methodology, which scaled up *ab initio* calculated data into elementary kinetic models to simulate polymer electrolyte membrane fuel cells transient operation[6]. Tang *et al.* formulated a multiscale approach based on the coupling of

dissipative particle dynamics simulations and macroscopic mathematical models to obtain a detailed understanding on membrane formation process via thermally induced phase separation method[7]. A multiscale approach was also proposed to model incipient crystallization in desalination membrane modules, focusing on solid phase generation phenomena and accounting for the membrane surface geometrical changes[8]. Sullivan *et al.*[9] proposed a multiscale model to investigate the transport through a microfiltration membrane; the model was obtained by coupling a macroscale approach, aimed at describing the flow in a tubular module, and a microscopic model, which accounted for membrane porous structure. Guillen and Hoek proposed a multiscale modeling approach to link microscopic and macroscopic transport phenomena in spiral wound elements[10]. A multiscale model was developed for reverse electrodialysis process in order either to describe the physical phenomena involved in the process or to achieve an optimal equipment design[11].

A multiscale model to simulate the UF process of BSA solutions was already published by some of the authors of this paper[12]. This multiscale model allowed predicting permeate flux decay starting from the knowledge of BSA fundamental features, namely the electrostatic surface charges and charge density as provided by ab initio calculations. The previous paper had to be considered as a "first brick" for the formulation of a more comprehensive and accurate modeling approach aimed at predicting the behavior of protein purification by UF. In the previous paper, in fact, the noncovalent interactions existing between proteins and the membrane surface, significantly affecting the evolution of the membrane permeability during typical UF processes,[13] were not taken into account. In the present work, the noncovalent proteins-surface interactions were accurately evaluated by a quantum and molecular mechanics approach and then incorporated in the previously formulated model[12]. The surface charges of PSU and BSA were calculated through a first-principle-based approach and accounted for the solution pH.

This *ab-initio* modeling allowed defining the actual structure of the first layers of adsorbed proteins and the equilibrium distance among them. Such an equilibrium distance, arbitrarily assumed in the previous paper,[12] was imposed as a minimum value of the distances between adjacent proteins accumulated in the compact layers of the deposit. In this way, a physical limit to both the void fraction and the additional resistance, as due to adsorbed macromolecules, was rigorously calculated, thus making the present multiscale model more physically consistent, general, and versatile. It is worthwhile remarking that the existence of such a minimum distance limit allows reliably explaining the achievement of a maximum compression of the cake. Thus, one of the most severe assumptions, exploited in ref[12], was eliminated in this study.

It is worth noting that also steric and electrostatic exclusion as well as pore blocking (or constriction) affect membrane filtration efficiency[14–17] and fouling. However, the description of this different fouling mechanism was far beyond the scope of this work and was not considered, considering that the computational effort required to perform the ab initio calculations was very high. For this reason, all the simulations were referred to as filtrations through membranes exhibiting high protein rejections.

It is worthwhile remarking that the present model was not based on adjustable parameters, except for some empirical constants to be used in the DLVO theory calculations. Nevertheless, these parameters were fixed at the beginning of simulations and were never tuned in order to get a better data fitting.

In fact, the main goal of the approach described in the present paper is definitely the development of a computational tool capable of accurately simulating the progress of the dead-end ultrafiltration process without resorting to any empirical or adjustable parameter.

3.2 Multi scale approach and experimental setup

3.2.1 Protein contact surface

The noncovalent interactions between proteins and the membrane surface are crucial in multiscale modeling of organic fouling. Surface charges of interacting systems are necessary to evaluate the involved long-range interactions. In particular, the surface charges of proteins depend on the nature of external amino acids, on their arrangement, and on the experimental conditions such as solvent, pH solvated ions, etc. The protein contact surface characterized by a proper thickness becomes a crucial point for the calculations of surface charges. To obtain different molecular surfaces, various algorithms are available in the open literature[18,19]. However, it is not easy to get a reliable protein surface with custom thickness, i.e. having an optimal number of amino acids allowing to calculate the surface charges through ab initio approaches. Herein, a bespoke algorithm was used to obtain the contact surface of BSA from its crystallographic structure at pH = 7, reproducing valleys, deep canyons, and flat regions as shown in Fig. 4.

The considered contact surface of BSA contained 3179 atoms; its area, $S_{vdW,}$ evaluated through the Analytical calculation of the van der Waals Surface and Volume (ASV) code[20] is equal to about 24000Å^2 (1.21 10^{-16} m^2). In order to consider only the surface facing outward from the protein, the value obtained by ASV is divided by two. Using the bespoke algorithm, a thickness of the protein surface has to be defined. Such a thickness was chosen small enough, as compared to the diameter of BSA, so that the thickness of protein crust was comparable to the sizes of its external amino acids.

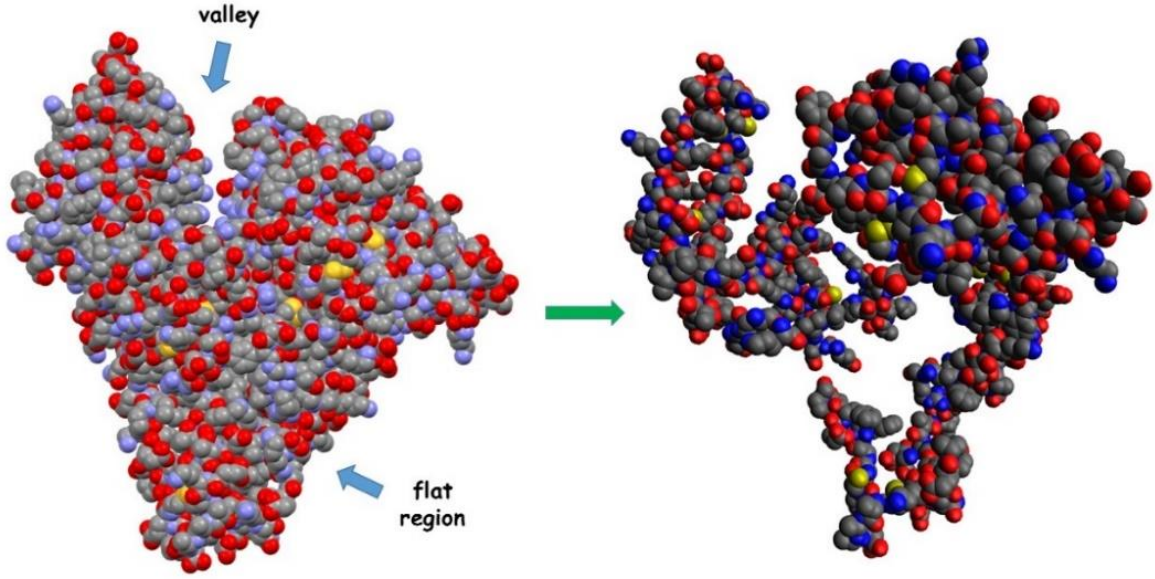

Figure 4 Structure of BSA at pH=7 showing valleys and flat regions (right side) and its 2D contact surface (left side) as coming out from the bespoke algorithm.

Using this criterion the difference between inner and outer facing surfaces can be considered as negligible. The $S_{\text{cont. surf}}$, equal to $S_{vdW}/2$, was used to define the diameter of an equivalent sphere with equal surface, named equivalent diameter, and equal to 8.8 nm. This diameter was used in the force balance equation at the microscopic level while the external amino acids were used to calculate the surface charges in order to obtain the total protein surface charge and density.

The surface charges were calculated in the frame of Density Functional Theory (DFT) using the ElectroStatic Potential (ESP) method as implemented in NWChem[21] that evaluates the atomic charges from the fit of the quantum mechanical electrostatic potential on a selected grid points centered on each external atoms of the protein. All quantum calculations were performed by using B3LYP[22] hybrid functional and double-ζ (6-31G) basis set for each atoms of the protein and membrane surfaces. The thresholds for the energy convergence in the self-consistent field procedure and the root mean square of the electron density were set to 10^{-6} (a.u.) and to 2×10^{-5} (a.u.), respectively.

3.2.2 Polysulfone surface model

Several computational approaches can be used to build dense polymeric surfaces[23–26]. Conformational systematic research (systematic rotor search) of the polysulfone functional groups, Ph-O-Ph, Ph-SO_2-Ph and Ph-isopropyl-Ph, was first performed using Avogadro code[27] and Universal Force Field. After that, for each functional group, the most stable conformers were optimized at quantum mechanics level using the D2 dispersion correction in order to consider the interaction between phenyl rings. The B3LYP[22] hybrid functional and double-ζ set were used. The geometries were optimized by analytical energy gradients and the quasi-Newton algorithm with approximate energy Hessian updates. The convergence criteria for the geometry optimizations, i.e. the maximum and root-mean-square gradient thresholds, were set equal to 4.5×10^{-4} and 3.0×10^{-4}, respectively, with the maximum and root-mean square of the nucleus Cartesian displacement vectors equal to 1.8 × 10−3 and 1.2 × 10−3 (a. u.), respectively. The optimized functional groups were used to build the polysulfone monomer once more optimized at the same level of theory. A second monomer was then added to the first one; the polymeric fragment was gradually lengthened, and each time it was optimized at the quantum level. A fragment of 16 monomers was built and used as the starting geometry for the successive Molecular Dynamics annealing. Isothermal–isobaric ensemble (NPT) simulations with P = 1 atm, a step of 1 fs, and cutoff of 9 Å were performed using the Amber force field (Amber99) and period boundary conditions. The sizes of the simulation box were Lx = 24.976 Å, Ly = 24.765 Å and Lz = 22.591 Å. Heating from 0 K up to 600 K was carried out followed by a cooling up to 300 K using a ΔT equal to 150 K. Simulations of 1 ns were performed for each temperature except for the last one (300 K) which lasted up to 18 ns. The energy of the fragment was minimized using the steepest descent algorithm with 103 steps. The system was considered as

equilibrated when the oscillations of total energy fell into 5% of its mean value and the Root Square Means Displacement converged into an asymptotic value, as shown in Fig. 5. The density of the polysulfone box, as obtained by the simulated annealing MD, was equal to 1100 kg/m^3. Using this value and taking into account the average porosity of UF-PSU membranes an apparent density equal to 200 kg/m^3 was obtained very close to that one of some of the most common UF PolySulfone membranes available on the market.

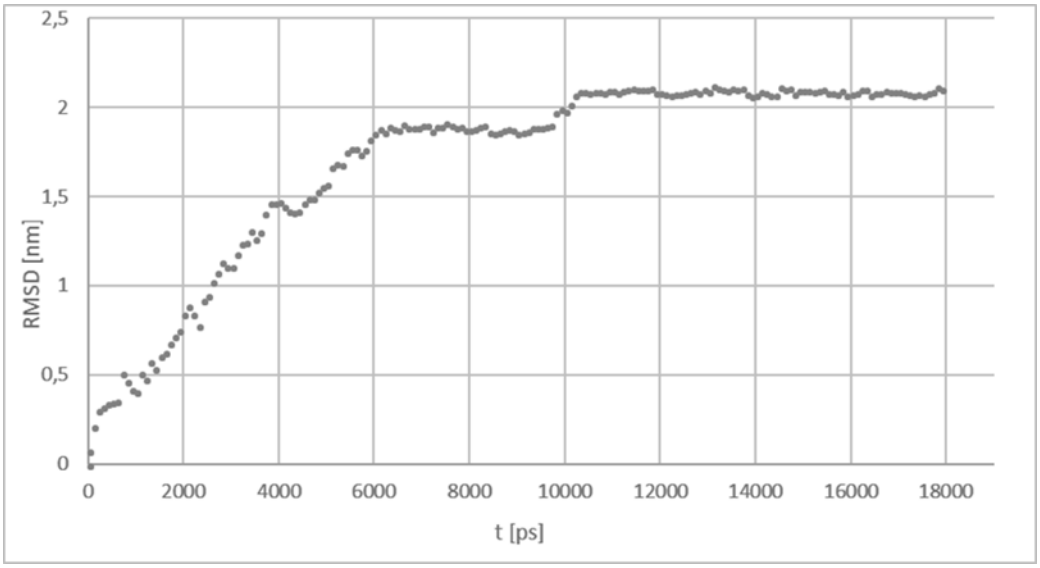

Figure 5 RMSD as function of simulation time (18 ns) at P=1 atm, T =300 K and step 1 fs.

It is worthwhile emphasizing that the simulation box was built starting from a polymer fragment obtained by ab initio optimizations and having a satisfactory number of monomers. Starting from a polymer fragment optimized at the first-principle level, the MD annealing procedure began at 0 K, thus reducing the dependence from initial conditions.

The partial atomic charges of the equilibrated polymer box were calculated with the same approach used for the calculation of BSA surface charges. However, in this case, the quantum calculation was carried out using the Continuum Conductor-like Screening Model (COSMO)[28] with a relative

dielectric constant equal to 2.2 in order to consider the water molecule in contact with polymer, i.e. confined in the equilibrated box. Finally, a polymer surface model showing x and y sizes equal to 99.904 and 99.060 Å, respectively, was built by replicating the already equilibrated box and keeping its thickness constant, i.e. *Lz* = 22.591 Å. These minima sizes were chosen in agreement with the BSA equivalent diameter to accommodate one protein on the polymer surface for the successive molecular mechanics optimizations. The model of the polymer surface was hence proportionally enlarged to accommodate two proteins, four and 16 macromolecules in order to reproduce the first layer of adsorbed proteins on the polysulfone surface.

3.2.3 Interaction potential energy

The interaction potential energy can be split into three contributions according to the approach reported by Mikael Lund and Bo Jönsson[29]:

$$u_{tot}(r_{ij}) = u_{hs}(r_{ij}) + u_{el}(r_{ij}) + u_{vdW}(r_{ij}) \tag{3.1}$$

$$u_{hs} = \begin{cases} \infty & r_{ij} < \frac{\sigma_{ii}+\sigma_{jj}}{2} \\ 0 & r_{ij} > \frac{\sigma_{ii}+\sigma_{jj}}{2} \end{cases} \tag{3.2}$$

$$u_{el}(r_{ij}) = \sum_i \sum_j \frac{q_i q_j}{4\pi\epsilon_0\epsilon_r r_{ij}} \tag{3.3}$$

$$u_{vdW}(r_{ij}) = 4\epsilon_{ij}\left[\left(\frac{\sigma_{ij}}{r_{ij}}\right)^{12} - \left(\frac{\sigma_{ij}}{r_{ij}}\right)^{6}\right] \tag{3.4}$$

The $u_{hs}(r_{ij})$ accounts for the repulsion of the electron clouds, and the usual hard-sphere approach was used[30]. The $u_{el}(r_{ij})$ term is the electrostatic Coulomb interaction; ε_0 and ε_r are the vacuum and relative dielectric permittivity, respectively, while q_i and q_j are the atomic surface charges of the

protein and the polymer surface models. The confined water was considered in the successive optimizations using a suitable relative dielectric constant equal to 2.2; this dielectric constant was also used in COSMO for the calculation of the surface charges. The hydrophobic (Van der Waals) interactions among proteins or between proteins and surface models were evaluated by a Lennard-Jones 12-6 potential; σ_{ii} and ε_{ii} parameters were taken from ref.[31]

As pointed out, the protein surface charges, q_i, were used to calculate the total surface charge, Q_{tot}, and the surface charge density by means of the same method adopted in the previous paper[12]:

$$Q_{\text{tot}} = \Sigma\, q_{i,\,out} + q_{i,ckbone} \qquad (3.5)$$

where $q_{i,out}$ are the partial charges of the amino acids functional groups showing outward direction, while the second term refers to the partial charges of the backbone of all external amino acids.

The effect of pH was also considered. In particular, the protonated form of the external residues depended on the difference between pH and pK_r, where K_r was the equilibrium constant of a specific functional group. For $pH > pK_r$ the predominant form is the deprotonated structure, whereas for $pH < pK_r$ the protonated form was the most abundant. Nevertheless, for particular pH values both forms had to be considered. The ratio between the deprotonated and protonated structure was calculated using the following relationship:

$$\frac{[\text{Depr}]}{[\text{Pr}]} = 10^{(\text{pH}-\text{pK}_r)} \qquad (3.6)$$

For instance, at pH=7, the aspartic and glutamic acids are fully deprotonated, whereas lysine and arginine are protonated. Concerning the functional group of the external histidine, the deprotonated form results 70%. Thus, all the external residues were protonated or deprotonated according to the Eq.3.6 by considering pH= 7.

3.2.4 Proteins-surface interaction

Geometry optimizations of proteins-surface nanostructures were performed to build a reliable layer of adsorbed proteins on the largest surface model. The equilibrium distance among proteins, $h_{min,}$ was hence calculated by the covered surface. As a result, a lower limit to the void fraction and additional resistance of the adsorbed proteins, useful in the modeling at a microscopic level, was calculated.

The minimum of potential energy (Eq 3.1), referred to as a single protein on the corresponding surface model, was initially searched. For this optimization, the two possible rotations (tetz and text) of the protein and the distance (d) from the surface were chosen as variables to optimize, Fig. 6.

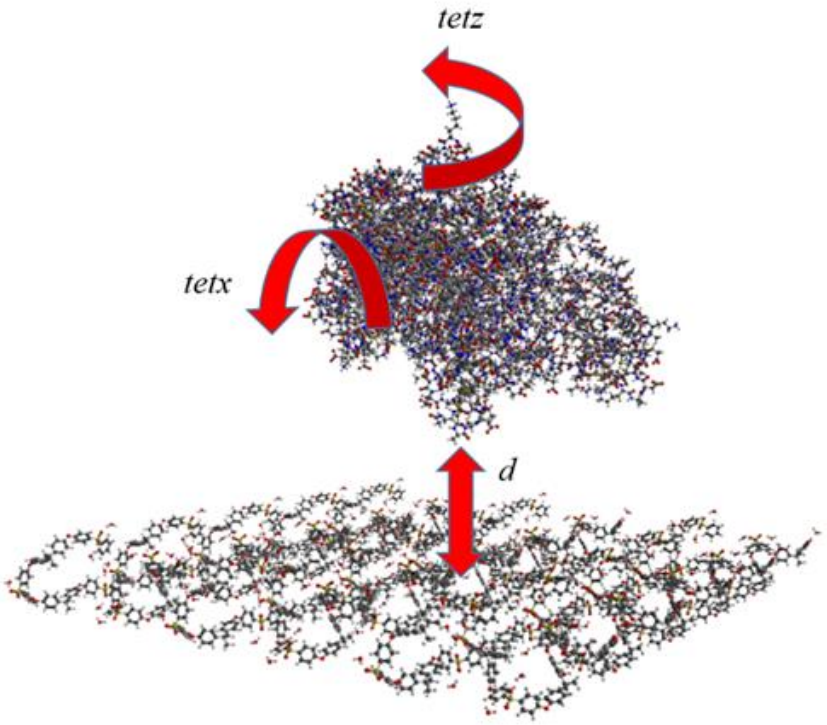

Figure 6 BSA-polysulfone (ball-stick) model, tetz, tetx *and* d *variables used to minimize the potential energy*

A preliminary grid-type search restricted to the rotational variables was performed. The orientations corresponding to the minimum of the potential energy were then used as a starting point for

subsequent optimizations by considering all three variables. These optimizations were performed using Levenberg–Marquardt (LM)[32] and Downhill simplex (D- simplex) [33] algorithms. The above-described procedure was repeated several times varying both the x- and the y-position of BSA interacting with the membrane surface, and it was found that the changes in potential energy were negligible (variations less than 0.1%), thus the surface model can be considered quite homogeneous allowing a significant reduction of computational effort.

Starting from this result, the position of a second protein (BSA2) interacting with an already-optimized BSA molecule (BSA1) was optimized. With reference to Fig.7, and starting from the calculated position of BSA1, as expressed by the two variables *text-opt* and *d-opt*, a set of new variables, considered as relevant to achieve the optimization of BSA2 position, was introduced.

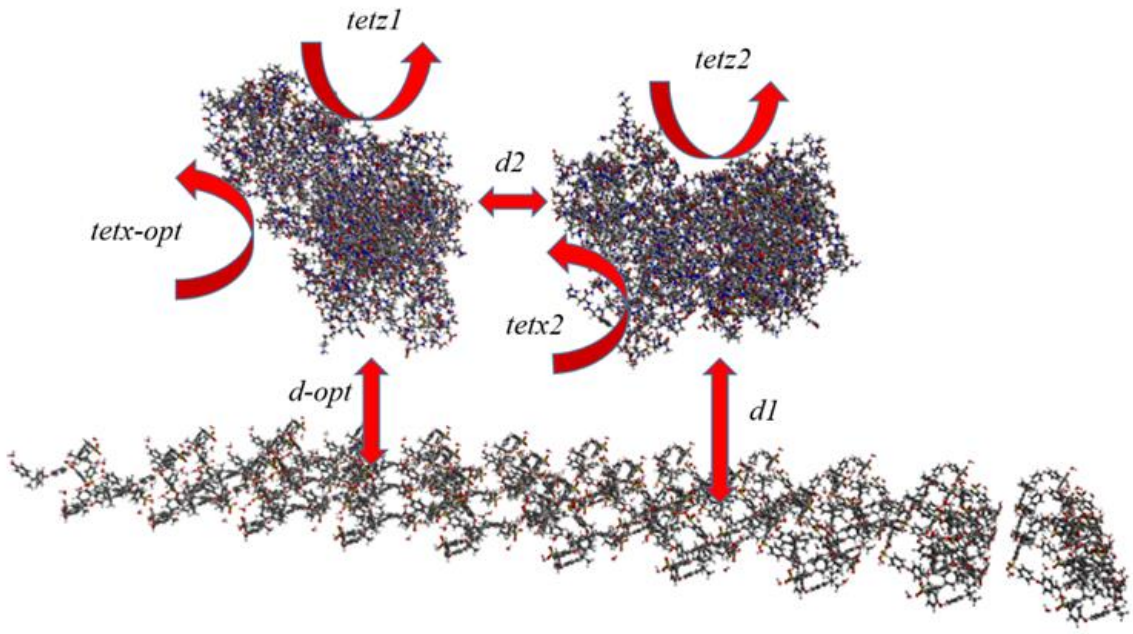

Figure 7 Second protein assembled to the first one adsorbed on the surface model (ball-stick). Variables used in the minimization of the potential energy of interaction.

These are two rotational angles (*tetz2*, *tetx2*), the distances between BSA2 and BSA1 and between BSA2 and surface, *d2* and *d1*, respectively; finally, the position of BSA2 around BSA1 is actually replaced by a z-rotation of the latter (*tetz1*). The minimization of the potential energy allowed obtaining the optimized position of BSA2 with respect to both the membrane surface and BSA1.

The optimized structure of the initial/first couple of BSA molecules was replicated along the x- and the y-axis so as to obtain a whole layer of proteins adsorbed on the membrane surface.

In particular, further optimizations were carried out to obtain the equilibrium distance, d^X, between the first and second couple of BSA molecules added along the x-axis. Moreover, the optimal distance, d^Y, between the first couple and a third couple added along the y-axis was calculated, and finally the orientation of the second BSA couple compared to the first one was optimized.

The so-calculated first layer of proteins adsorbed on the membrane surface was then used to find the position of a BSA molecule belonging to the second layer. Three initial positions of this protein, (A) face-centered, (B) body-centered, and (C) top position, were chosen in addition to two heights (z = 100 Å and z = 400 Å, respectively). A schematic grid representing these initial positions was presented in Fig. 8. Five variables, namely the x, y, and z coordinates and two rotational angles, were considered as relevant for the minimization of potential energy aimed at calculating the equilibrium position of this protein on the first layer. It is worthwhile noting that x and y sizes of the polysulfone surface were lengthened with respect to the minimum sizes so as to locate all 16 proteins.

Finally, both the orientation and distances of a second adjacent protein belonging to the second layer were optimized using the same procedure adopted for the optimization of a couple of BSA molecules; this procedure leads to an optimal packaging of BSA accumulated on the membrane surface in the compact cake.

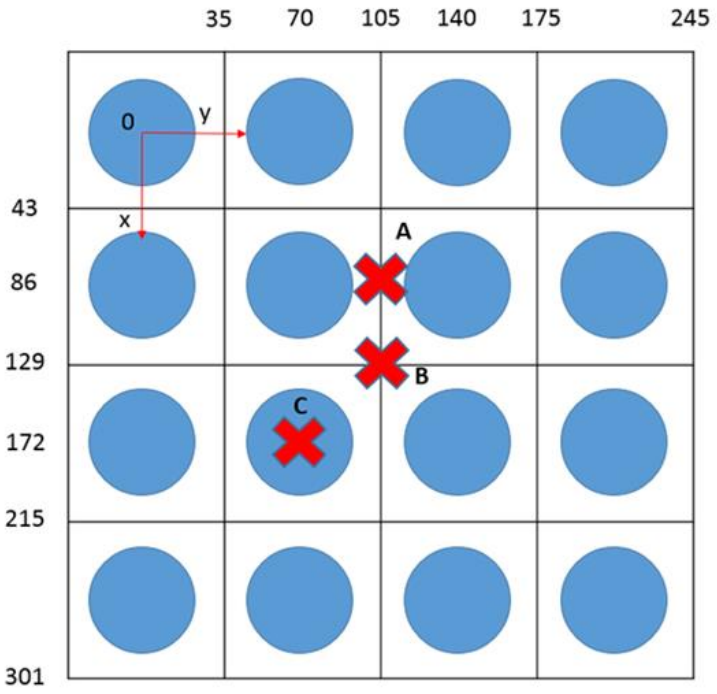

Figure 8 Schematic grid representing the three initial positions (red crosses) of a protein belonging to the second layer. Light blue circles represent proteins of the first layer.

3.2.5 Microscopic and Macroscopic models

Assuming a body-centered cubic symmetry in the forces balance at microscopic scale aimed at predicting the buildup of macromolecules deposit, each particle was subjected to the surface forces as due to both the n–1 and n+1 layers, according to the Harmant and Aimar model[34]. In the multiscale framework already formulated by some of the authors of the present paper[12], the surface forces, according to the DLVO theory[35], were expressed as functions of the protein surface potential, ψo, and the equivalent diameter of BSA resulting from the smaller time- and space scales. In turn, the surface potential was calculated as a function of the dielectric constant of medium, the reciprocal of the Debye–Huckel parameter, expressed according to the relations proposed in the Karthik and Das Gupta work[36], and the surface charge density. The equivalent diameter was calculated in section 3.2.1,

while the Hamaker constant and collision diameter were evaluated as reported in ref.[12]. Finally, the surface forces also depended on the distance (h) between proteins belonging to adjacent layers of the deposit. A central protein in the deposit could also be subjected to the viscous force expressed by the modified Stokes relation[37] and to the diffusive forces occurring in the opposite direction. The modified Stokes relation depended on the equivalent diameter, on the permeate flux, and on the void fraction of the deposit[38]; moreover, the latter depends on the protein–protein distance, h, and on the number of layers, n, constituting the deposit.

The force balance relation[34] had to be solved for all the deposit layers starting from the bulk and up to the membrane surface. The forces balance was solved iteratively obtaining a distribution of *h* with respect to *n* [12]; in this work a lower limit to the *h* values was imposed, i.e. h_{min}, calculated at nanoscale level. As a result, a lower bound of deposit void fraction and of the additional resistance to filtration, as due to deposit buildup, was calculated. The equilibrium distance, h_{min}, represented the lower limit of the h distance that, instead, varies as the filtration proceeds. This lower limit was calculated by molecular mechanics optimizations in order to take into account the maximum compression of the adsorbed proteins. In fact, the electrostatic repulsive forces beyond this equilibrium distance did not allow any further compression of the proteins, while the modified Stokes relation and the other forces control, at the microscale level, the deposit compression. The model, as formulated in ref.[34], describes the protein deposit on the membrane surface at the microscale level using nondeformable spheres. Thus, it assumes that water permeation did not change markedly the protein conformation as the filtration proceeds. As pointed out, the cake compression was taken into account at the microscopic level by means of the forces balance (modified Stokes relation), while the effect of water permeation on the conformation of individual proteins was considered as negligible due to the low transmembrane pressures characterizing dead-end ultrafiltration.

Although the forces balance describing the cake formation did not explicitly consider any conformational changes of BSA, it is worthwhile remarking that protein transport through the compact cake was dynamically simulated. In fact, it was assumed that the molecules adsorbed on the membrane surface diffuse through the few free volumes, whereas, at the same time, other BSA molecules enter into the compact cake through the top layer from solution bulk. Such a transport mechanism is described by the macroscopic scale equations as explained in the previous paper[12].

For each simulation time, a specific resistance of the deposit was calculated using the void fraction and the equivalent diameter. Finally, the permeate flux was calculated using the so-called total resistance defined as the sum of membrane resistance, assumed as constant, and the cake specific resistance multiplied its mass per unit area, i.e. the additional resistance R_{add} (t). More details about the implementation of the iterative procedure, aimed at calculating both the specific resistance and the deposit structure, as well as the implementation of the macroscopic model predicting permeate flux decay, could be found in ref.[12].

As already pointed out in previous sections, the development of a rigorous methodology aimed at estimating all the mutual interactions existing between different BSA molecules accumulating on a polymeric membrane and the membrane surface itself was the main objective of this work. Such a methodology, based on accurate (and time-consuming) calculations performed at both subnanoscopic and nanoscopic scales, has to be considered as a significant novelty in the literature and, therefore, was described in a detailed way. Some other aspects, referred, in the developed multiscale framework, to either microscopic or macroscopic scales, were not described with the same level of accuracy, since the exploited methodology was already reported in ref.[12]. However, is wise to have a conceptual scheme outlining how the small scale computations lead to compute the relevant parameters in the macroscale model as reported in Fig.9.

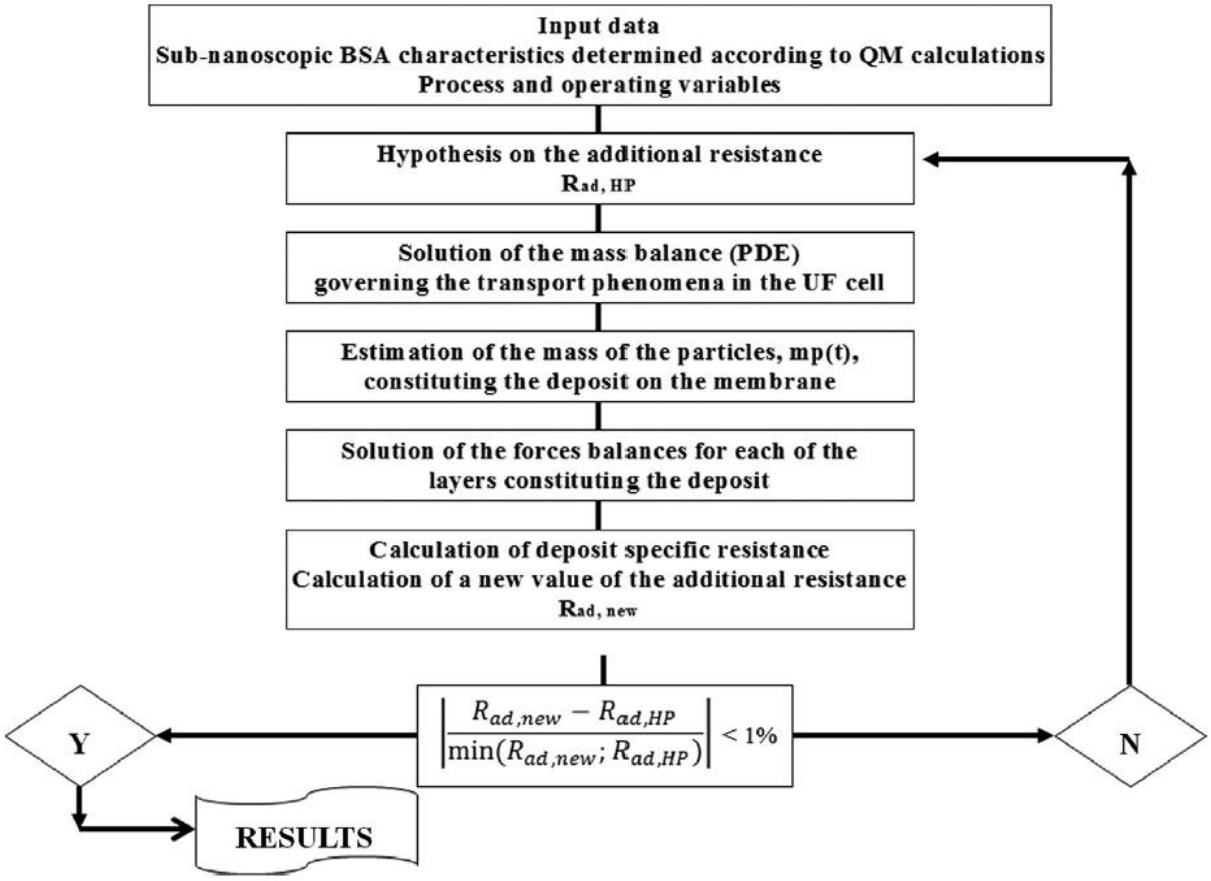

Figure 9: Schematic representation of the formulated multi-scale model[12].

3.2.6 Experimental setup

Inputs, achieved in subnanoscopic and nanoscopic scales, were ascertained by undertaking experiments aimed at measuring the zeta potential of BSA solutions. The solutions were prepared using bovine serum albumin (BSA; A 9647, obtained from Sigma-Aldrich (Dorset, UK)) dissolved in deionized water (Milli Q system, Millipore, Gradient model) showing a resistivity of 18.3 MΩ cm. Two different concentrations of NaCl of analytical grade (obtained from Merck, Germany) were also used in order to analyze the effects of ionic concentration on the zeta potential. The protein solutions were titrated from pH value 7.5 to 4.9 using 0.1 M HCl and 0.1 M KOH (Merck, Germany) under

constant stirring. Before each titration, freshly prepared protein solutions were filtered using 0.45 μm PVDF filter. All measurements were performed using protein solutions with a concentration of 10g/L. The zeta potential of BSA solutions were determined by phase analysis light scattering (PALS) for the 0.001 M and 0.1 M NaCl concentrations; a Malvern Zetasizer, NANO ZS (Malvern Instruments Limited, UK) was used. Each data value is an average of five measurements. The instrument software calculated the zeta potential through the electrophoretic mobility by the Henry equation:

$$\mu_E = \frac{2\varepsilon\zeta\ f(\kappa a)}{3\eta} \tag{3.7}$$

Where μ_E is the electrophoretic mobility, ε is the absolute dielectric constant of solution, ζ the zeta potential, κ is the reciprocal electrical double layer which depends on ionic strength of the solution, η is the viscosity of solution, *a* is BSA radius and *f* (κα) is Henry's corrective term. Assuming the double layer thickness much smaller than the particle size, the Smoluchowski approximation was used in the calculations. The Debye screening length or electrical double layer thickness, κ^{-1} (nm), was calculated as:

$$\kappa^{-1} = \left(\frac{\varepsilon_0 \varepsilon_r k_B T}{2000 e^2 I N} \right)^{0.5} \tag{3.8}$$

where ε_0 and ε_r are the dielectric constants of free space (8.854×10^{-12} C V^{-1} m^{-1}) and water (78.5), k_B is Boltzmann's constant (1.38×10^{-23} J K^{-1}), *T* is the absolute temperature (K) and *e* is the magnitude of the electron charge (1.6022×10^{-19} C). *N* is Avagadro's number ($6.02 \times 10^{23} mol^{-1}$), and *I* is the ionic strength of the salt solution (M).

3.3 Results and Discussion

3.3.1 Surface Charge Density

The protein surface charges were calculated by the ESP method; the functional groups of the external amino acids were protonated or deprotonated according to the Eq.3.6 in order to take into account the effect of pH. The surface charges were used to evaluate the total charge, Q_{tot}, according to Eq.3.5, obtaining −15.82 $a.u.$, and the surface charge density, evaluated as the ratio between Q_{tot} and $S_{cont.surf}$, i. e. q''= Q_{tot}/ $S_{cont.surf.}$. The computed q'' was equal to −0.021 (C/m^2) in good agreement with the values reported in literature[39,40]. In addition, q'' and the equivalent diameter were used to calculate the protein surface potential obtaining -75 mV. Interestingly, the surface charges calculated by the Löwdin method yields a value of q'' equal to -0.012 C/m^2 and a BSA surface potential equal to -49 mV[12]. The accuracy of these parameters, used to define the surface and viscous forces in the simulations at microscopic scale, was verified experimentally. Measures of BSA solutions Z-potential were reported, as a function of three pH values and two NaCl concentrations, in Fig. 10. For pH = 7 and a ionic concentration equal to 1x10^{-4} M, the experimental value of the Z-potential is -26 mV. This value is close to the surface potential obtained using the surface charge density evaluated with Löwdin surface charges, whereas the agreement is worse using the ESP charges. Although ESP charges provided less accurate Z-potential with respect to the Löwdin charges, they were used because the objective of this work was to model an effective polymer surface interacting with the adsorbed proteins including the effect of this interaction in the already-developed multiscale framework.

Thus, the proposed modeling does not lose validity if the Löwdin surface charges is used.

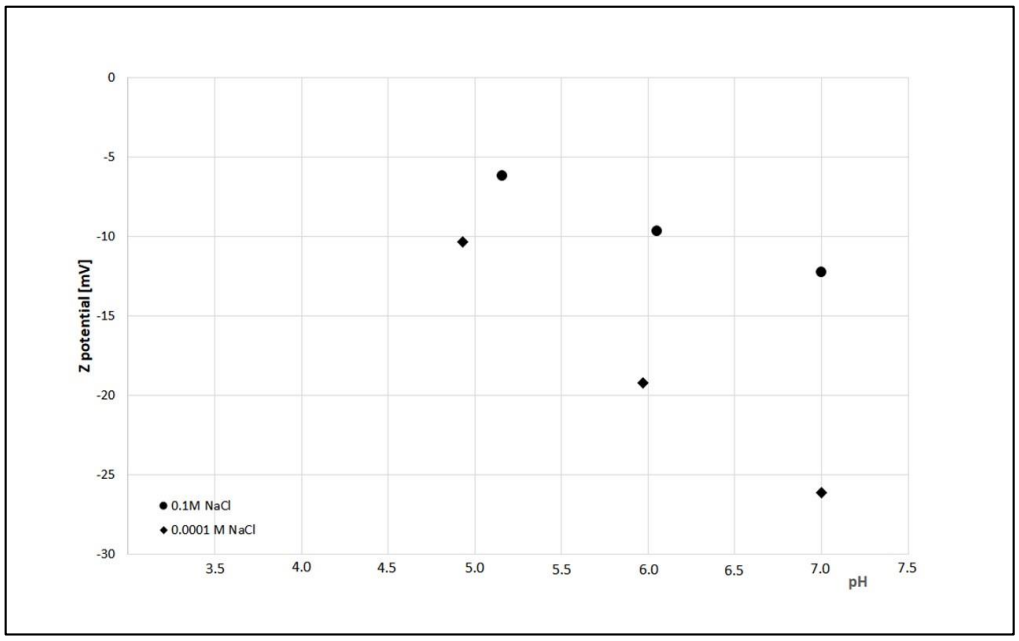

Figure 10 BSA solution Z-potential measurements performed at three pH and two NaCl concentrations.

3.3.2 Protein packing on polysulfone surface

The equilibrium distances between adjacent proteins adsorbed on the polymer surface, and their mutual orientation were calculated following the procedure described in paragraph *3.2.4*.

A grid-type search was first performed considering the rotations of one protein as shown in Fig. 6; 256 orientations were explored in order to find the starting point near the minimum. The LM and D-simplex methods allowed obtaining the final protein dispositions corresponding to the minima of potential energy. Although D-simplex provided a lower potential energy as compared to the LM, both the minima configurations were used for subsequent optimizations. An analogous grid-type search was performed for the optimization of the structure of a couple of BSA molecules, exploring 512 orientations and keeping $d2$ equal to the equivalent diameter while $d1$ equal to d_{opt} evaluated by the single protein optimization (see Fig. 7). For the latter optimization, three algorithms were used: LM, D-simplex and Sequential Quadratic Programming (SQP). All the algorithms converged into

structures similar to those ones found by the grid-type search. The LM method yielded a minimum with the lowest energy as compared to the other algorithms, thus, the structure of a couple of BSA molecules obtained by the LM method was chosen to develop the first layer of adsorbed proteins according to the procedure illustrated in section *3.2.4*. The optimized couple of the BSA system interacting with the surface was replicated along the x- and y-axis and the d^Y, d^X and *tetz* variables were again optimized. The first protein layer formed by 16 macromolecules was built (see Fig. 8) to predict the position of one protein belonging to the second layer of the compact deposit.

The optimal position of this protein was obtained starting from three initial points (face-centered, body-centered, and top position) and using the LM algorithm. The optimized sites were shown in Fig.11.

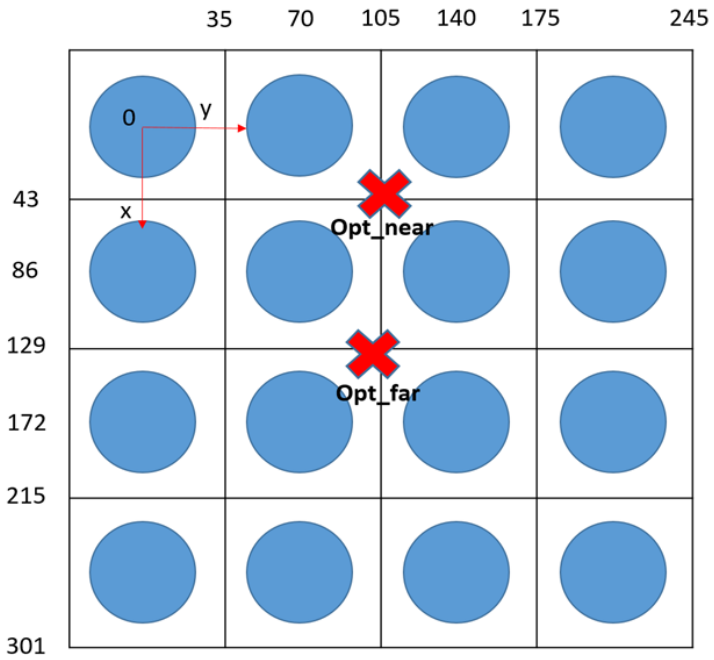

Figure 11 Schematic grid to represent the optimized positions of one protein belonging to the second layer of the compact deposit on the polymer surface (red crosses: Opt_near initial height = 100 Å Opt_far initial = 400 Å). Proteins of the first layer in blue

The optimal position of protein did not depend on its initial positions and heights, and interestingly the optimized structures could be associated with a body-centered cubic geometry. This result was particularly important since in previous works the bcc symmetry was assumed on empirical basis only[34]. Instead, in the present paper, this symmetry was the result of rigorous calculations, namely the subsequent geometry optimizations of increasing nanostructures, without resorting to any empirical assumption but exploiting surface charges derived from quantum-based calculations and also considering the effect of pH. The minimum distance among the adsorbed proteins was computed from the MM optimizations and imposed as lower bound in the microscopic forces balance. Thus, the upper limit of the additional resistance, associated with the obtained the protein maximum packing on the polysulfone surface, was consistent with the symmetry used in the forces balance. It is important to point out that in the previous works[12,34] the minimum distance among the adsorbed proteins had been empirically assumed; instead, in this work it was calculated. In particular, h_{min} was calculated as the difference between the center-to-center equilibrium distance, derived from the optimizations of the proteins position on the second layer and the equivalent diameter (Fig. 12); h_{min} was equal to 1.3 Å.

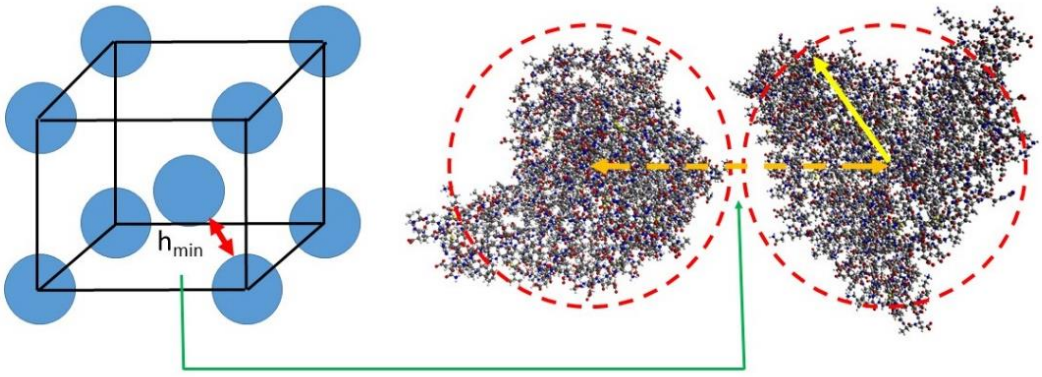

Figure 12 Center-to-center equilibrium distance (dotted arrow) obtained by MM optimizations, equivalent radius (continuous arrow) obtained from the protein contact surface and $h_{min,}$ *(lower bound) calculated from the difference between equilibrium distance and equivalent diameter.*

h_{min} was not the minimum distance among the atoms of the contact surface, but the difference between proteins equilibrium distance and equivalent diameter as shown in Fig. 12. In the microscale the atoms-formed protein was modeled as an equivalent sphere with a specific radius, and this condition was necessary when the scale was expanded; hence, the use of h_{min}, in conjunction with the equivalent diameter, allowed predicting the final void fraction of the compact cake in a physically consistent way.

3.3.3 Macro results of multi-scale modeling

The BSA ultrafiltration process was simulated in order to obtain the actual proprieties of fouling coat and some macroscopic quantities such as the permeate flux $J(t)$ and the additional resistance $R_{ad}(t)$. A dead-end filtration, using membrane module with a filter surface of 25 cm^2, a temperature of 20°C and constant transmembrane pressure (TMP) was simulated. The simulations lasting 40 minutes were performed with BSA concentration of 10 g/l. The TMP ranged from 1 to 3 bar with increments of 0.5 while high protein rejections, *Rej*, were analyzed for each pressure: 0.9825, 0.985, 0.9875, 0.99[41].

The protein-protein distance in the deposit layers, *h (n)*, as function of the layer number, correlated to height of the proteins from the surface, is showed in Fig. 13. Two characteristic portions of protein deposit were clearly visible: the compact layers on the membrane surface (inner part) and the loose layers (outer part), typical of solution bulk.

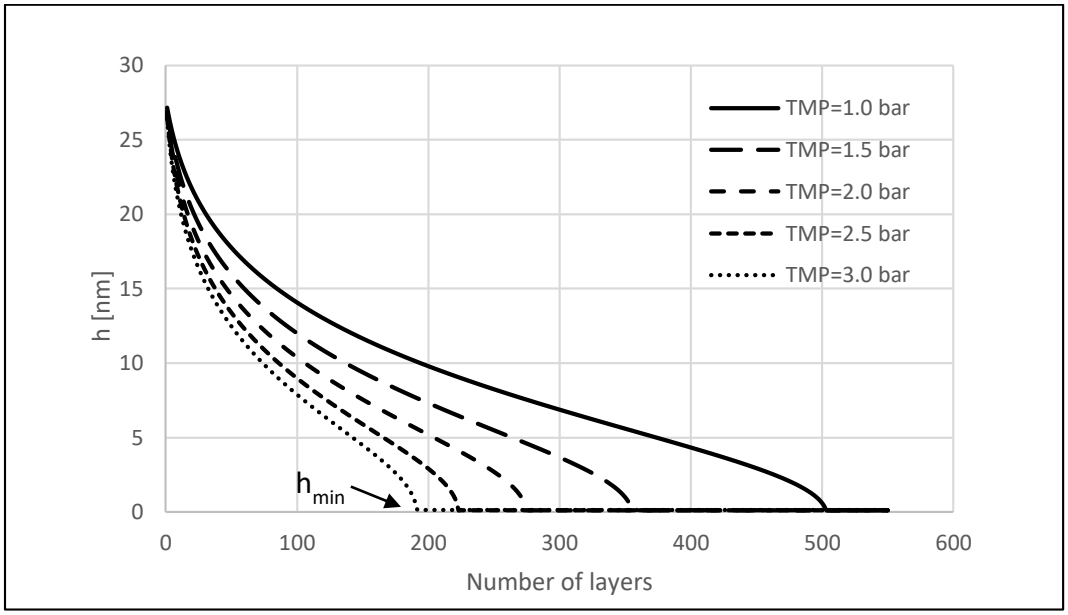
30
25
20
15
10
5
0
h [nm]
0
100
200
300
400
500
600
Number of layers
TMP=1.0 bar
TMP=1.5 bar
TMP=2.0 bar
TMP=2.5 bar
TMP=3.0 bar
h min

(a)

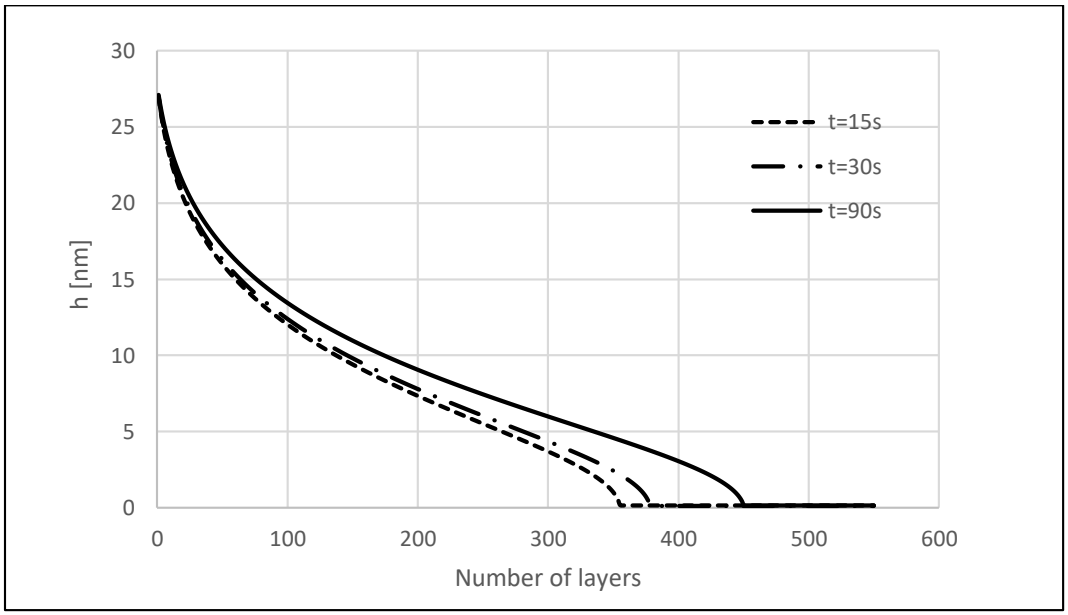
30
25
20
15
10
5
0
h [nm]
0
100
200
300
400
500
600
Number of layers
t=15s
t=30s
t=90s

(b)

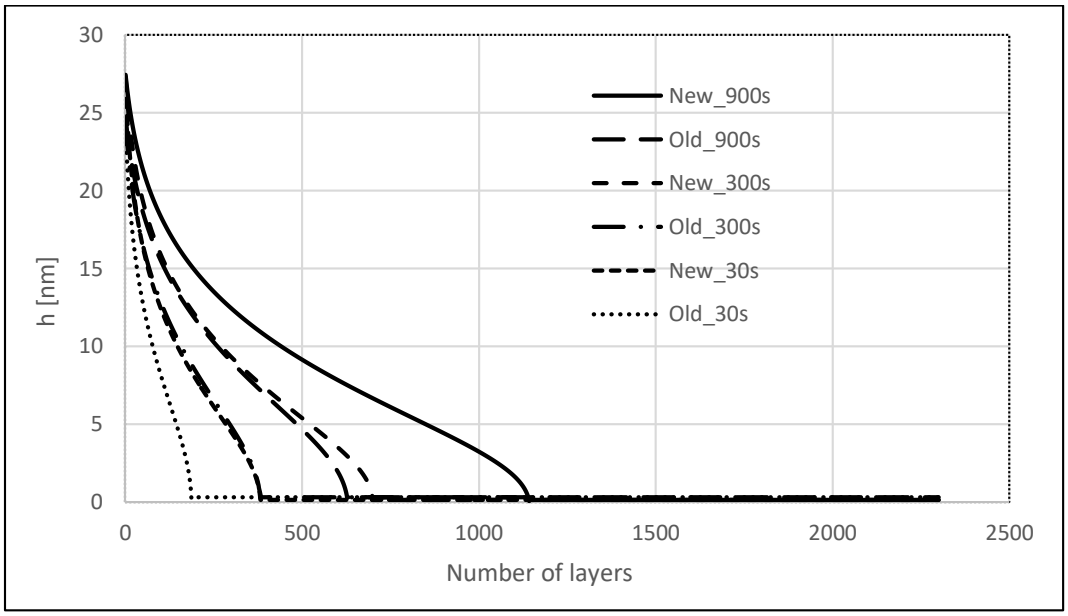

(c)

Figure 13 Protein-protein distance vs *number of layers a) for different transmembrane pressures,* Rej*=0.9875, t=15s; b) for different filtration times, Rej = 0.9875, TMP = 1.5 bar; c) for the old and new models at different filtration times, Rej = 0.9875, TMP = 2 bar, t = 30, 300, 900 s.*

In particular, for higher values of TMP the number of loose layers was markedly reduced with respect to the number of loose layers calculated at lower TMP (Fig.13a). In addition, for higher filtration times the number of loose layers was markedly increasing with respect to the number of loose layers obtained at lower filtration times (Fig.13b). This result was physically consistent. The simulations reported in Fig.13a lasted 15s since at this time the equilibrium distance among the proteins in the inner part of the deposit, i.e. h_{min}, was reached. Fig.13c reported a comparison between the present and previous multiscale models, expressed as the protein–protein distance vs the number of layers, calculated at either short or long filtration times. The observed differences between the two approaches were to be ascribed to the subnanoscopic and nanoscopic scale calculations performed, in the present paper, and referred to BSA surface potential, as well as the equivalent protein diameter and the Molecular Mechanics calculations performed to properly take into account the interactions between the first layer of adsorbed BSA and the polymeric membrane.

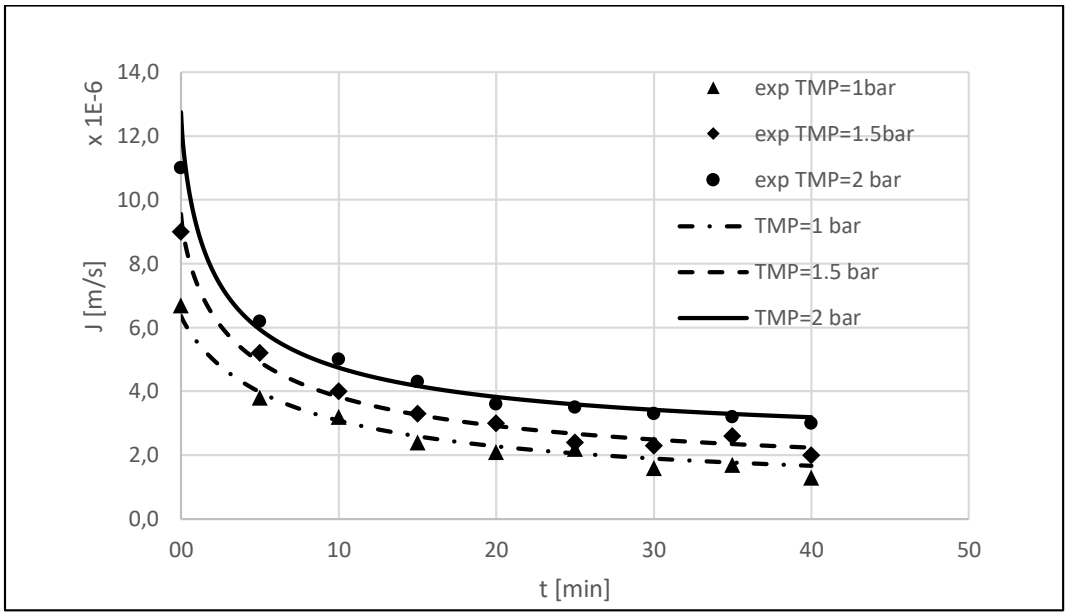

Figure 14 Comparison between simulated and experimental permeate flux decay using Rej *= 0.9875. Details of the measurements can be found in ref.*[12].

In Fig. 14, the simulated permeate fluxes, *J* (t), were compared with the experimental values obtained for three TMP and membrane rejection equal to 0.9875. The procedure, apparatus and experimental conditions are equal to those used in the previous work[12]. Fig. 14 showed a good agreement between the simulated flux decay performed by the present improved multiscale model and the experimental values. The permeate flux *J* (t) and the additional resistance R_{add} (t) were reported in both Fig. 15 and 16 for different *Rej* and TMP equal 1.5 bar. In appendix section, these macroscopic quantities were reported for the other transmembrane pressures. A membrane with large rejection restrained more proteins forming at the same time a larger number of layers on the membrane surface; hence, the flux decay was more pronounced, as shown in Fig. 15. Moreover, for lower values of membrane rejection to BSA (e.g., 0.9825), the ultrafiltration process reached a steady state more quickly as compared to higher values of rejection (0.99) for which the steady state was reached later.

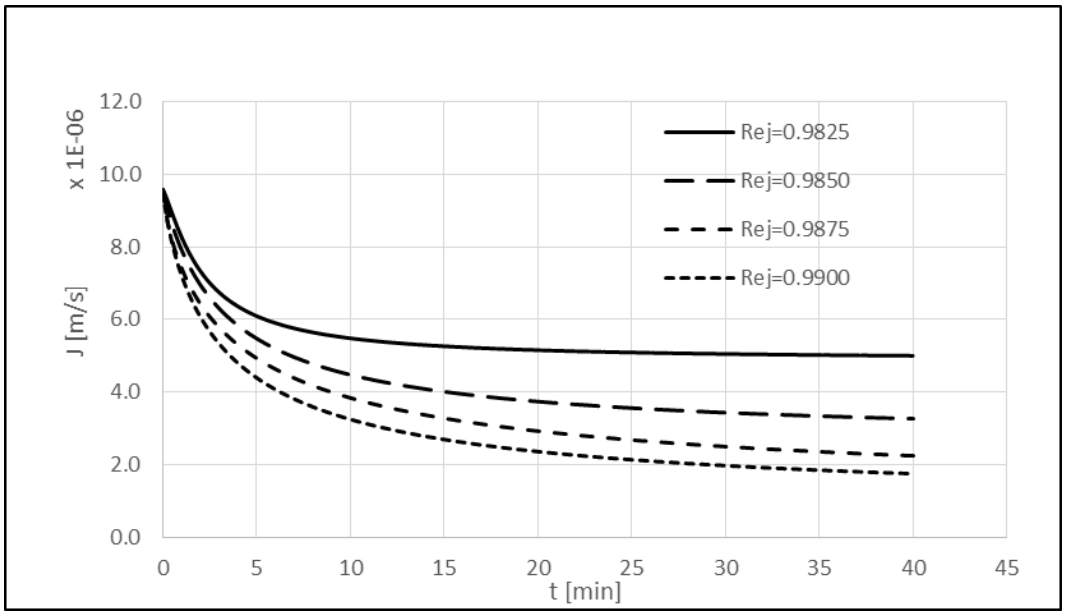

Figure 15 Permeate flux vs *simulation time at = 1.5 bar for different membrane rejections.*

In fact, as soon as the steady state was reached, the molar flux of the BSA through the membrane, as described by the macroscopic model[12], balances the deposit growth.

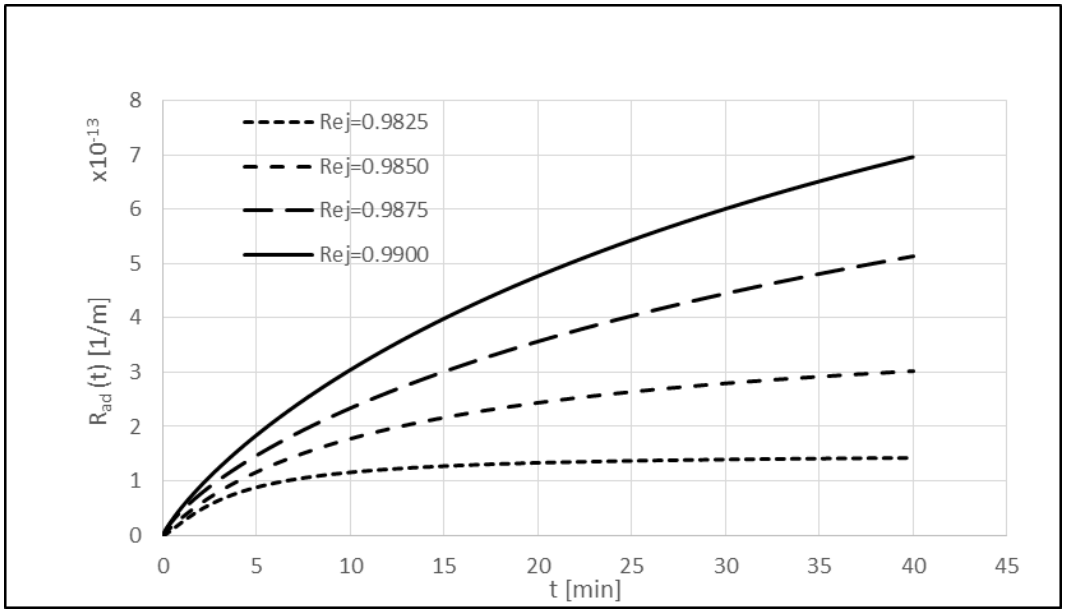

Figure 16 Additional resistance vs *simulation time at TMP = 1.5 bar for different membrane rejections.*

The trends of permeate flux vs time, *J* (t), were reported in Fig.17 for different transmembrane pressures. The permeate fluxes obtained with different values of membrane rejection were reported in the Appendix section, where it was possible to observe that with the decrease in membrane rejection, an effective steady state was achieved for all the considered values of TMP. Thus, the present improved multiscale approach, which did not use an arbitrary upper limit for the calculation of the additional resistance as due to compact deposit, was in a remarkable agreement with the experimental results.

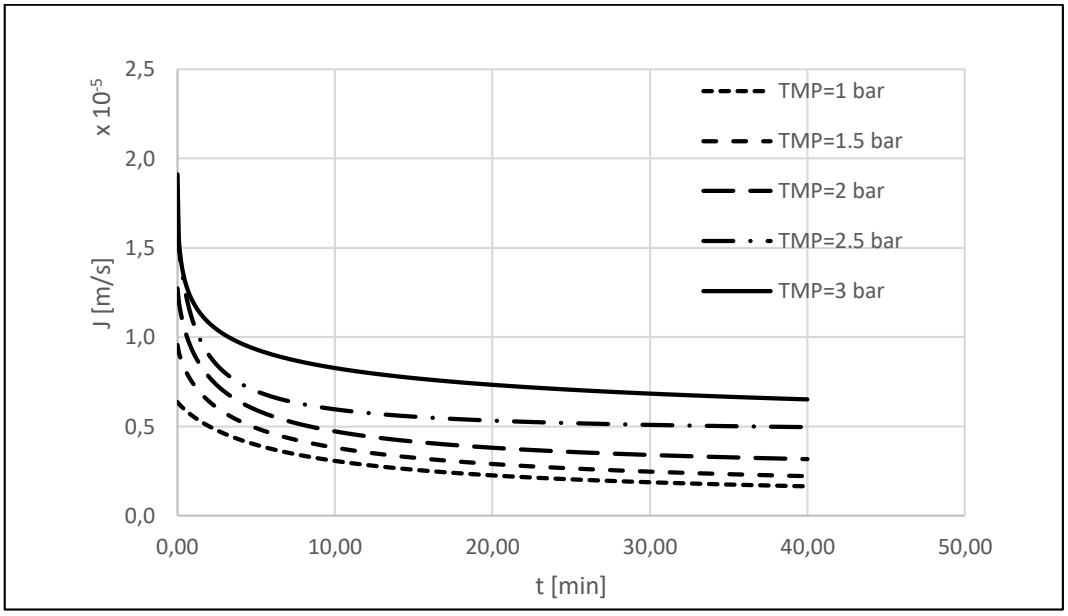

Figure 17 Permeate flux vs simulation time using Rej=0.9875 and the considered TMP.

Some of the simulations carried out in the previous work[12] were compared with those ones performed herein and were shown in Figs 18a and b. A lower permeate flux decay was achieved simulating the dead-end UF process by the present model in two typical conditions.

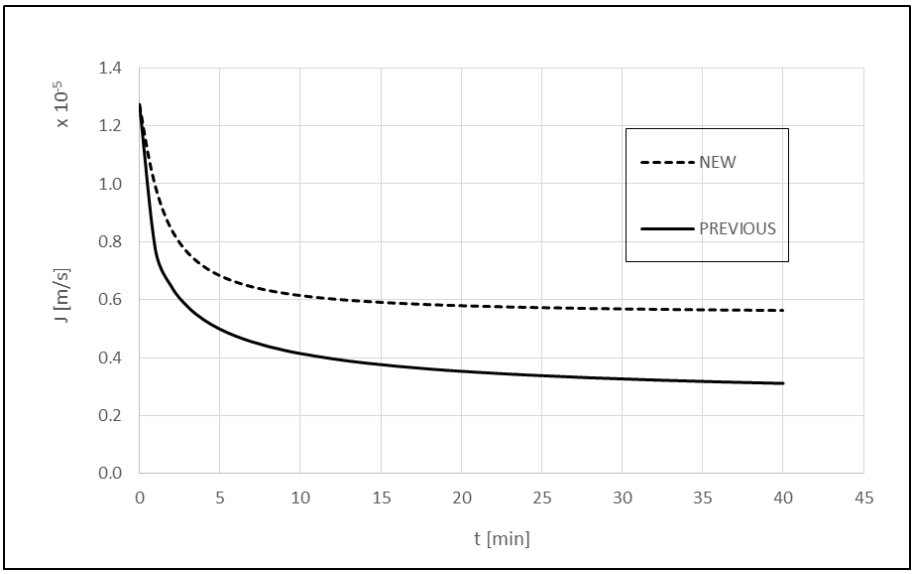

(a)

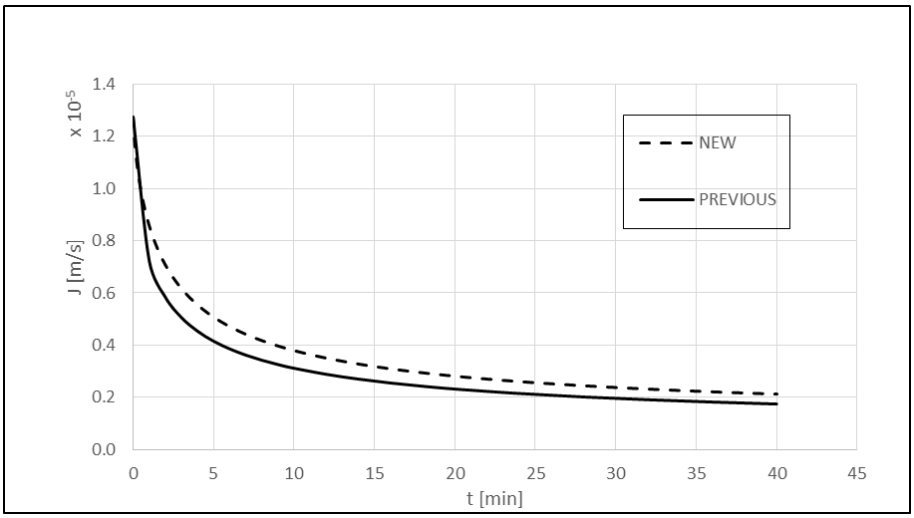

(b)

Figure 18 Decays of the permeate fluxes as obtained by the new and previous work: a) Rej= 0.985 and TMP= 2 bar; b) Rej 0.99, TMP =1.5 bar.

For low *Rej*=0.985, the modified multiscale approach yielded a steady state permeate flux, whereas the permeate flux modeled by the previous approach did not allow for reaching an actual steady state. The void fraction of the compact cake calculated by the previous model was equal to 0.37, whereas it was equal to 0.35 in the present case; such a difference in void fraction was not so big to justify the

different behavior observed in terms of permeate flux. The different trend could be traced comparing some of the basic parameters calculated at both subnanoscopic and nanoscopic scales. Using the protein surface charges evaluated (previous work) by the Löwdin approach, the value of q'' was -0.012 C/m^2 and the surface potential -4.9 mV, whereas using the ESP charges, the surface charge density and potential were equal to -0.021 (C/m^2) and to -75mV, respectively. The higher density of surface charges and potentials caused a higher proteins repulsion and consequently a different structure of the whole deposit on the membrane surface. Although, under the same operating conditions, the thickness of the protein deposit was the same, the thickness of loose layers was greater in the present simulations with respect to the previous ones, thus a smoother flux decay had to be expected.

3.4 Conclusions

Some of the authors of this paper previously proposed a multiscale approach for modeling membrane fouling in the ultrafiltration process where interactions between proteins and the membrane surface were not taken into account. In this paper, the missing membrane-protein interactions were evaluated via a first-principle based approach. The noncovalent interactions were accurately evaluated by quantum and molecular mechanics simulations and incorporated in the previously formulated multiscale model. A final (lower limit) void fraction and additional resistance, caused by the first layer of the adsorbed proteins and required in the microscopic forces balance, were evaluated by the optimizations of progressively increasing nanostructures describing the membrane surface and the adsorbed first layer of proteins, thus making the present multiscale model more physically consistent. The surface charges of both BSA and polysulfone surface were evaluated at the quantum level considering the solution pH; they were used to get some fundamental parameters,

such as the protein surface potential and the charges density. Validation of these quantities was carried out by measurements of BSA Z-potential, and the agreement with the experimental value was remarkable. Moreover, a good agreement between the simulated flux decay and the corresponding experimental values was observed. The permeate flux decay and the additional resistance, R_{ad} (t), at different *Rej* and transmembrane pressures, were simulated together with the structure of the BSA deposit.

The formulated multiscale framework is now ready to attain another step forward since it has been already planned to achieve a more accurate *ab-initio* description of proteins ultrafiltration process taking into account other fouling effects, such as the steric and electrostatic exclusion as well as the pore blocking.

References

(1) Fermeglia, M.; Pricl, S. Multiscale Modeling for Polymer Systems of Industrial Interest. *Prog. Org. Coatings* **2007**, *58* (2–3), 187–199.

(2) Chen, L.; Feng, Y.-L.; Song, C.-X.; Chen, L.; He, Y.-L.; Tao, W.-Q. Multi-Scale Modeling of Proton Exchange Membrane Fuel Cell by Coupling Finite Volume Method and Lattice Boltzmann Method. *Int. J. Heat Mass Transf.* **2013**, *63*, 268–283.

(3) Shi, M.; Printsypar, G.; Duong, P. H. H.; Calo, V. M.; Iliev, O.; Nunes, S. P. 3D Morphology Design for Forward Osmosis. *J. Memb. Sci.* **2016**, *516*, 172–184.

(4) Oliveira, L. F. L.; Jallut, C.; Franco, A. A. A Multiscale Physical Model of a Polymer Electrolyte Membrane Water Electrolyzer. *Electrochim. Acta* **2013**, *110*, 363–374.

(5) Oliveira, L. F. L.; Laref, S.; Mayousse, E.; Jallut, C.; Franco, A. A. A Multiscale Physical Model for the Transient Analysis of PEM Water Electrolyzer Anodes. *Phys. Chem. Chem. Phys.* **2012**, *14* (29), 10215–10224.

(6) de Morais, R. F.; Sautet, P.; Loffreda, D.; Franco, A. A. A Multiscale Theoretical Methodology for the Calculation of Electrochemical Observables from Ab Initio Data: Application to the Oxygen Reduction Reaction in a Pt(111)-Based Polymer Electrolyte Membrane Fuel Cell. *Electrochim. Acta* **2011**, *56* (28), 10842–10856.

(7) Tang, Y.-H.; Lin, H.-H.; Liu, T.-Y.; Matsuyama, H.; Wang, X.-L. Multiscale Simulation on the Membrane Formation Process via Thermally Induced Phase Separation Accompanied with Heat Transfer. *J. Memb. Sci.* **2016**, *515*, 258–267.

(8) Kostoglou, M.; Karabelas, A. J. On Modeling Incipient Crystallization of Sparingly Soluble Salts in Frontal Membrane Filtration. *J. Colloid Interface Sci.* **2011**, *362* (1), 202–214.

(9) P. Sullivan, N.; E. Wentz, J.; Abraham, J. *Multi-Scale Modeling of Tubular Cross-Flow*

Microfiltration of Metalworking Fluids; 2012; Vol. 7.

(10) Guillen, G.; Hoek, E. M. V. Modeling the Impacts of Feed Spacer Geometry on Reverse Osmosis and Nanofiltration Processes. *Chem. Eng. J.* **2009**, *149* (1–3), 221–231.

(11) Tedesco, M.; Cipollina, A.; Tamburini, A.; Bogle, I. D. L.; Micale, G. A Simulation Tool for Analysis and Design of Reverse Electrodialysis Using Concentrated Brines. *Chem. Eng. Res. Des.* **2015**, *93*, 441–456.

(12) De Luca, G.; Bisignano, F.; Paone, F.; Curcio, S. Multi-Scale Modeling of Protein Fouling in Ultrafiltration Process. *J. Memb. Sci.* **2014**, *452*, 400–414.

(13) Szymczyk, A.; Fievet, P. Investigating Transport Properties of Nanofiltration Membranes by Means of a Steric, Electric and Dielectric Exclusion Model. *J. Memb. Sci.* **2005**, *252* (1–2), 77–88.

(14) Molek, J.; Ruanjaikaen, K.; Zydney, A. L. Effect of Electrostatic Interactions on Transmission of PEGylated Proteins through Charged Ultrafiltration Membranes. *J. Memb. Sci.* **2010**, *353* (1–2), 60–69.

(15) Polyakov, Y. S.; Zydney, A. L. Ultrafiltration Membrane Performance: Effects of Pore Blockage/Constriction. *J. Memb. Sci.* **2013**, *434*, 106–120.

(16) Mehta, A.; Zydney, A. L. Effect of Membrane Charge on Flow and Protein Transport during Ultrafiltration. *Biotechnol. Prog.* **2006**, *22* (2), 484–492.

(17) Burns, D. B.; Zydney, A. L. Contributions to Electrostatic Interactions on Protein Transport in Membrane Systems. *AIChE J.* **2001**, *47* (5), 1101–1114.

(18) Connolly, M. L. Analytical Molecular Surface Calculation. *J. Appl. Crystallogr.* **1983**, *16* (5), 548–558.

(19) Connolly, M. L. The Molecular Surface Package. *J. Mol. Graph.* **1993**, *11* (2), 139–141.

(20) Petitjean, M. On the Analytical Calculation of van Der Waals Surfaces and Volumes: Some Numerical Aspects. *J. Comput. Chem.* **1994**, *15* (5), 507–523.

(21) Valiev, M.; Bylaska, E. J.; Govind, N.; Kowalski, K.; Straatsma, T. P.; Van Dam, H. J. J.; Wang, D.; Nieplocha, J.; Apra, E.; Windus, T. L.; et al. NWChem: A Comprehensive and

Scalable Open-Source Solution for Large Scale Molecular Simulations. *Comput. Phys. Commun.* **2010**, *181* (9), 1477–1489.

(22) Becke, A. Density Functional Thermochemistry III The Role of Exact Exchange. *J. Chem. Phys.* **1993**, *98*, 5648–5652.

(23) Brunello, G.; Lee, S. G.; Jang, S. S.; Qi, Y. A Molecular Dynamics Simulation Study of Hydrated Sulfonated Poly(Ether Ether Ketone) for Application to Polymer Electrolyte Membrane Fuel Cells: Effect of Water Content. *J. Renew. Sustain. Energy* **2009**, *1* (3), 33101–33115.

(24) Heuchel, M.; Böhning, M.; Hölck, O.; Siegert, M. R.; Hofmann, D. Atomistic Packing Models for Experimentally Investigated Swelling States Induced by CO2in Glassy Polysulfone and Poly(Ether Sulfone). *J. Polym. Sci. Part B Polym. Phys.* **2006**, *44* (13), 1874–1897.

(25) Lins, R. D.; Vorpagel, E. R.; Guglielmi, M.; Straatsma, T. P. Computer Simulation of Uranyl Uptake by the Rough Lipopolysaccharide Membrane of Pseudomonas Aeruginosa. *Biomacromolecules* **2008**, *9* (1), 29–35.

(26) Hofmann, D.; Fritz, L.; Ulbrich, J.; Schepers, C.; Bhning, M. Detailed-Atomistic Molecular Modeling of Small Molecule Diffusion and Solution Processes in Polymeric Membrane Materials. *Macromol. Theory Simulations* **2000**, *9* (6), 293–327.

(27) Hanwell, M. D.; Curtis, D. E.; Lonie, D. C.; Vandermeerschd, T.; Zurek, E.; Hutchison, G. R. Avogadro: An Advanced Semantic Chemical Editor, Visualization, and Analysis Platform. *J. Cheminform.* **2012**, *4*, 1–17.

(28) Klamt, A.; Schüürmann, G. COSMO: A New Approach to Dielectric Screening in Solvents with Explicit Expressions for the Screening Energy and Its Gradient. *J. Chem. Soc., Perkin Trans. 2* **1993**, *2*, 799–805.

(29) Lund, M.; Jönsson, B. A Mesoscopic Model for Protein-Protein Interactions in Solution. *Biophys. J.* **2003**, *85* (5), 2940–2947.

(30) Zhou, A. Q.; O'Hern, C. S.; Regan, L. The Power of Hard-Sphere Models: Explaining Side-Chain Dihedral Angle Distributions of Thr and Val. *Biophys. J.* **2012**, *102* (10), 2345–2352.

(31) Morris, G. M.; Goodsell, D. S.; Huey, R.; Olson, A. J. Distributed Automated Docking of

Flexible Ligands to Proteins: Parallel Applications of AutoDock 2.4. *J. Comput. Aided. Mol. Des.* **1996**, *10* (4), 293–304.

(32) Weisstein, Eric, W. Levenberg-Marquardt Method. *http://mathworld.wolfram.com/Levenberg-MarquardtMethod.html* **2014**, 683.

(33) Press, W.; Teukolsky, S.; Vetterling, W.; Flannery, B. Downhill Simplex Method in Multidimensions. *Numer. recipes C art Sci. Comput.* **1992**, 408–412.

(34) Harmant, P.; Aimar, P. Coagulation of Colloids Retained by Porous Wall. *AIChE J.* **1996**, *42* (12), 3523–3532.

(35) Yu, Y.; Ma, L.; Xu, H.; Sun, X.; Zhang, Z.; Ye, G. DLVO Theoretical Analyses between Montmorillonite and Fine Coal under Different PH and Divalent Cations. *Powder Technol.* **2018**, *330*, 147–151.

(36) Karthik, V.; DasGupta, S.; De, S. Modeling and Simulation of Osmotic Pressure Controlled Electro-Ultrafiltration in a Cross-Flow System. *J. Memb. Sci.* **2002**, *199* (1), 29–40.

(37) Happel, J. Viscous Flow in Multiparticle Systems: Slow Motion of Fluids Relative to Beds of Spherical Particles. *AIChE J.* **1958**, *4* (2), 197–201.

(38) Dassios, G.; Vafeas, P. The 3D Happel Model for Complete Isotropic Stokes Flow. *Int. J. Math. Math. Sci.* **2004**, *46*, 2429–2441.

(39) de la Casa, E. J.; Guadix, A.; Ibáñez, R.; Camacho, F.; Guadix, E. M. A Combined Fouling Model to Describe the Influence of the Electrostatic Environment on the Cross-Flow Microfiltration of BSA. *J. Memb. Sci.* **2008**, *318* (1–2), 247–254.

(40) Fukuzaki, S.; Urano, H.; Nagata, K. Adsorption of Bovine Serum Albumin onto Metal Oxide Surfaces. *J. Ferment. Bioeng.* **1996**, *81* (2), 163–167.

(41) Ali, N.; Sofiah, H.; Asmadi, A.; Endut, A. Preparation and Characterization of a Polysulfone Ultrafiltration Membrane for Bovine Serum Albumin Separation: Effect of Polymer Concentration. *Desalin. WATER Treat.* **2011**, *32* (1–3), 248–255.

Chapter 4

Enzyme Immobilization on Polymer Membranes: A Quantum and Molecular Mechanics Study

Petrosino, F.; Curcio, S.; Chakraborty, S.; De Luca, G. Enzyme Immobilization on Polymer Membranes: A Quantum and Molecular Mechanics Study. Computation 2019, 7, 56. https://www.mdpi.com/2079-3197/7/4/56

Enzyme Immobilization on Polymer Membranes: A Quantum and Molecular Mechanics Study

Francesco Petrosino[a], Stefano Curcio[a], Sudip Chakraborty[a] and Giorgio De Luca[b]

[a]*Department of Computer Engineering, Modeling, Electronics and Systems (D.I.M.E.S.), Laboratory of Transport Phenomena and Biotechnology, University of Calabria, Ponte P. Bucci, cubo 39/c, 87036 Rende (CS), Italy;*

[b] *Institute on Membrane Technology, ITM-CNR, Ponte P. Bucci, cubo 17/c, 87036 Rende (CS), Italy*

Abstract

Adsorption of the phosphotriesterase on polysulfone membrane surface was investigated in this paper through a double-scale computational approach. Surface charges of enzyme as well as membrane were calculated at sub and nanoscale whist protein adsorption was simulated at bigger scale. Adsorption energies were calculated as a function of the enzyme-surface distance and for each distance several protein rotations were tested in order to found the most stable orientations of the macromolecule. The results of this model were useful to obtain information about adhesion of the enzyme and to give indications on the orientations of its binding site. Adsorption energies agreed with the literature data, furthermore the binding site of the immobilized phosphotriesterase was less accessible with respect to native enzyme due to the steric hindrance of the polymer surface; thus, a reduction of its efficiency is expected. The proposed methodology made use of fundamental quantities, calculated without resorting to adjustable or empirical parameters, providing basic outputs useful for ascertaining enzymatic catalysis rate.

Keywords: Enzyme adsorption and orientation, polysulfone membrane, Density Functional Theory, double-scale computational modeling.

4.1 Introduction

Nowadays a significant growth of research activities in multiscale modeling is observed, with applications in many areas including material sciences, fluid mechanics, chemistry, and biology. It is widely recognized that multiscale techniques will become an essential part of computational science and engineering. In this frame, however, the crucial point is represented by the reliable calculation of some key parameters that are associated to smaller scales[1,2].

In recent years, enzymatic productivity has been rapidly increasing through the improvement of genetic engineering, microbial cultivation technologies and wild type strain screening technology, together with the understanding of enzymatic biosynthesis mechanisms [3]. This advance is providing different kinds of enzymes exhibiting improved activities, which is leading to a massive. use of enzymes in industrial processes. Enzymes play key roles in numerous biotechnology products and processes that are commonly encountered in the production of food and beverages, cleaning supplies, clothing, paper products, pharmaceuticals, and monitoring devices [4]. At present, the most frequently enzymes used in biotechnology are hydrolases, which catalyze molecular breakdown. Enzymatic chiral selectivity has been exploited to prepare enantiomerically pure pharmaceuticals, agro-chemicals, chemical feedstocks, and food additives [5]. Most of currently used industrial enzymes are hydrophilic, being used for the degradation of various natural substances. Proteases remain the dominant enzyme type for their extensive use in the detergent and in the dairy industries. In this frame, Phosphotriesterase (PTE) has been also used for the hydrolysis of common pesticides such as glyphosate, due to the high efficiency of glyphosate abatement exhibited by this enzyme [6].

Immobilization of enzymes on the external or internal (pore) membrane surfaces is widely used in biotechnology industries [7 8], where immobilization is generally achieved by establishing non-covalent interactions between protein and polymeric surface without chemical modifications of membranes and enzymes [9]. As a result, non-covalent adsorption is an interesting research topic and computational

methodologies able to optimize and control this process in a larger scale [10,11] are highly desirable. However, due to some process limitations, several aspects need to be improved in order to increase the immobilized enzyme activity and re-usability. In this framework, it is essential to formulate advanced and reliable computational methodologies to optimize the enzyme immobilization without resorting adjustable or empirical parameters.

An advanced modeling aimed to describe the enzyme adsorption on polymeric membranes surface was developed in this work. In particular, the immobilization of phosphotriesterase (PTE) on polysulfone (PSU) surface was studied at a fixed pH *via* a quantum and molecular mechanics approach (QM/MM) without resorting adjustable parameters. This approach achieved fundamental results, like adsorption energies and enzyme orientation on the polymer surface. The absorption energy is an important property to predict the enzyme adhesion on the membrane surface hence to predict possible releases of the macromolecule in solution. Moreover, the geometries of the immobilized protein, i.e. its orientations, can be used in a meso-scale modeling to describe the diffusion of the substrate towards the catalytic site in order to check possible steric hindrance of the surface.

The proposed methodology was implemented to provide an innovative tool that starting from the calculation of sub-nano quantities can be used to develop advanced membrane bioreactors. In particular, this model was developed, in the frame of previous works [12,13], to provide basic outputs useful for ascertaining enzymatic catalysis rate for which both the molecular orientation and the adsorption energy are fundamental. In this way, a series of accurate simulations can be planned for achieving a true optimization of PTE immobilization before performing the experimental tests.

4.2 Computational approach

4.2.1 Quantum calculations

The adsorption of macromolecules on polymer surfaces is mainly controlled by electrostatic and hydrophobic interactions, as well as by hydrogen bond at very short distances; thus, the surface charges of interacting systems are necessary to accurately evaluate short- and long-range electrostatic contributions. Surface charges of proteins largely depends on the nature of the external amino acids and conditions, like pH, solvent and ionic strength. In general, *ab-initio* (quantum mechanics)-based methods are usually used for the calculation of partial charges considering the effect of specific conditions and avoiding the use of the classic Force Fields. However, the calculation of the partial charges via quantum approaches is time consuming, especially for proteins formed by thousands of atoms. For this reason, herein, a contact surface of the PTE was first determined through a home-made algorithm and using the crystallographic structure of the enzyme at pH=7 [14]. The electrostatic charges on large fragments of external amino acids were calculated in the frame of Density Functional Theory (DFT) using the Löwdin method as implemented in NWChem [15]. All quantum calculations were performed by using the B3LYP [16] hybrid functional and double-ζ basis set (6-31G*) for each atom of the enzyme and polysulfone surfaces. The thresholds for the energy convergence in the self-consistent field procedure and the root-mean-square of the electron density were set to 10^{-6} (au) and to 2×10^{-5} (au), respectively. The Löwdin method was chosen for its low dependence on the orbitals basis set and it was also used to calculate the distributions of charges on the PSU model surface. It is important to emphasize that once the Cartesian coordinates of the atoms on the enzyme surface were determined, these were grouped in large fragments containing more than 500 atoms; then DFT calculations of the point charges were performed using these fragments and not on the individual amino acids. In this way the protonated and deprotonated forms of the external amino acids can be

evaluated more accurately *via* an ab-initio approach. A dense polymeric surface was obtained through a Molecular Dynamics simulated annealing as described in detail in Ref.[12], hence the atomic coordinates of the equilibrated surface model were used for the calculation of the partial charges at quantum mechanics level through the same computational approach used for the enzyme charges calculation. Nevertheless, in case of the surface charges of the polymer, the Continuum Conductor-like Screening Model (COSMO) [17] was used with a relative dielectric constant equal to 4 in order to consider the molecules of water in close contact with the polymer surface, i.e. confined. The equilibrated PSU unit cell with L=7.2 nm, was translated in the X and Y directions obtaining 3 cells for each axis so that the QM/MM calculations did not suffer from the edges effect.

The pH was also considered in the calculations of PTE surface charges. Specifically, the protonated form of the external residues forming a fragment depends on the difference between pH and pK_r, with K_r equal to the equilibrium constant of the amino acid's functional group. For $pH > pK_r$ the deprotonated form is predominant, whereas protonated forms result the most abundant for $pH < pK_r$. However, for specific pH values, both forms had to be considered. Thus, the ratio between the deprotonated [D] and protonated [P] external amino acid was calculated at pH =7 using the following relationship:

$$\frac{[D]}{[P]} = 10^{(pH - pK_r)} \qquad (4.1)$$

The external residues of the PTE were then protonated or deprotonated according the ratios obtained from relationship (1). It is worth noting that the pH value is closely related to the structure of the enzyme used to carry out the DFT calculations; thus, simulations at different pH would require the crystallographic structure of the protein corresponding to that value.

4.2.2 Molecular mechanics optimizations

Following the approach used in the previous work and by Mikael Lund and Bo Jönsson [12,18], the potential energy, characterizing the interaction between proteins and polymer surface, can be divided into three different parts:

$$u_{tot}(r_{ij}) = u_{hs}(r_{ij}) + u_{el}(r_{ij}) + u_{vdW}(r_{ij}) \tag{4.2}$$

$$u_{hs} = \begin{cases} \infty & r_{ij} < \frac{\sigma_{ii}+\sigma_{jj}}{2} \\ 0 & r_{ij} > \frac{\sigma_{ii}+\sigma_{jj}}{2} \end{cases} \tag{4.3}$$

$$u_{el}(r_{ij}) = \sum_i \sum_j \frac{q_i q_j}{4\pi\epsilon_0 \epsilon_r r_{ij}} \tag{4.4}$$

$$u_{vdW}(r_{ij}) = 4\epsilon_{ij}\left[\left(\frac{\sigma_{ij}}{r_{ij}}\right)^{12} - \left(\frac{\sigma_{ij}}{r_{ij}}\right)^{6}\right] \tag{4.5}$$

The $u_{hs}(r_{ij})$ term takes into account the repulsion of electron clouds through hard-spheres [19]. The Coulomb interaction was considered in $u_{el}(r_{ij})$ defined by the atomic surface charges, q_i and q_j, of the protein and polymer surface, respectively, and evaluated through the DFT calculations. ϵ_r and ϵ_0 are the relative and *vacuum* dielectric permittivity; in agreement with the value used for the calculation of the partial charges on polysulfone $\epsilon_r = 4.0$ was used in relationship (4.4) for very close interacting systems and $\epsilon_r = 78.2$ for weakly interacting systems. Finally, to evaluate the hydrophobic (van der Waals) interaction, the Lennard-Jones 12-6 potential was used; ϵ_{ij} and σ_{ij} parameters were taken from ref. [20,21].

Bespoke Matlab [22] functions were implemented to calculate the total interaction energy according to the eqs.4.2-4.5 in which a 3D grid-type calculation was performed. The radial points refer to PTE-

PSU distance, d, along the Z axis perpendicular to the polymer surface, as shown in Fig.19, whilst the angular points are related to protein rotations with respect to Z and X (tetz, tetx) (Fig.19).

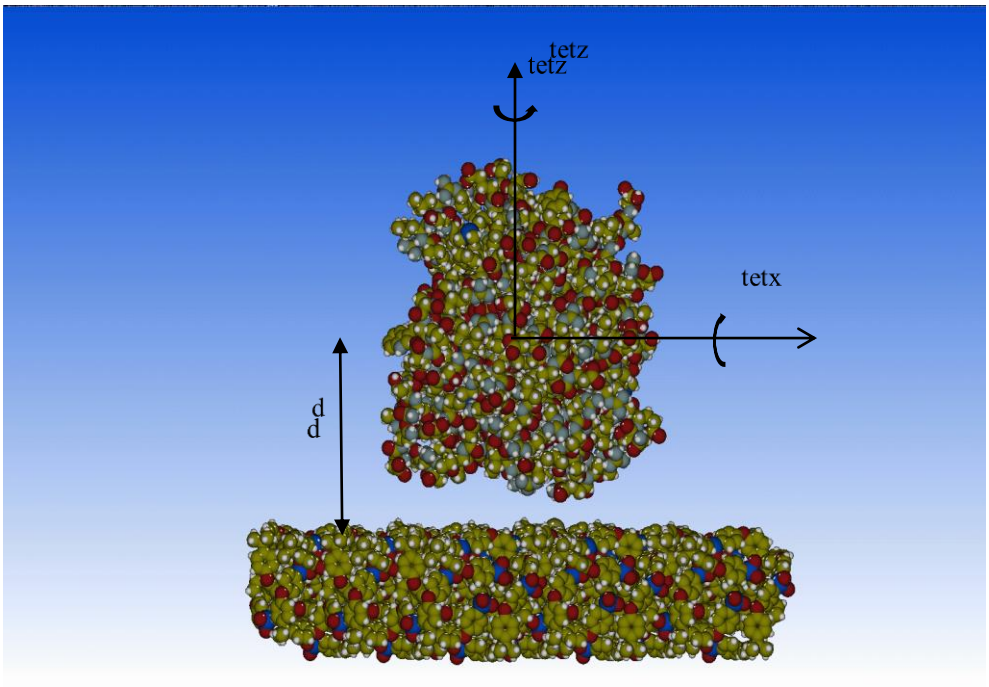

Figure 19 PTE on polysulfone surface, d= protein-surface distance, tetz and tetx protein rotations around Z and X axis, respectively, used for the calculation of the interaction energy.

Potential energy was obtained as a function of the protein-surface distance (d) and global and local minima were characterized. The d values ranged between 24 Å and 60 Å and a step of 1 Å was used, whilst, for each distance, 16 rotations of macromolecule were evaluated (Fig.19).

4.3 Results and Discussion

The interaction energy as a function of the enzyme-surface distance was shown in Fig.20, and as expected, various local minima and a global minimum were found. The potential energy profile showed a complete overview of the interaction energy from very close distances to weakly interacting systems or non-interacting systems, i.e. the enzyme in solution at 60 Å.

A global minimum was found at a distance of 30 Å from PSU surface with a total energy equal to -107.96 Kcal/mol. The nearest local minima were found at d= 27 Å and 35 Å with interactions energies of -97.57 and -82.44 Kcal/mol, respectively. Other local minima were found further from the surface with interaction energies considerably higher than -107.96 Kcal/mol, thus they were not considered in the analysis of the enzyme orientation since jumps for thermal vibrations in these minima are difficult, at room temperature. Instead, the energy differences between the global and the two nearest minima were 10 Kcal/mol and 25 Kcal/mol. Hence, considering a distribution of the macromolecules among these minima, an adsorption energy ranging betwen -82.44 Kcal/mol and -107.96 Kcal/mol is expected. Experimental values around -30 kcal/mol are reported in ref while values around -70 kcal/mol can be found in ref.18, then an average value of -50 kcal /mol can be assumed. The theoretical adsorption energies are in good agreement with the above experimental values[18-20] since the latter are obtained with respect to a reference system in standard condition, thus a scaling of the theoretical values should be considered. Nevertheless, reproducing the order of magnitude of the adsorption energy, through an *ab-initio* quantum method without using adjustable parameters, is a satisfactory result; finally the proposed QM/MM modeling can be used in comparative studies.

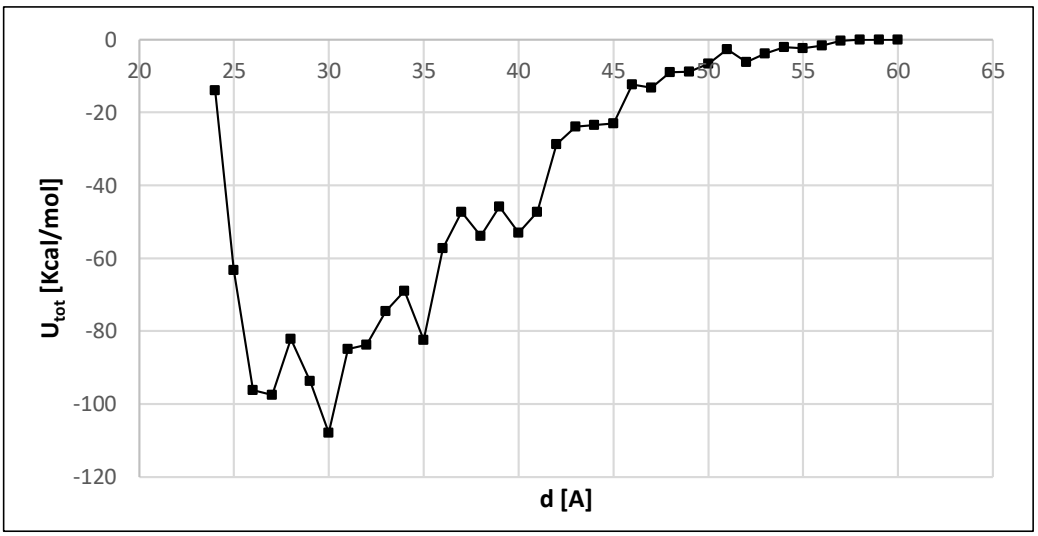

Figure 20 Enzyme-PSU interaction energy, U_{tot}, versus *enzyme-surface distance obtained by QM/MM calculations*

The orientation of the PTE on the PSU surface, corresponding to the global minimum, was showed in Fig.21. In particular, the orientation of the contact surface, used in the QM/MM calculations, was shown in Fig.21a and b, whilst the complete structure of the enzyme in the same orientation was reconstructed in Fig.21c. and d. One of the goals of this work was to elucidate the stable orientations of the enzyme on the PSU membrane surfaces then to provide supramolecular structures (enzyme-surface) for modeling the substrate diffusion at higher scale. Nevertheless, the supramolecular structures can be used to investigate the steric hindrance of the catalytic site due to the polymeric surface. This can be achieved by analyzing the position of the two zinc atoms present in the catalytic site of the PTE and responsible for the glyphosate hydrolysis. Also, the binding site, close to the enzyme surface and responsible for the selective adsorption of the substrate can be monitored. Hence, analyzing the position of these atoms with respect to the membrane surface the steric hindrance can be predicted.

Comparing Fig.21a (side view) and 20b (top view), it is clear that the two zinc atoms are difficult to reach from the bulk (solution) side, on the contrary, these atoms were visible from the side of the supramolecular structure that means that the substrate must arrive from this direction to reach the binding site. This result is clearer when the complete structure of the enzyme was shown in the same orientation, as in Fig.21c and d. In particular, the zinc atoms are still visible from side view, Fig.21c, but when the supramolecular structure is rotate in order to show the top view (bulk side) these atoms are no longer visible (Fig.21d). In solution, the substrate molecules can easily reach the binding site without barriers because the enzyme is free, instead for adsorbed enzymes the steric hindrance of the surface makes this difficult.

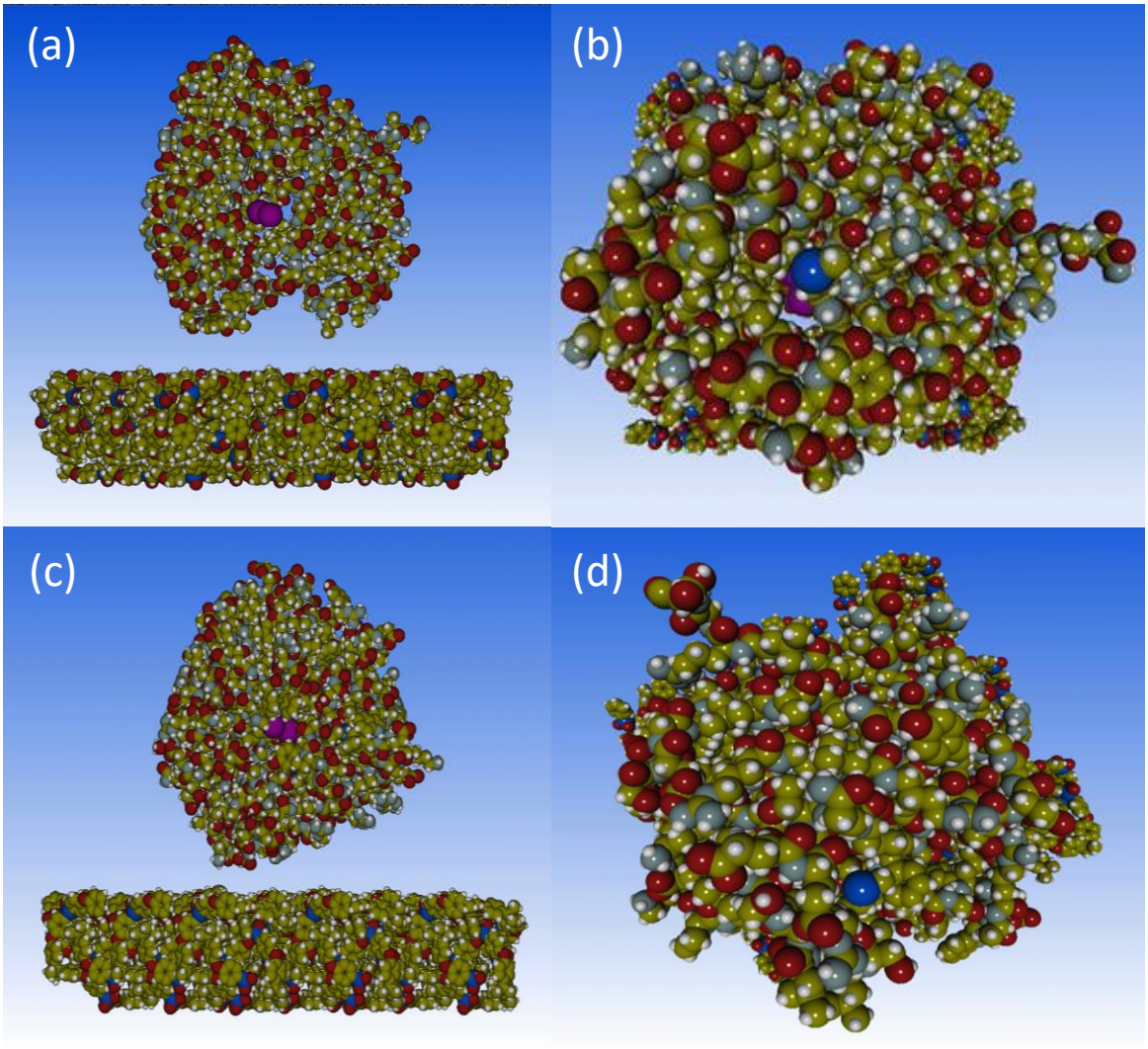

Figure 21 Adsorbed PTE on the PSU model surface in the global minimum (-107.96 Kcal/mol at 30 Å). (a) and (b) side and top view of the contact surface, respectively; (c) and (d) side and top view of full enzyme in the same orientation, respectively. Zinc atoms were shown in fuchsia.

Starting from the position corresponding to the global minimum, the enzyme was rotated by 90 degrees around the X axis (tetx = 90°, Fig.19) to make the zinc atoms more accessible from the bulk side as shown in Fig.22a. This Fig. showed that the two atoms of zinc were more visible with respect to Fig.21b which refers to the enzyme at the same distance but not rotated. Unfortunately, the energy cost for this rotation is 83.09 Kcal/mol. This energy gap is too high to allow this spin at room temperature; thus, the enzyme fails to rotate and direct the binding site toward the bulk. As shown in Fig.22b (side view of the rotated enzyme), a rotation of the protein around the X axis greater than 90

degrees (tex > 90) would make the metal atoms more accessible for the substrate from the solution. However, in this case, the protruding amino acid residue would touch the surface of the polysulfone.

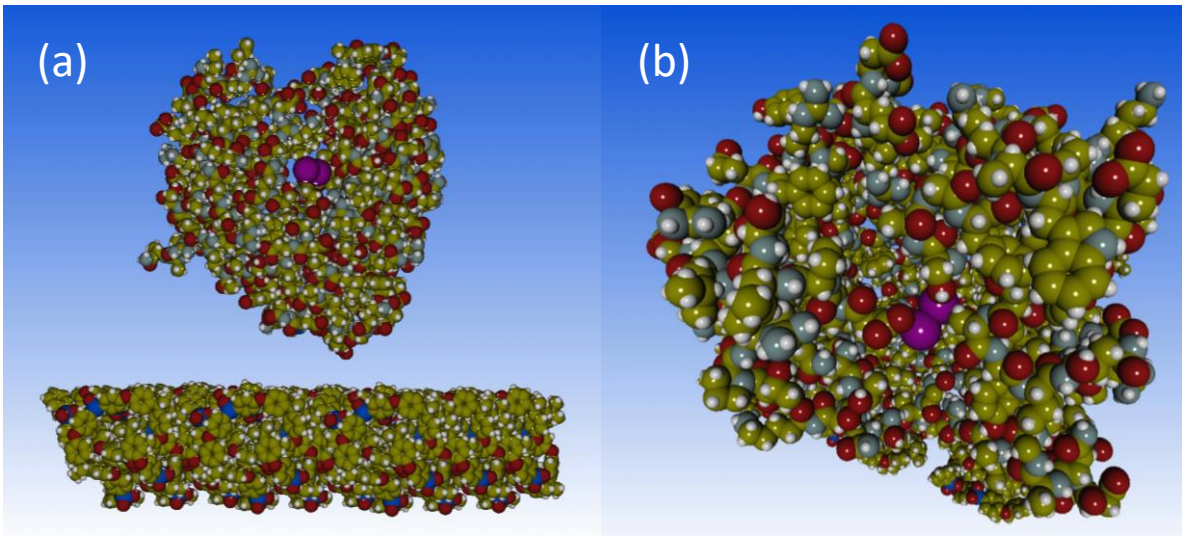

Figure 22 Adsorbed PTE on the PSU surface at d=30 Å but rotated by 90 degrees around the X axis. (a) and (b) top and side view of the contact surface. Zinc atoms were shown in fuchsia.

As regard the orientations of the PTE associated to the local minima, the same conclusion can be drawn as shown in Fig.23. For both minima, the two atoms of zinc are clearly visible from the side of the supramolecular structure whereas they were difficult to reach for the substrate from the bulk side. Moreover, concerning the rotations of the enzyme around the X axis to make metal atoms more accessible, i.e tex=90 or tex> 90, results similar to those found for the PTE rotations, adsorbed in the global minimum, were obtained.

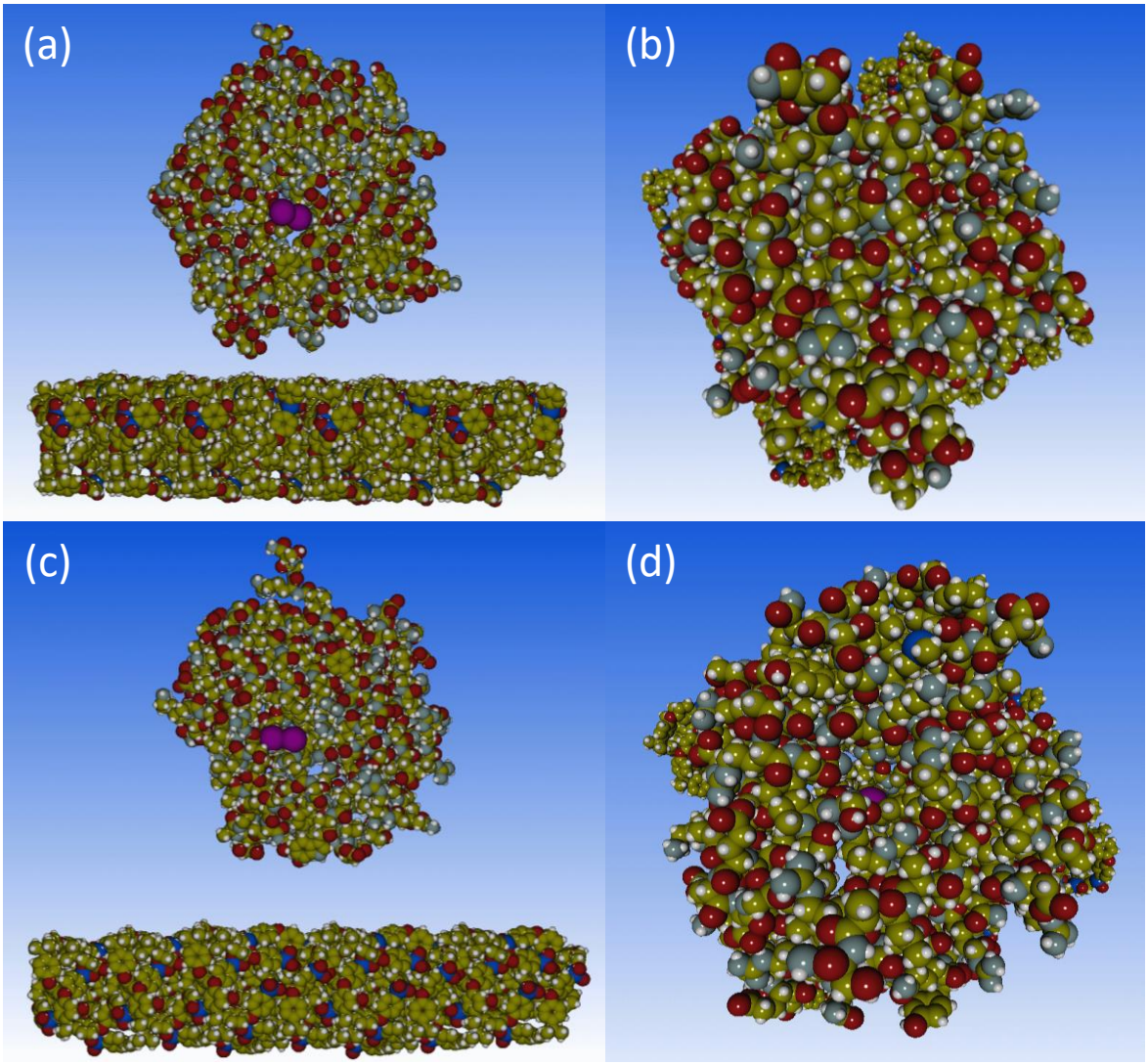

Figure 23 Adsorbed PTE on the PSU model in the local minima. (a) and (b) side and top view of the PTE-PSU structure corresponding to minimum with interaction energies of -97.57 Kcal/mol at 27 Å., respectively; (c) and (d) side and top view of the PTE-PSU structure corresponding to minimum with interaction energies of -82.44 Kcal/mol at 35 Å, respectively. Zinc atoms were shown in fuchsia.

In summary, this modeling showed that the binding site of the adsorbed PTE is less accessible with respect to the native enzyme due to the steric hindrance of the polymer surface. As a result, the adsorbed enzyme should reduce its activity; i.e. a reduction of the enzyme efficiency is expected since the substrate can reach the binding site laterally and nearby adsorbed enzyme could hinder its access. This depends on the enzyme-enzyme equilibrium distance and protein concentration; the analysis of these aspects will be the subject of a subsequent work.

4.4 Conclusions

A model based on quantum and molecular mechanics calculations was proposed in this work to simulate the enzyme adsorption on polysulfone membrane surface. The modeling aims to achieve the following objectives: the calculation of the enzyme-surface interaction energies and the orientation of the absorbed enzymes on the membrane surface in order to predict possible steric hindrance for the substrate. The surface charges of the PTE were calculated by an accurate quantum mechanics approach at pH =7, whilst a PSU surface model was defined by a molecular dynamics simulated annealing. Electrostatic charges of the polymer surface were calculated using the same quantum approach without resorting adjustable or empirical parameters. The interaction energy between enzyme and membrane surface was evaluated as a function of protein-surface distance considering several rotations of the PTE for each distance. The final result was the calculation of potential energy profile as well as macromolecular structures that can be used as inputs in large scale model development. The computed interaction energies are in good agreement with adsorption free energies reported in literature; this means that the considered enzyme can be effectively adsorbed on PSU. However, an accurate analysis of the protein orientations suggested that the binding site of the immobilized enzyme is less accessible with respect to the pristine PTE due to the steric hindrance of the polymer surface; thus, a reduction of the enzyme efficiency is expected. The proposed methodology made use of fundamental quantities and it was designed to provide basic outputs useful for ascertaining enzymatic catalysis rate, i.e. kinetic proprieties from immobilization features, important for designing of enzymatic bioreactors.

Acknowledgments:

The authors are grateful to CINECA for the use of High-Performance Computers.

References

(1) Weinan, E.; Li, X.; Vanden-Eijnden, E. Some Recent Progress in Multiscale Modeling; 2004. https://doi.org/10.1007/978-3-642-18756-8_1.

(2) Horstemeyer, M. Multiscale Modeling: A Review. In *Practical Aspects of Computational Chemistry*; 2009; pp 87–135. https://doi.org/10.1007/978-90-481-2687-3_4.

(3) Parekh, S.; Vinci, V. A.; Strobel, R. J. Improvement of Microbial Strains and Fermentation Processes. *Applied Microbiology and Biotechnology*. 2000, pp 54(3) 287-301. https://doi.org/10.1007/s002530000403.

(4) Gurung, N.; Ray, S.; Bose, S.; Rai, V. A Broader View: Microbial Enzymes and Their Relevance in Industries, Medicine, and Beyond. *BioMed Research International*. 2013. https://doi.org/10.1155/2013/329121.

(5) Underkofler, L. A.; Barton, R. R.; Rennert, S. S. Production of Microbial Enzymes and Their Applications. *Applied Microbiology* **1958**, *6* (3), 212–221.

(6) Raushel, F. M.; Holden, H. M. Phosphotriesterase: An Enzyme in Search of Its Natural Substrate. *Adv. Enzymol. Relat. Areas Mol. Biol.* **2000**, *74*, 51–93.

(7) Nguyen, H.; Kim, M. An Overview of Techniques in Enzyme Immobilization. *Appl. Sci. Converg. Technol.* **2017**, *26* (6), 157–163. https://doi.org/10.5757/ASCT.2017.26.6.157.

(8) DiCosimo, R.; McAuliffe, J.; Poulose, A. J.; Bohlmann, G. Industrial Use of Immobilized Enzymes. *Chem Soc Rev* **2013**, *42* (15), 6437–6474. https://doi.org/10.1039/c3cs35506c.

(9) Datta, S.; Christena, L. R.; Rajaram, Y. R. S. Enzyme Immobilization: An Overview on Techniques and Support Materials. *3 Biotech* **2013**, *3* (1), 1–9. https://doi.org/10.1007/s13205-012-0071-7.

(10) Kazemi, P.; Renka, R. J. A Levenberg–Marquardt Method Based on Sobolev Gradients. *Nonlinear Analysis* **2012**, *16* (75), 6170–6179. https://doi.org/10.1016/j.na.2012.06.022.

(11) Han, L.; Neumann, M. Effect of Dimensionality on the Nelder–Mead Simplex Method. *Optimization Methods & Software - OPTIM METHOD SOFTW* **2006**, *21*, 1–16. https://doi.org/10.1080/10556780512331318290.

(12) Curcio, S.; Petrosino, F.; Morrone, M.; De Luca, G. Interactions between Proteins and the Membrane Surface in Multiscale Modeling of Organic Fouling. *Journal of Chemical Information and Modeling* **2018**, *58* (9), 1815–1827. https://doi.org/10.1021/acs.jcim.8b00298.

(13) De Luca, G.; Bisignano, F.; Paone, F.; Curcio, S. Multi-Scale Modeling of Protein Fouling in Ultrafiltration Process. *Journal of Membrane Science* **2014**, *452*, 400–414. https://doi.org/10.1016/j.memsci.2013.09.061.

(14) Zhang, L.; Wang, H.; Liu, X.; Zhou, W.; Rao, Z. The Crystal Structure of the Phosphotriesterase from M. Tuberculosis, Another Member of Phosphotriesterase-like Lactonase Family. *Biochem. Biophys. Res. Commun.* **2019**, *510* (2), 224–229. https://doi.org/10.1016/j.bbrc.2019.01.069.

(15) Valiev, M.; Bylaska, E. J.; Govind, N.; Kowalski, K.; Straatsma, T. P.; Van Dam, H. J. J.; Wang, D.; Nieplocha, J.; Apra, E.; Windus, T. L.; et al. NWChem: A Comprehensive and Scalable Open-Source Solution for Large Scale Molecular Simulations. *Computer Physics Communications* **2010**, *181* (9), 1477–1489. https://doi.org/10.1016/j.cpc.2010.04.018.

(16) Malki, Z. E.; Bouzzine, S. M.; Bejjit, L.; Haddad, M.; Hamidi, M.; Bouachrine, M. Density Functional Theory [B3LYP/6-311G(d,p)] Study of a New Copolymer Based on Carbazole and (3,4-Ethylenedioxythiophene) in Their Aromatic and Polaronic States. *Journal of Applied Polymer Science* **2011**, *122* (5), 3351–3360. https://doi.org/10.1002/app.34395.

(17) Klamt, A.; Schüürmann, G. COSMO: A New Approach to Dielectric Screening in Solvents with Explicit Expressions for the Screening Energy and Its Gradient. *J. Chem. Soc., Perkin Trans. 2* **1993**, *2*, 799–805. https://doi.org/10.1039/P29930000799.

(18) Lund, M.; Jönsson, B. A Mesoscopic Model for Protein-Protein Interactions in Solution. *Biophysical Journal* **2003**, *85* (5), 2940–2947. https://doi.org/10.1016/S0006-3495(03)74714-6.

(19) Zhou, A. Q.; O'Hern, C. S.; Regan, L. The Power of Hard-Sphere Models: Explaining Side-Chain Dihedral Angle Distributions of Thr and Val. *Biophysical Journal* **2012**, *102* (10), 2345–2352. https://doi.org/10.1016/j.bpj.2012.01.061.

(20) Morris, G. M.; Goodsell, D. S.; Huey, R.; Olson, A. J. Distributed Automated Docking of Flexible Ligands to Proteins: Parallel Applications of AutoDock 2.4. *J Computer-Aided Mol Des* **1996**, *10* (4), 293–304. https://doi.org/10.1007/BF00124499.

(21) 7. Van der Waals Potential Energy http://www.csb.yale.edu/userguides/datamanip/autodock/html/Using_AutoDock_305.a.html (accessed Jul 17, 2019).

(22) Attaway, S. *Matlab: A Practical Introduction to Programming and Problem Solving*; Butterworth-Heinemann, 2009.

Chapter 5

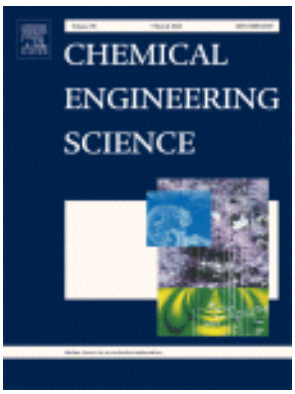

Osmotic pressure and transport coefficient in ultrafiltration: a Monte Carlo study using quantum surface charges

Submitted for publication CES-D-19-02719

Osmotic pressure and transport coefficient in ultrafiltration: a Monte Carlo study using quantum surface charges

F. Petrosino[a], Y. Hallez[b], G. De Luca[c], S. Curcio[a]

[a]*Department of Computer Engineering, Modeling, Electronics and Systems (D.I.M.E.S.), Laboratory of Transport Phenomena and Biotechnology, University of Calabria, Ponte P. Bucci, cubo 39/c, 87036 Rende (CS), Italy;*

[b]*Laboratoire de Génie Chimique, Université de Toulouse, CNRS, INPT, UPS, Toulouse, France;*

[c]*Institute on Membrane Technology, ITM-CNR, Ponte P. Bucci, cubo 17/c, 87036 Rende (CS), Italy;*

Abstract

The calculation of the Osmotic Pressure and the Diffusion Coefficient, characterizing the cake layer developing during the Ultrafiltration (UF) of Bovine Serum Albumin (BSA), through a Multiscale Model based on Quantum Mechanics (QM) and Monte Carlo methods (MC) was the aim of this work. From the *ab-initio* results described in previous works, the distribution of the BSA surface charges was used. A home-made Metropolis MC algorithm, aimed at simulating the formation of BSA loose or concentrated layers during membrane operations, was also implemented. In such a MC algorithm, a DLVO energy calculation methodology of the adsorbed system was developed. Different MC simulations and Hypernetted Chain theory (HNC) calculations were performed so to determine both the Osmotic Pressure and the Diffusion Coefficient of BSA according to the Chun and Bowen approach, thus allowing a comparison between the calculated values of osmotic pressure and a set of experimental data taken from the literature. Such a comparison showed a good agreement between the simulated and the experimental results.

Keywords: multiscale modeling, ab-initio modeling, theory of liquids, computational chemistry, membrane fouling, bovine serum albumin.

5.1 Introduction

Many models aimed either at the description of the fouling formation during UF through stochastic approaches or at the calculation of osmotic pressure were formulated[1-7]. *Kim A. and Hoek E.* proposed a statistical mechanical approach for predicting the long-term gradual flux decline due to colloid-cake formation in dead-end membrane filtration[8]. *Chen Y. and Kim H.* proposed an on-lattice Monte Carlo model referred to a two dimensional membrane pore and surface and simulated the pore blocking and the cake formation[9]. *J. Flora* proposed a stochastic approach to model the fouling of ultrafiltration membrane surfaces[10]. *Bowen W. et al.* proposed a mathematical *a priori* model for predicting osmotic pressure of electrostatically stabilized colloids in UF process; the colloidal interactions were described by the Wigner-Seitz cell approach and the osmotic pressure calculation was essentially based on the addition of different contributions to the interaction energy in agreement with the extended Deryaguin–Landau–Verwey–Overbeek (DLVO) theory[11]. *Roa R. et al.* proposed different approaches to calculate the Osmotic Pressure of solutes accumulating on the membrane surface during the UF process; in particular, either a macroscopic description of cross-flow UF of non-ionic microgels modeled as solvent-permeable spheres[12] or a theoretical description based on the one-component macroion fluid model (OCM)[13] were proposed.

However, these papers and many others available in the literature, do not contain a complete multi-scale approach, actually oriented to the simulation of UF process starting from the ab-initio knowledge acquired at sub-nanoscopic scale. In most of the papers, only partial multi-scale pathways, which generally describe the system behaviour at a mesoscopic scale or are based on a set of experimental parameters such as the colloidal charge, have been developed.

The actual aim of a complete multi-scale approach is to provide a comprehensive, theoretical model, which can predict macromolecules structuration or aggregation and, then, the permeate flux decay

typical of UF, starting from fundamental quantities, namely the electrostatic surface charges of the macromolecule under study, resulting from the *ab-initio* calculations.

Two papers describing a complete multi-scale model for the simulation of UF processes were already published by some of the authors of the present work.[14,15] The first one[14] had to be considered as a "first brick" for the formulation of a more comprehensive and accurate modeling approach aimed at predicting the behavior of protein purification by UF. In fact, the noncovalent interactions existing between the protein molecules and the membrane surface, which significantly affect membrane permeability during UF[16], were not taken into account. In the second paper[15], the noncovalent proteins-surface interactions were accurately evaluated by a quantum and molecular mechanics approach. This *ab-initio* modeling allowed defining the actual structure of the first layer of adsorbed proteins and the equilibrium distance among them. In this way, a physical limit to both the volume fraction and the additional resistance, as due to adsorbed macromolecules, was rigorously calculated. However, in these papers[14,15] only the interactions between a limited number of macromolecules and the surface was analyzed. Nevertheless, the methods used to simulate the phenomena in mesoscopic and macroscopic scales were founded on a major assumption: the formation of the protein deposit layers towards the bulk, in fact, was simulated through a force balance written with reference to a specific protein packing symmetry that yielded a compactly ordered cake. Although, the noncovalent proteins-surface interactions were accurately evaluated by a quantum and molecular mechanics approach[14,15] and, as a result, the structure of the first layer of proteins adsorbed on membrane surface was obtained by calculating the equilibrium distance between them, a body-centered cubic structure symmetry was assumed. A physical limit for both the volume fraction and the additional resistance, as due to either the compact or the loose proteins deposit, was rigorously calculated presuming that this symmetry held also for the loose layers.

The present paper, starting from the fundamental parameters already calculated in the described articles, is intended to propose a stochastic procedure for the simulation of cake layer formation

during UF processes without exploiting any protein packing assumptions. In addition, the calculations of the osmotic pressure and of the diffusion coefficient of BSA in the cake have been performed more rigorously, using this calculated structure.

A Metropolis Monte Carlo procedure has been implemented in a home-made algorithm. A number of simulation boxes large enough to be representative of the proteins layers were analyzed. The potential energy calculation relied on the DLVO pair potential, with a Yukawa model for electrostatic interactions and a van der Waals contribution. Periodic boundary conditions were enforced in the 3 space directions to simulate a large enough volume as compared to the colloid scale but small enough as compared to a macroscopic concentration polarization layer.

It was therefore possible to calculate the osmotic pressure of the deposit layer as a function of the volume fraction related to the total potential characterizing the considered box system. From the generalized virial pressure equation, the formulation for the osmotic pressure calculation was obtained[13,17,18]. Moreover, the diffusion coefficient was evaluated by the approaches based on the *Donnan* equilibrium[19] and *Kirkwood and Buff* theory[20] as exploited in *Roa R. et al.* papers[13,21].

It is worthwhile remarking that the present model did not make use of any adjustable parameter since its inputs were represented by fundamental quantities calculated by ab-initio methods; this allows developing a computational tool capable of accurately simulating colloids adsorption in UF process without resorting to any empirical or adjustable parameter.

5.2 Theoretical

5.2.1 Quantum mechanics calculations

The protein surface charges are necessary to evaluate the electrostatic short- and long-range interactions by the present multi-scale approach. The distribution of surface charges depends on the arrangement and of the nature of external amino-acids, as well as on the experimental conditions such

as type of solvent, pH, solvated ions, etc. Thus, the external amino acids defining the protein surface were preliminarily identified. A home-made algorithm was implemented so as to obtain the coordinates of the BSA external amino-acids from its crystallographic structure.[15]

The atomic partial charges were calculated in the frame of the Density Functional Theory (DFT) using two quantum approaches[14]: the Electro-Static Potential (ESP) and the Löwdin methods as implemented in NWChem[22] code. It is worthwhile remarking that the atomic partial charges were evaluated taking into account both the protonation and the de-protonation of external amino acids according to the pH value related to the structure of the considered BSA, as shown in [14]. The ESP method allowed evaluating the atomic charges from the fitting of the quantum mechanical electrostatic potential on selected grid points centered on each of the atoms of the aforementioned calculated external surface[15]. Finally, the BSA total charge number, Z, was evaluated[14]. The computed total charge was in good agreement with the reported values[23,24]. Moreover, it is important to emphasize that this fundamental property was calculated without resorting to any adjustable parameter.

5.2.2 Colloid interaction potential energy

The study of colloidal interactions by MC simulations is very effective since it is explicitly based on the knowledge of the interaction potential, which depends on both the polydispersity and the volume fraction.[25]

Here BSA is coarse grained as a sphere with a bare charge $Z \cdot e$ given by QM calculations and an equivalent radius of a=3.2nm permitting to conserve the protein volume approximately. It is worthwhile noting that this value as also been exploited in the literature[11].

The total potential energy was split up into three contributions. A hard sphere part, an electrostatic potential and a van der Waals potential. The hard-sphere contribution was classically implemented as:

$$\boldsymbol{U_{HS}(r_{ij}) = \begin{cases} \infty, & r_{ij} \leq \sigma \\ 0, & r_{ij} > \sigma \end{cases}} \quad \textbf{(5.1)}$$

Where r_{ij} is the center to center distance and $\sigma = 2a$ the overlap limit distance between two interacting spheres.

The electrostatic repulsion potential can be considered as the characterizing part of the total interactions and is usually represented as the Static Screened Coulomb Potential (SSCP) also known as Yukawa Potential (YP).[26] For two microion dressed charged colloid spheres of radius a at centre-to-centre distance r_{ij}, the YP can be modeled as:

$$\boldsymbol{U_{elc}(r_{ij}) = l_B\, Z_{eff}{}^2 \left(\frac{\exp(k_{eff}\, a)}{1 + k_{eff}\, a}\right)^2 \frac{\exp(-k_{eff}\, r_{ij})}{r_{ij}}\; K_B\, T} \quad \textbf{(5.2)}$$

Which is valid for non-overlapping spheres.

Here, $l_B = e^2/(4\,\pi\,\varepsilon_0\,\varepsilon_R\,K_B\,T)$ is the Bjerrum length of the suspending fluid and e, ε_0, ε_R, K_B and T, are, respectively, the electron charge, the void and relative dielectric constants, the Boltzmann constant and the operating temperature. Z_{eff} and k_{eff} are the colloid effective charge number and effective screening parameter, respectively. These parameters are equal to the bare charge Z and to the inverse Debye length k for dilute suspensions of weakly charged objects. In highly charged or concentrated suspensions, they can be computed from Z, k and the volume fraction with so-called renormalization methods.

Even if the long range repulsive Yukawa potential is the characterizing contribution in the considered system, the attractive contributions should also be evaluated by the van der Waals (vdW) formulation:[27]

$$\boldsymbol{U_{vdw}(r_{ij}) = -\frac{A_{eff}}{6}\left[\frac{2a^2}{r_{ij}^2 - 4a^2} + \frac{2a^2}{r_{ij}^2} + \ln\left(1 - \frac{4a^2}{r_{ij}^2}\right)\right]} \quad \textbf{(5.3)}$$

The effective Hamaker constant, A_{eff}, incorporates, to some extent, the electrodynamic retardation and non-additivity effects on the dispersion forces.[27]

For dispersions of highly charged colloidal particles, U_{vdw} becomes completely masked by the electrostatic part U_{elc}. In this case, the colloidal particles (with associated microion layer) are usually referred as Yukawa spheres, since their microstructural properties are determined only by the Yukawa-like exponentially screened Coulomb potential U_{elc}.[27]

It is assumed that the total potential energy of a N-particle liquid system can be approximated by a sum of pair interactions. Under the premise of this pairwise additivity assumption, the thermodynamic and microstructural properties of the fluid are solely expressible in terms of $u_{tot}(r_{ij}) = U_{HS}(r_{ij}) + U_{elc}(r_{ij}) + U_{vdw}(r_{ij})$ and of its associated Radial Distribution Function (RDF), $g(r)$ [28]. It should be noted that the vdW term is sometimes negligible in the calculation of the osmotic pressure. It will be the case in the present work, as shown later.

5.2.3 Monte Carlo simulation method

The Monte Carlo (MC) method is a stochastic simulation procedure especially suitable to problems involving particle(s) dynamics due to its capability to evaluate each discrete particle displacement.[29] The used scheme for the implementation of the present simulation code is based on the Metropolis Monte Carlo approach thanks to which the total energy of the system, based on the exploited energy calculation, is used as a criterion for evaluating the acceptance or rejection of each single MC step.

The Metropolis method starts with a tentative random location of the considered system of particles. Defining an ensemble where the number of particles, simulation box volume and temperature are fixed (NVT ensemble), a set of particles coordinate can be randomly evaluated inside the specified box.

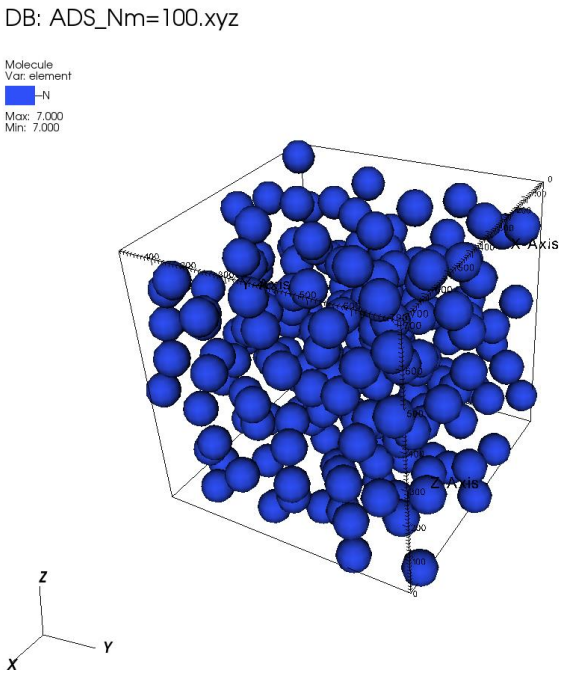

Figure 24: First random configuration of an MC box.

The method proceeds with the random choice of a particle, its random displacement of a fixed distance δr_{max} and the evaluation of the MC move. One point to note is that it is necessary to protect against a trial move, which might result in a significant molecular overlap. However, with the implementation of the explained hard sphere contribution in potential energy calculation, the colloids overlapping can be excluded.

The maximum allowed displacement δr_{max} governs the size of the trial MC move. If this parameter is too small, a large fraction of displacement is accepted but the phase space of the system is explored slowly. If δr_{max} is too large, nearly all the trial moves are rejected and the possible movement through

the phase space is rather limited. An optimal value of δr_{max}, equal to colloid radius a, was therefore chosen to perform the simulations.

Several details on the implemented procedure will be presented hereafter in the subsequent sections of the manuscript.

5.2.4 Theoretical approaches

The structures resulting from the MC simulations were firstly compared to those calculated by solving the Ornstein-Zernike (OZ) equation with the Hypernetted-Chain (HNC) closure[30].

The osmotic pressure calculation was performed by[13]:

$$\frac{\boldsymbol{\beta\,\Pi}}{\boldsymbol{n}} = \mathbf{1} + \mathbf{4}\,\boldsymbol{\pi}\,\boldsymbol{\phi}\,\boldsymbol{g}(\boldsymbol{\sigma}^{+}) - \frac{\mathbf{2}\,\boldsymbol{\pi}}{\mathbf{3}}\,\boldsymbol{n}\int_{\sigma^{+}}^{\infty}\frac{\boldsymbol{\partial}\,\boldsymbol{\beta}\,(\boldsymbol{U_{elc}} + \boldsymbol{U_{vdw}})(\boldsymbol{r})}{\boldsymbol{\partial}\,\boldsymbol{r}}\,\boldsymbol{g}(\boldsymbol{r})\,\boldsymbol{r^{3}}\,\boldsymbol{dr} \qquad \textbf{(5.4)}$$

Where $\beta = 1/(K_B\,T)$, $n = N_c/\,V$ was the colloidal number concentration, $g(\sigma^{+})$ was the RDF function value at $r = \sigma^{+}$. The 1 on the right hand side is the ideal contribution. The second and third terms are contributions from contacts and non-contact interactions, respectively. When using an effective potential such as U_{elc}, two other terms can appear in this relation. One is the so-called "volume term" and the other is an integral involving a density derivative of U_{elc}[31]. They are important when the effective charge and screening length differ significantly from their bare values. In the present work, the colloidal charge is quite low and the salt content quite high so renormalization has only a mild effect and these two terms can be omitted.

The concentration-dependent collective diffusion coefficient, $D_c(\phi)$, was expressed as:[13]

$$\boldsymbol{D_c(\phi)} = \boldsymbol{D_0}\,\frac{\boldsymbol{K(\phi)}}{\boldsymbol{\chi_{osm}}} \qquad \textbf{(5.5)}$$

Where $D_0 = K_B\,T/(6\,\pi\,\eta_0\,a)$ was the single particle diffusion coefficient, η_0 the water viscosity, $K(\phi) = (1-\phi)^{5.1}$ was the long-time sedimentation coefficient[21] and χ_{osm} was the osmotic compressibility coefficient, which can be expressed as:

$$\frac{1}{\chi_{osm}} = \frac{\partial(\beta\Pi)}{\partial n}\bigg|_T \qquad \textbf{(5.6)}$$

Taking into account that $n\,V_c = \phi$ where the colloid volume V_c can be exploited from the radius a, a final expression for diffusion coefficient was therefore obtained as:

$$D_c(\phi) = \frac{2a^2}{9\eta_0}\,(1-\phi)^{5.1}\,\frac{\partial\Pi}{\partial\phi}\bigg|_T \qquad \textbf{(5.7)}$$

Starting from the total energy derived from the Monte Carlo simulations, Eqs.5.4-7 allowed calculating both the Osmotic Pressure and the Diffusion Coefficient of BSA as a function of the volume fraction (or concentration) of colloids.

5.3 Numerical implementation

The complete multi-scale framework implementation started from the ab-initio knowledge acquired at both sub-nanoscopic and nanoscopic scales, and was therefore independent on experimental or empirical information. The fundamental linking parameter, namely the BSA surface charge distribution, was exploited so to achieve the proper scale transition, allowing the calculation of the total, bare charge number, Z.

The MC simulations used to compute the osmotic pressure and the diffusion coefficient are based on the effective electrostatic potential U_{elc} involving an effective charge and an effective screening length. These parameters were obtained with the Extrapolated Point Charge (EPC) renormalization method[31] with the bare charge Z computed with Quantum Mechanics as input parameter.

The other required inputs of MC simulations were: the number of adsorbed molecules, N, the simulation box volume fraction, ϕ, the system temperature, T, the Boltzmann Constant K_B, the minimum distance, σ, the radius, a, the maximum number of iterations, max_iter, the overlapping energy limit U_{tot_max}, which represents the highest energy value of overlapped spheres in the hard sphere energy approach, the parameter d_gr, which represented the number of MC steps whenever the box structure and the RDF files are saved, the parameter lay_tick used to define the layer thickness in the calculation of the RDF and the $seed$ value used to control the random generation[32].
A total potential energy code was implemented in agreement with Eqs. 1-3 for a macromolecules coordinates matrix. The $\varepsilon_0, \varepsilon_R$ and A_{eff} constants were defined within the simulation code.

For each volume fraction, ϕ, 8 sets of simulations were performed with 8 different seeds related to the number of available processors. For each of the considered seeds, a max_iter number of MC iterations were performed.
A characteristic number of MC iterations $n_{MC\ ch}$ was set on the basis of the steps, which were actually necessary to notice an initial decrease in system energy. After different tests, a number of 3 $n_{MC\ ch}$ accepted displacements was considered as adequate to obtain satisfactory RDFs and osmotic pressure results.
Two Intel Xeon CPU E5-2609 v2 processors were used on 8 cores and the calculation times in the case of high volume fractions were equal, on average, to about 72 hours.

5.4 Results and discussions

In this section, the fundamental results deriving from sub-nano and nanoscopic scales are firstly illustrated, together with the results of MC simulations calculated in a range of concentrations deriving from the flux-decay profiles characterizing the ultrafiltration process[14,15]. The validation of

MC code carried out by the Hypernetted-Chain (HNC) theory[33] is then presented. Finally, the calculations of the Osmotic Pressure and the Diffusion Coefficient for an experimental study available in the literature[11], are reported. The theoretical calculations of the Osmotic Pressure were performed by the HNC theory too. It was then possible to carry out both a theoretical analysis and an experimental validation of the formulated computational model.

5.4.1 Ab-initio total protein charge and minimum distance

The surface charges distribution calculation was performed by the ESP method[14,15,34]. At pH=7, the external amino-acids functional groups were protonated or deprotonated as described in section 2.1. The surface charges were used to evaluate the protein total charge, obtaining -15.82 atomic units. Consequently, the colloid charge number Z=15.82 was used as a bare charge in the model.

The exploited radius was equal to $a = 32$ Å [11]. The center to center minimum distance among the adsorbed proteins, $\sigma = 64$ Å, was imposed as the lower bound in total energy calculation for MC simulations.

5.4.2 MC simulation sets and code validation

An NVT ensemble was defined to perform the MC simulations. A set of volume fractions was defined in agreement with a previously obtained ultrafiltration concentration-polarization profiles[15] as illustrated in Fig.25. Referring to Fig.10 of previous work[15] the disperse cake profile was analyzed. The deriving concentration diagram for an ultrafiltration time of $3200s$, a transmembrane pressure of 1.5 bar and a membrane rejection of 0.9875, was discretized. Different characteristic points as a set of corresponding volume fractions were obtained.

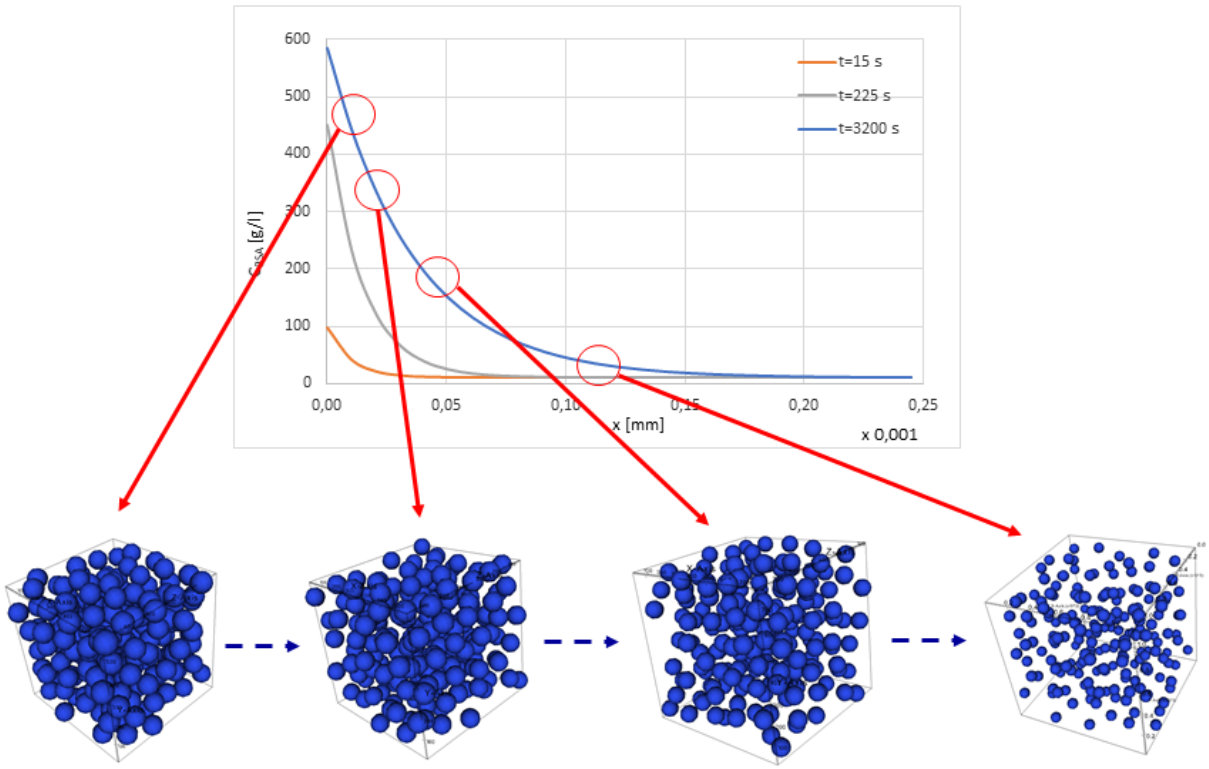

Figure 25:Concentration-polarization profile discretization for a volume fraction set choice. BSA ultrafiltration on polysulfone membrane TMP=1.5bar, membrane Rejection Rej=0.9875, for a filtration time of 3200s (considered curve)[15]

Thanks to these considerations, a volume fraction, ϕ, ranging between 0.05 and 0.30 was chosen. As a trade-off between a high enough box dimension and an affordable computer effort, a number of BSA colloids, N, equal to 200 was chosen. From a fixed N and ϕ the simulation box volume was calculated. The other input parameters were $T = 300\ K$, $\max\_iter = 1.5 \cdot 10^4$, $U_{tot\_max} = 10^{13} J$, $d\_gr = 100$, $lay\_tick = 2$ Å. The ε_R constant was fixed equal to the water dielectric constant, $\varepsilon_R = 81.07$ and $A_{eff} = 1.354 \cdot 10^{-20} J$.

For MC calculations validation a total charge number $Z_{eff} = Z = 15.82$ was set up. A ionic strength, $I = 0.15\ M$, was analyzed in order to compare the simulation results as provided by the present multiscale model to the experimental data reported in the literature[11], giving a screening parameter equal to $k_{eff} = k = 1/(8.0068 \cdot 10^{-10}) = 1.2489 \cdot 10^9$.

As shown in Fig.26, after 5000 MC iterations the total energy was stable with a rather small fluctuation around the equilibrium state.

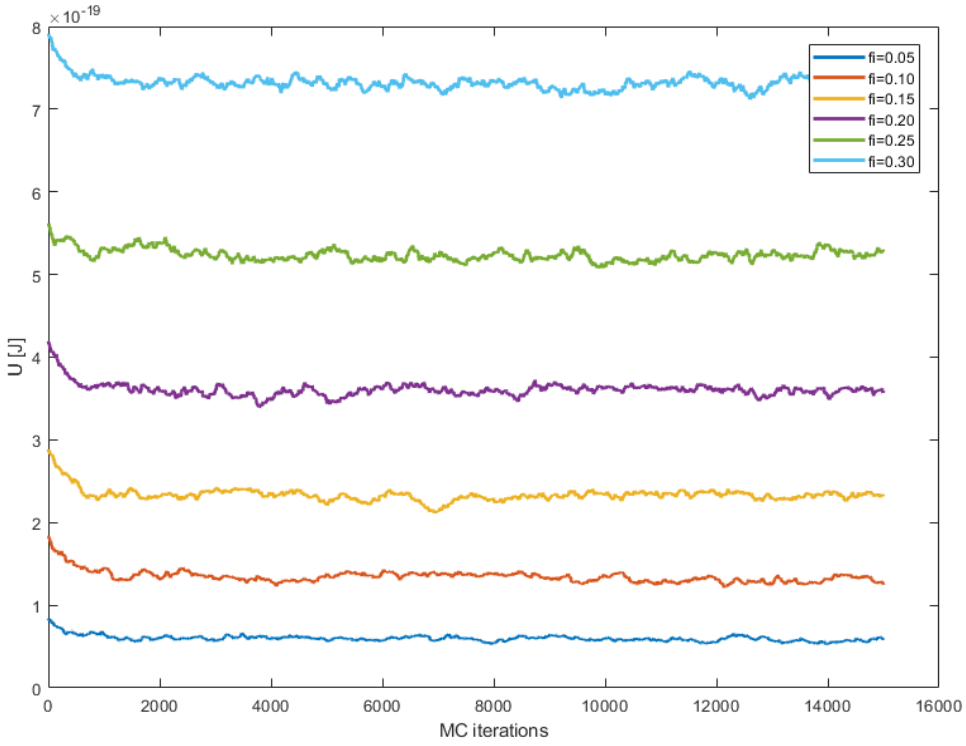

Figure 26: Total energy profile as function of MC iterations for different volume fractions. $Z = 15.82, I = 0.15M, pH = 7,\ a = 32$ Å, $\sigma = 64$ Å, $T = 300\ K$

The Metropolis algorithm was first validated in the case of hard sphere interactions (Fig.27). Then, for a more complete test, the RDFs produced by MC simulations considering both hard sphere collisions and effective electrostatic interactions were also compared to RDFs calculated theoretically with HNC. As shown in Figs. 27-28 a very good agreement between these techniques can be observed for hard sphere and Yukawa-type electrostatic potential, which validates our MC implementation.

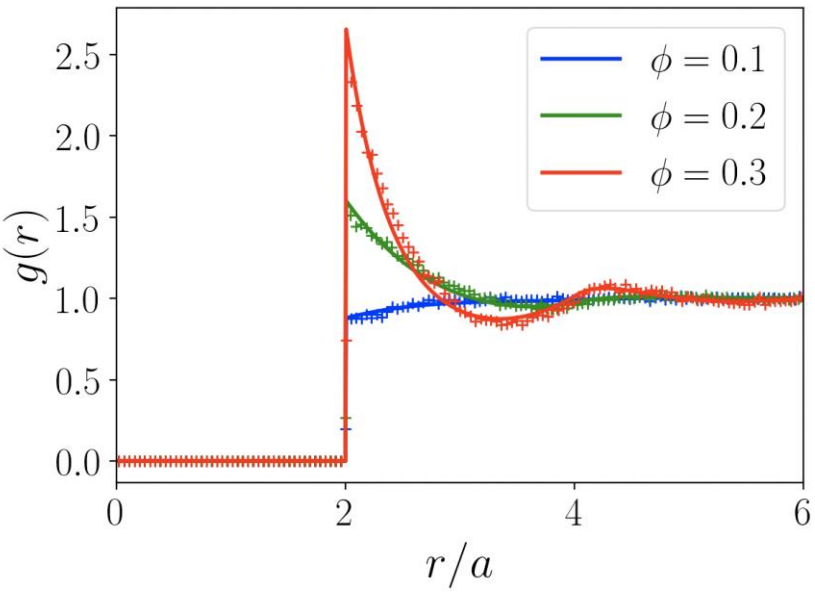

Figure 27 Hard-Sphere potential RDFs validations. + is the MC simulation points, lines the HNC theory results. r/a is the normalized distance with colloids radius a. Z=15.82, I=0.15M, pH=7, a=32 Å, σ=64 Å, T=300 K

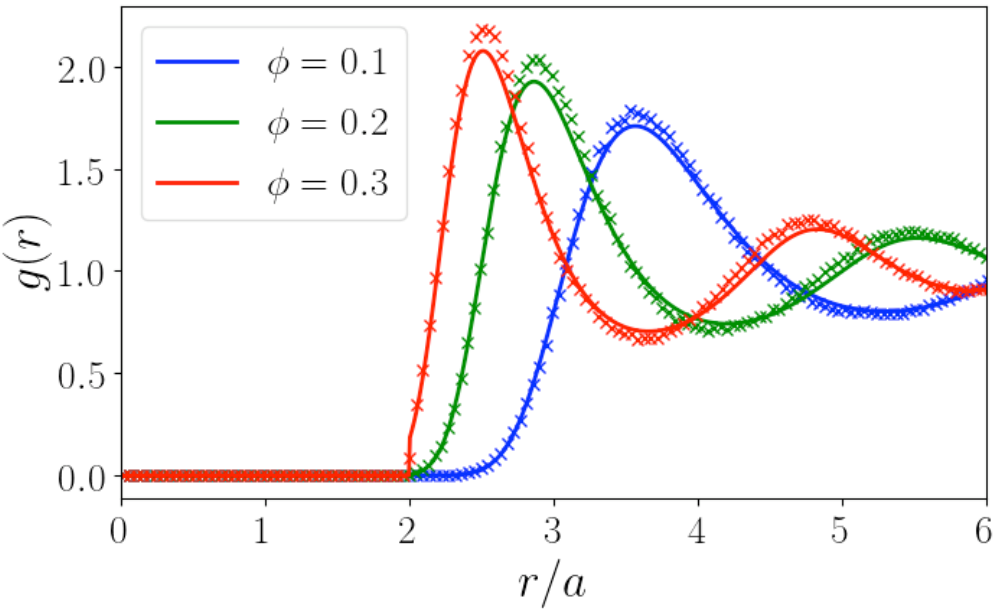

Figure 28 Yukawa potential RDFs validations. + is the MC simulation points, lines the HNC theory results. r/a is the normalized distance with colloids radius a. Z=15.82, I=0.15M, pH=7, a=32 Å, σ=64 Å, T=300 K

The Yukawa case shows $g(2a) \rightarrow 0$, which means that contacts are not much present.

Therefore, it was decided to perform some other simulations without considering the van der Waals contribution.

5.4.3 Osmotic Pressure and Diffusion Coefficient

Once the MC model was validated, different sets of simulations were performed on the basis of the previously defined total bare charge number Z and screening parameter k.

The energy set from MC simulations is reported in Fig.28.

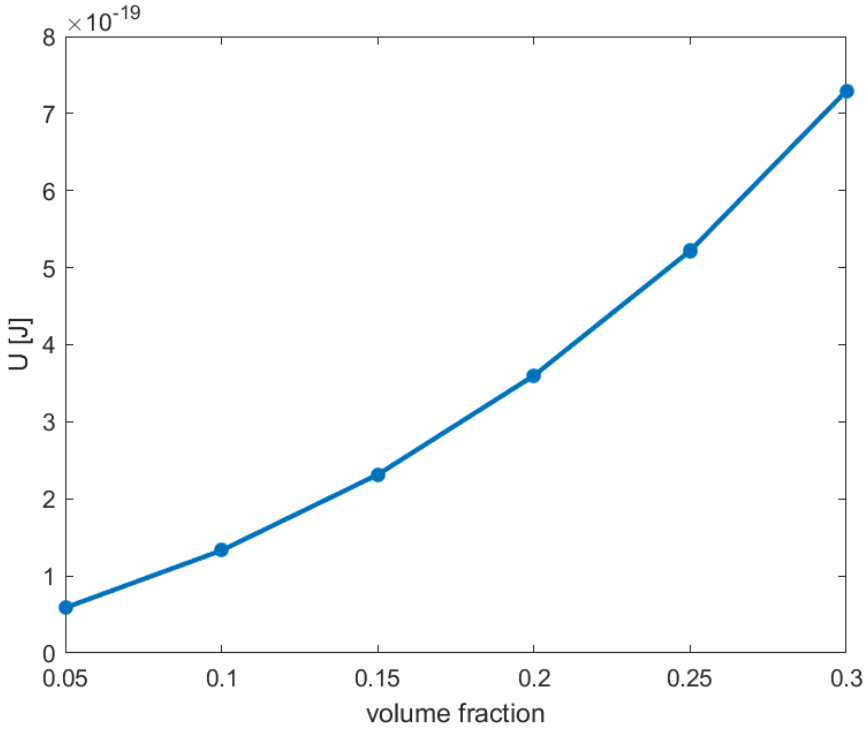

Figure 29 Total energy as function of volume fraction for Yukawa potential total energy. Z=15.82, I=0.15M, pH=7, a=32 Å, σ=64 Å, T=300 K

The total Yukawa energy compared to the $K_B\,T$ value is $\sim 0.5\,K_BT$ energy per colloid particle.

The osmotic pressure was carried out using Eq.5.4. Moreover, in order to achieve the experimental validation of the present model, a set of data reported in *Bowen et al.* paper[11], were taken as reference. A comparison of MC results with both HNC theory and *Bowen et al.* data[11] is reported in Fig.30.

Osmotic pressure Π was reported like P_{osm} in the following data and figures independently.

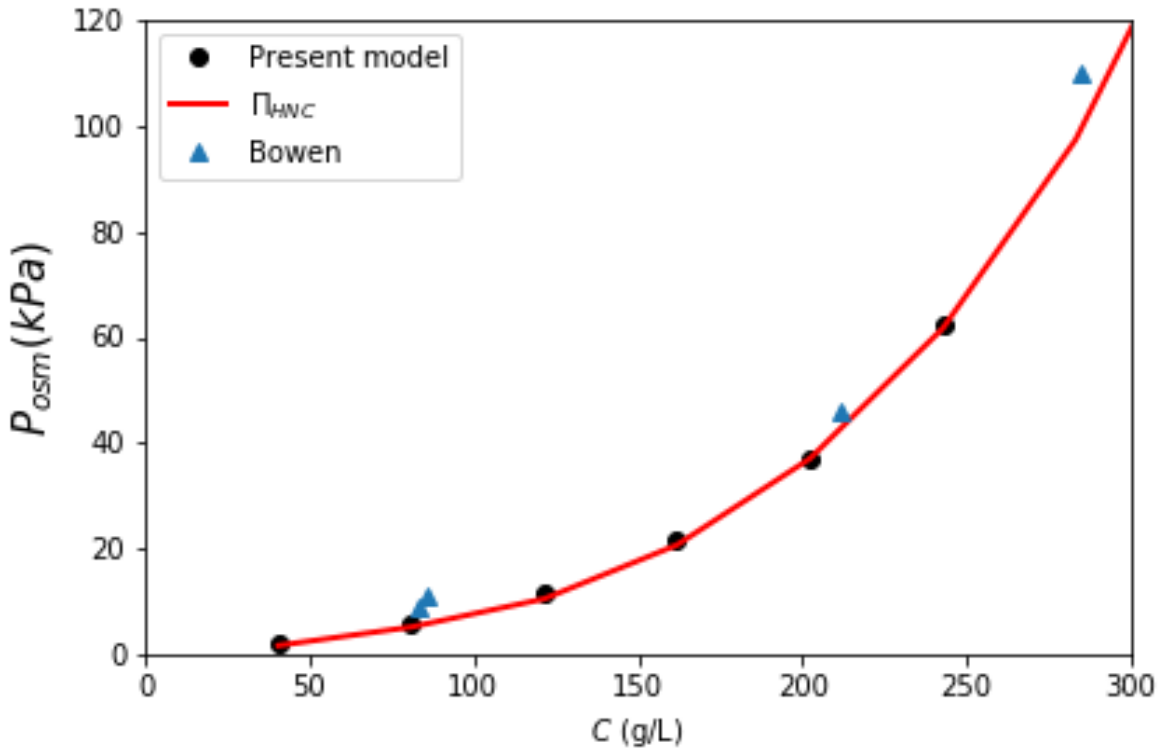

Figure 30 Osmotic pressure comparison as function as colloid concentration between the presented model Monte Carlo results (black dots), HNC theory results (red line) and experimental data. Ionic Strength 0.15M, pH=7. Concentration in g/L in agreement with literature11

The results show a good agreement between the present multiscale theoretical model, based both on the ab-initio knowledge acquired at sub-nanoscopic scale and on MC simulations, and the experimental data, with maximum relative errors equal to 6%.

Once the pressure calculation has been validated, basing on the Eq. 5.4, three osmotic pressure contributions were analyzed and reported in Fig. 31.

The linear colloidal ideal gas contribution P_{id} denoted a medium of 15% of the total pressure. However, for very dilute system it represented the characterizing contribution due to the assimilation of the system to an ideal one. The contact and non-contact interaction pressure contributions contributed more or less equally to the total pressure. As expected, at high concentrations these interaction contributions dominate the total pressure.

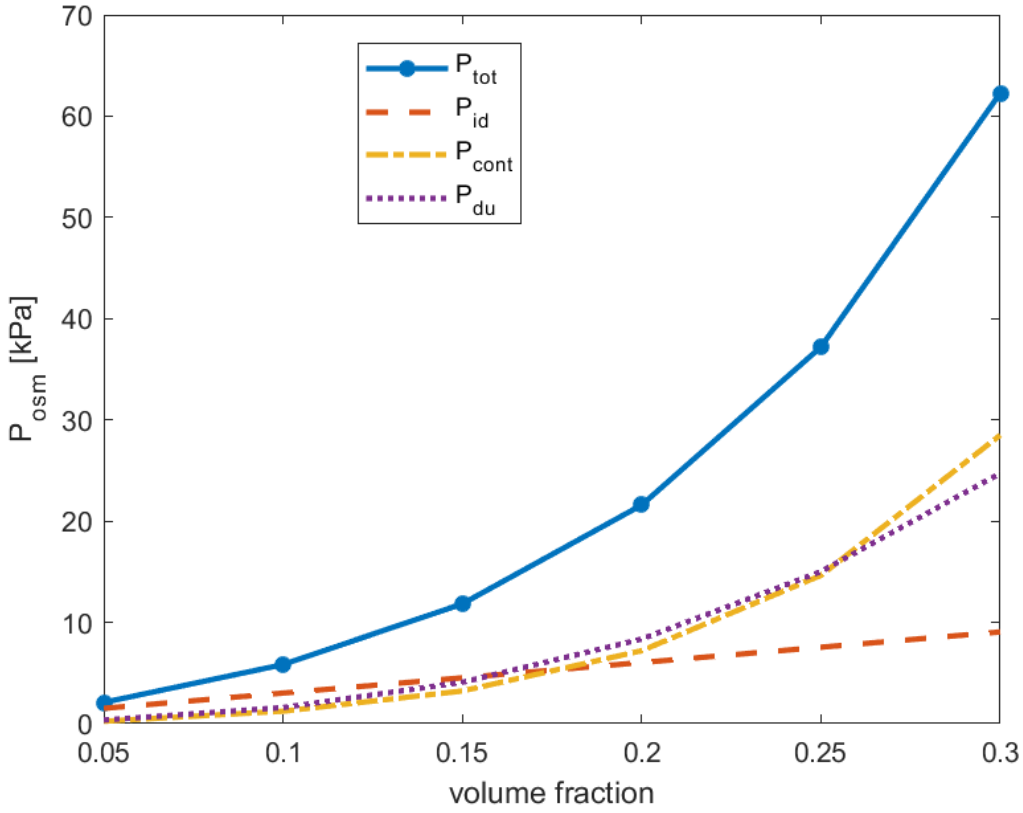

Figure 31 Model predicted osmotic Pressure of the fouling cake as function of volume fraction during ultrafiltration process for Yukawa potential formulation. Total osmotic pressure in continuous line and the three different contributions basing on Eq.4. Z=15.82, I=0.15M, pH=7, a=32 Å, σ=64 Å, T=300 K. Process conditions: TMP=1.5bar, Rej=0.9875, t=3200s.

It is worthwhile stressing how a knowledge of the osmotic pressure of colloidal systems is crucial in design and operation of different industrial processes. Pressure driven ultrafiltration processes are becoming widely used in concentration of colloidal and bio-colloidal suspensions where osmotic pressure within the polarized layer play a key role on the global process performance.

At this level it was possible to derive an important transport property of the deposit layer starting from sub-nanoscopic information: the diffusion coefficient was calculated using Eqs. 5.5-7 and was reported in Fig.32.

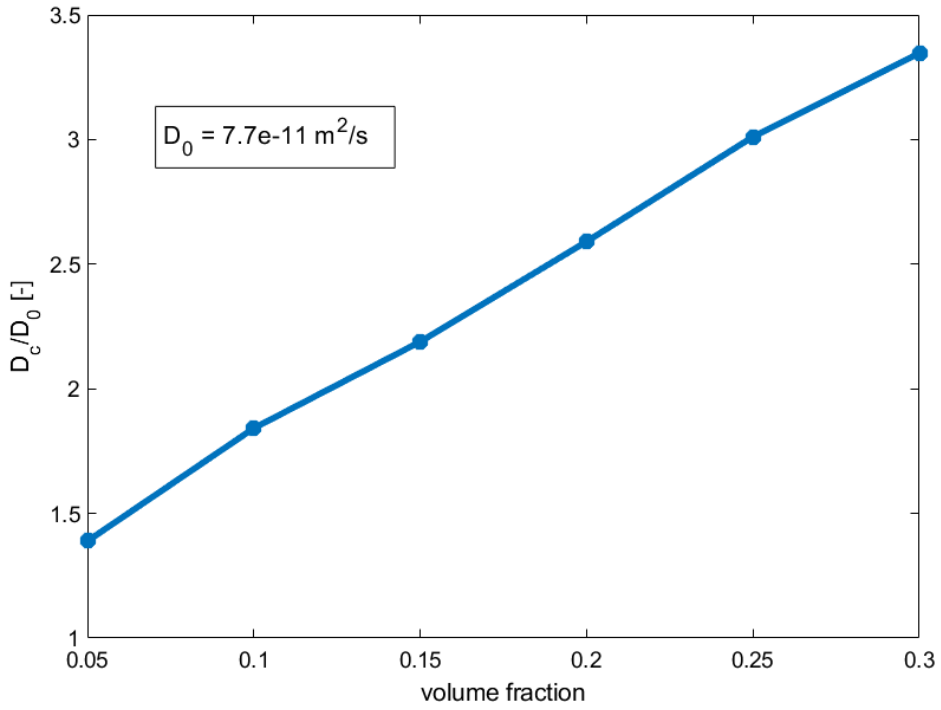

Figure 32 Model predicted diffusion coefficient, D_c/D_0, of the fouling cake as function of volume fraction during ultrafiltration process for Yukawa potential formulation. D_0=7.7 10^{-11} m^2/s
Z=15.82, I=0.15M, pH=7, a=32 Å, σ=64 Å, T=300 K.
Process conditions: TMP=1.5bar, Rej=0.9875, t=3200s.

The diffusion coefficient trend presented a smooth rising trend in agreement with similar literature data[13]. This is the signature of repulsive electrostatic interactions promoting the classical Brownian collective diffusion.

Once again it is worthwhile remarking that fundamental transport property like diffusion coefficient results a first brick of macroscopic scale process simulation.

5.5 Conclusions

In the present work, key macroscopic quantities of ultrafiltration processes, i.e. osmotic pressure and diffusion coefficient, were obtained starting from the BSA surface charges through a rigorous quantum ab-initio method regardless of any empirical parameters at fixed pH. The very crucial quantity, the colloid charge number, was exploited from quantum mechanics approach rather than

using different experimental fitted values. It is worthwhile emphasizing that the present work makes use of different theories and merges all of them according to a real multiscale approach which starts at sub-nanoscopic scale.

In other previous works a fouling modelling approach in UF processes considered equilibrium quantities to characterize the adsorbed compact cake and classical force balance for the description of loose layers. In the present one a stochastic approach, based on a metropolis MC method, was used to describe the fouling formation. The formulated model was validated by well-assessed colloid physics theoretical methods and a very good agreement was actually observed.

Moreover, a good agreement between osmotic pressure and corresponding experimental data taken from the literature was remarked.

Quantum Mechanics is a powerful tool to access detailed properties of colloids involved in UF, but its application is limited to the scale of one object and it does not account for entropic effects driving the meso-structure of colloidal dispersions. On the other hand, Monte Carlo simulations are designed to capture the structuration at this meso-scale, but they require the detailed characteristics of colloids (as the surface charge) as input parameter.

The multiscale framework presented here combines these two approaches to get the best of both worlds. It can be used as a “first-brick” for different processes simulations, as a mean to compute thermodynamic and transport properties of colloidal dispersions. In addition, this multiscale framework could be used to predict partial or total aggregation for example.

The next step would be to introduce a third component at even large scale: the transport coefficients, computed from the present multiscale framework, can be considered as input parameters for a continuous description of mass and momentum transfers at the scale of processes with a Computational Fluid Dynamics approach. This will be conducted using MC box meshes in CFD simulations obtaining different fouling cake properties, such as the cake permeability.

Appendix: Nomenclature

a	Protein radius	$[m]$
A_{eff}	Effective Hamaker constant	$[J]$
d_gr	MC steps files saving	$[-]$
D_c	Diffusion coefficient	$[m^2/s]$
$D_\mathbf{0}$	Single particle diffusion coefficient	$[m^2/s]$
e	Electron charge ($-1.60217646 \cdot 10^{-19}$)	$[C]$
$g(r)$	Radial distribution function	$[-]$
k	Inverse of Debye length	$[m^{-1}]$
K	Long time sedimentation coefficient	$[-]$
K_B	Boltzmann constant ($1.3806503 \cdot 10^{-23}$)	$[J/K]$
l_B	Bjerrum length	$[m]$
lay_tick	RDF layer thickness	$[A]$
max_iter	Maximum number of MC iterations	$[-]$
n	Colloidal number concentration	$[m^{-3}]$
$n_{MC\ ch}$	Characteristic MC steps number	$[-]$
n_{res}	Reservoir ion density	$[m^{-3}]$
N_c	Number of colloids	$[-]$
r_{ij}	Proteins centre to centre distance	$[m]$
$seed$	Seeds MC number	$[-]$
T	Temperature	$[K]$
TMP	Transmembrane pressure	$[Pa]$
U_{elc}	Electrostatic energy contribution	$[J]$
U_{HS}	Hard Sphere energy contribution	$[J]$
U_{tot}	Total interaction energy (=A)	$[J]$
U_{vdw}	van der Waals energy contribution	$[J]$

U_{tot_max}	Overlapping energy limit	$[J]$
V	Simulation volume	$[m^3]$
V_c	Total volume of colloids	$[m^3]$
Z	Colloid charge number	$[-]$
β	Energy constant (=$1/(K_B T)$)	$[J^{-1}]$
δr_{max}	Random displacement	$[m]$
ε_R	Relative dielectric constant (81.07)	$[-]$
ε_0	Void dielectric constant $8.8541878 \cdot 10^{-12}$	$[C^2/(J\,m)]$
η_0	Water viscosity	$[Pa\,s]$
Π	Osmotic pressure	$[Pa]$
σ	Centre to centre minimum distance	$[m]$
ϕ	Volume fraction	$[-]$
$\boldsymbol{\chi_{osm}}$	Osmotic compressibility coefficient	$[-]$

References

(1) Cheng, T. W.; Yeh, H. M.; Gau, C. T. Flux Analysis by Modified Osmotic-Pressure Model for Laminar Ultrafiltration of Macromolecular Solutions. *Sep. Purif. Technol.* **1998**, *13*, 1–8.

(2) Chakraborty, S.; Loutatidou, S.; Palmisano, G.; Kujawa, J.; Mavukkandy, M. O.; Al-Gharabli, S.; Curcio, E.; Arafat, H. A. Photocatalytic Hollow Fiber Membranes for the Degradation of Pharmaceutical Compounds in Wastewater. *J. Environ. Chem. Eng.* **2017**, *5*, 5014–5024.

(3) Zin, G.; Penha, F. M.; Rezzadori, K.; Silva, F. L.; Guizoni, K.; Petrus, J. C. C.; Oliveira, J. V.; Di Luccio, M. Fouling Control in Ultrafiltration of Bovine Serum Albumin and Milk by the Use of Permanent Magnetic Field. *J. Food Eng.* **2016**, *168*, 154–159.

(4) Nath, A.; Mondal, S.; Chakraborty, S.; Bhattacharjee, C.; Chowdhury, R. Production, Purification, Characterization, Immobilization, and Application of β-Galactosidase: A Review. *Asia-Pacific J. Chem. Eng.* **2014**, *9*, 330–348.

(5) Saha, K.; R, U. M.; Sikder, J.; Chakraborty, S.; da Silva, S. S.; dos Santos, J. C. Membranes as a Tool to Support Biorefineries: Applications in Enzymatic Hydrolysis, Fermentation and Dehydration for Bioethanol Production. *Renew. Sustain. Energy Rev.* **2017**, *74*, 873–890.

(6) Suki, A.; Fane, A. G.; Fell, C. J. D. Flux Decline in Protein Ultrafiltration. *J. Memb. Sci.* **1984**, *21*, 269–283.

(7) Bolton, G.; LaCasse, D.; Kuriyel, R. Combined Models of Membrane Fouling: Development and Application to Microfiltration and Ultrafiltration of Biological Fluids. *J. Memb. Sci.* **2006**, *277*, 75–84.

(8) Kim, A. S.; Hoek, E. M. V. Cake Structure in Dead-End Membrane Filtration: Monte Carlo Simulations. *Environ. Eng. Sci.* **2002**, *19*, 245–254.

(9) Chen, Y.; Kim, H. Monte Carlo Simulation of Pore Blocking and Cake Formation by Interfacial Interactions during Membrane Filtration. *Desalination* **2008**, *233*, 258–266.

(10) Flora, J. R. V. Stochastic Approach to Modeling Surface Fouling of Ultrafiltration Membranes. *J. Memb. Sci.* **1993**, *76*, 85–88.

(11) Bowen, W. R.; Williams, P. M. The Osmotic Pressure of Electrostatically Stabilized Colloidal Dispersions. *J. Colloid Interface Sci.* **1996**, *184*, 241–250.

(12) Roa, R.; Zholkovskiy, E. K.; Nägele, G. Ultrafiltration Modeling of Non-Ionic Microgels. *Soft Matter* **2015**.

(13) Roa, R.; Menne, D.; Riest, J.; Buzatu, P.; Zholkovskiy, E. K.; Dhont, J. K. G.; Wessling, M.; Nägele, G. Ultrafiltration of Charge-Stabilized Dispersions at Low Salinity. *Soft Matter* **2016**, *12*, 4638–4653.

(14) De Luca, G.; Bisignano, F.; Paone, F.; Curcio, S. Multi-Scale Modeling of Protein Fouling in Ultrafiltration Process. *J. Memb. Sci.* **2014**, *452*, 400–414.

(15) Curcio, S.; Petrosino, F.; Morrone, M.; De Luca, G. Interactions between Proteins and the Membrane Surface in Multiscale Modeling of Organic Fouling. *J. Chem. Inf. Model.* **2018**, *58*, 1815–1827.

(16) Szymczyk, A.; Fievet, P. Investigating Transport Properties of Nanofiltration Membranes by Means of a Steric, Electric and Dielectric Exclusion Model. *J. Memb. Sci.* **2005**, *252*, 77–88.

(17) Deserno, M.; von Grünberg, H. H. Osmotic Pressure of Charged Colloidal Suspensions: A Unified Approach to Linearized Poisson-Boltzmann Theory. *Phys. Rev. E. Stat. Nonlin. Soft Matter Phys.* **2002**, *66*, 011401.

(18) Hansen, J. P.; McDonald, I. R. *Theory of Simple Liquids*; 2006, Academic Press.

(19) Stell, G.; Joslin, C. G. The Donnan Equilibrium: A Theoretical Study of the Effects of Interionic Forces. *Biophys. J.* **1986**, *50*, 855–859.

(20) Braga, C.; Smith, E. R.; Nold, A.; Sibley, D. N.; Kalliadasis, S. The Pressure Tensor across a Liquid-Vapour Interface. *J. Chem. Phys.* **2018**, *149*, 044705.

(21) Roa, R.; Zholkovskiy, E. K.; Nägele, G. Ultrafiltration Modeling of Non-Ionic Microgels. *Soft Matter* **2015**, *11*, 4106–4122.

(22) Valiev, M.; Bylaska, E. J.; Govind, N.; Kowalski, K.; Straatsma, T. P.; Van Dam, H. J. J.; Wang, D.; Nieplocha, J.; Apra, E.; Windus, T. L.; et al. NWChem: A Comprehensive and Scalable Open-Source Solution for Large Scale Molecular Simulations. *Comput. Phys. Commun.* **2010**, *181*, 1477–1489.

(23) de la Casa, E. J.; Guadix, A.; Ibáñez, R.; Camacho, F.; Guadix, E. M. A Combined Fouling Model to Describe the Influence of the Electrostatic Environment on the Cross-Flow Microfiltration of BSA. *J. Memb. Sci.* **2008**, *318*, 247–254.

(24) Fukuzaki, S.; Urano, H.; Nagata, K. Adsorption of Bovine Serum Albumin onto Metal Oxide Surfaces. *J. Ferment. Bioeng.* **1996**, *81*, 163–167.

(25) Iacovella, C. R.; Rogers, R. E.; Glotzer, S. C.; Solomon, M. J. Pair Interaction Potentials of Colloids by Extrapolation of Confocal Microscopy Measurements of Collective Suspension Structure. *J. Chem. Phys.* **2010**, *133*, 164903.

(26) Edwards, J. P.; Gerber, U.; Schubert, C.; Trejo, M. A.; Weber, A. The Yukawa Potential: Ground State Energy and Critical Screening. *Prog. Theor. Exp. Phys.* **2017**, *2017*, 083A01.

(27) Nägele, G. The Physics of Colloidal Soft Matter. *Mater. Struct.* **2004**, *2*, 674–688.

(28) Vlugt, T. J. H. *Introduction to Molecular Simulation and Statistical Thermodynamics*; 2009, Delft, The Netherlands.

(29) Chen, J. C.; Elimelech, M.; Kim, A. S. Monte Carlo Simulation of Colloidal Membrane Filtration: Model Development with Application to Characterization of Colloid Phase Transition. *J. Memb. Sci.* **2005**, *255*, 291–305.

(30) Howard L. Lemberg; Frank H. Stillinger. Application of Hypernetted-Chain Integral Equations to a Central-Force Model of Water. **1976**, *32*, 353–362.

(31) Boon, N.; Guerrero-García, G. I.; Van Roij, R.; De La Cruz, M. O. Effective Charges and Virial Pressure of Concentrated Macroion Solutions. *Proc. Natl. Acad. Sci. U. S. A.* **2015**, *112*, 9242–9246.

(32) Matsumoto, M.; Nishimura, T. Mersenne Twister: A 623-Dimensionally Equidistributed Uniform Pseudo-Random Number Generator. *ACM Trans. Model. Comput. Simul.* **1998**, *8*, 3–30.

(33) Hallez, Y.; Meireles, M. Fast, Robust Evaluation of the Equation of State of Suspensions of Charge-Stabilized Colloidal Spheres. *Langmuir* **2017**, *33*, 10051–10060.

(34) Zeng, J.; Duan, L.; Zhang, J. Z. H.; Mei, Y. A Numerically Stable Restrained Electrostatic Potential Charge Fitting Method. *J. Comput. Chem.* **2013**, *34*, 847–853.

Chapter 6

Theoretical modeling of UF fouling at micro-CFD scale: the case of BSA

An extended abstract

Theoretical modeling of UF fouling at micro-CFD scale: the case of BSA

Francesco Petrosino[a], and Giorgio De Luca[b], Stefano Curcio[a]

[a] *Department of Informatics, Modeling, Electronics and Systems Engineering (D.I.M.E.S.), Laboratory of Transport Phenomena and Biotechnology, University of Calabria, Ponte P. Bucci, cubo 42/a, 87036 Rende (CS), Italy;*

[b] *Institute on Membrane Technology, ITM-CNR, Ponte P. Bucci, cubo 17/c, 87036 Rende (CS), Italy*

Abstract

The aim of this work was the macroscopic characterization of fouling structure formation occurring during the Ultra-Filtration (UF) of Bovine Serum Albumin (BSA). A twisted Monte-Carlo (MC)/Computational-Fluid-Dynamic (CFD) approach was developed in order to obtain macroscopic fluid-dynamic proprieties.

Different fluid-dynamic simulations, performed on the basis of the knowledge acquired by a MC analysis, which resulted in a set of boxes of adsorbed molecules, were performed. In particular, thanks to the MC results, various 3D structures were developed and characterized. These structures represented the deposit layers, which formed at different distances from the membrane. Using some well-assessed computer-aided tools, these geometries were imported in a simulation environment and several meshes were created to perform micro-fluid dynamic calculations (m-FD). From these simulations, a set of macroscopic parameters was calculated. The resistance to flow of deposit layers accumulated on the membrane surface, R_{add}, normally estimated by experimental methods, was therefore computed starting from the *ab-initio* knowledge acquired at sub-nanoscopic scale.

Keywords: multiscale modeling, diffusion coefficient, Monte Carlo, *ab-initio* modeling, Computational-Fluid-Dynamic

6.1 Introduction

Fluid dynamics is one of the most important and interesting fields of technology because of the wide variety of its possible applications. The need for a deeper understanding of the complex phenomena involved in the fluid-dynamic analysis of real systems has inspired numerous advances in applied mathematics, computational physics and experimental techniques. One of the major problems in fluid-dynamics analysis is represented by the fact that the governing equations (the Navier-Stokes equations) have no general analytical solution, and the determination of reliable computational solutions is definitely very challenging[1].

Different innovations have been proposed for the fluid-dynamic characterization of miniaturized devices, which might be particularly useful is several engineering applications, as well as in biology, chemistry, and physics[1]. In particular, micro-fluidic and nano-fluidic systems[2], consisting of channels that are smaller than 1 millimeter or 1 micron, respectively, need to be properly designed and controlled by advanced models and reliable computational methods. These models can result of particular interest in many other areas of science and technology, like for instance in membrane processes. Membrane based technologies are receiving considerable attention over the past years for their effectiveness in achieving proteins concentration[3]. However, one of the major limitations is represented by permeate flux decay, since some of the components contained in feed solution tend to accumulate on the membrane surface, thus originating the so-called concentration polarization phenomena or determining the formation of a cake, which may result in pores plugging[4]. It is well known that these phenomena are strictly related to the fluid-dynamic conditions chosen to perform membrane filtration. Thus, accurate predictions of fouling, resulting in correct estimations of permeate flux decay, allow evaluating membrane processes efficiency and optimizing their performance. In order to achieve these objectives, it is necessary to model the momentum and mass transfer taking place both in the bulk and close to the membrane surface[5].

A variety of possible CFD applications have been developed to predict the behavior of membrane separation processes[6]. *B. Marcos and al.* proposed a transient model based on the finite element method to simulate the flow and the solute concentration profiles developing in an ultrafiltration unit[3]. *Z. Cui* proposed a multi-scale approach to analyze the coupling of the system hydrodynamics, boundary layer transport, membrane permeation, electrostatic and hydrophobic interactions and its effects on protein transmission and membrane selectivity[7]. *L Jianxin et al.* proposed a numerical method to investigate the membrane fouling phenomenon during microfiltration of semiconductor wastewater[8]. *F. Vinther et al.* studied the influence of back-shock frequency on the net flux at different transmembrane pressures and cross-flow velocities by a CFD approach[9].

However, in these and in many other works available in the literature, a purely macroscopic fluid-dynamic approach was used without exploiting any information, estimated by a proper analysis performed at microscopic scale and referred to fouling cake development. Only experimental or empirical parameters were used to define the macroscopic problem and to solve the Navier-Stokes equations[10]. Some effective quantities, i.e. the effective diffusion coefficient in the concentration-polarization layers, were defined, taking into account the existence of a microporous-like medium but without analyzing the actual micro-structure of deposit layers accumulated on the membrane surface.

Some of the authors of this work have already developed a multiscale model aimed at describing the membrane fouling in UF processes[11]. The overall additional resistance, as due to both the compact and loose layers of the deposit, was computed by a classical force balance and an unsteady-state mass transfer model was formulated to describe the behavior of a dead-end UF unit. The formulated force balance was strictly related to a fixed and a-priori-chosen packing structure and no disordered displacement of the macromolecules, especially in the loose layers, was considered.

On the other hand, in a previously submitted paper (chapter5), a home-made Metropolis MC algorithm, aimed at simulating the arrangement of both the loose and the concentrated layers which

develop during the UF process, was implemented. By such an approach, a set of MC boxes, representing the local values of BSA concentration inside the Concentration-Polarization (CP) layers, was obtained.

In the present paper, a stochastic-derived structure was analyzed and a twisted MC/CFD procedure was presented to achieve a micro-CFD scale analysis based on the MC box and, therefore, without exploiting any effective macroscopic coefficient, generally introduced in the literature to characterize the UF process. An on-line linking procedure between the MC box generator and the CFD analysis was implemented by a home-made mesh creator code and a parametric sweep simulation, continuously changing the box structure and, hence, the CP concentration profile, was performed.

Such a procedure allowed obtaining detailed fluid dynamic information about the deposit layer structure without defining any empirical or adjustable parameter but either setting the measurable permeate flux through the filtration system and calculating the pressure drop or imposing the measurable pressure-drop and measuring the flux. The additional resistance as due to cake formation on the membrane surface, R_{add}, was calculated as a function of the operating variables. Moreover, this fundamental result was compared to some previously published approaches, currently available in the literature[11–13].

It is worthwhile observing that the present approach did not make use of any effective parameter since its inputs were represented by the stochastic MC boxes exploited from a computational and rigorous model formulated at microscopic scale, which, in turn, was based on the determination of some fundamental quantities calculated by *ab-initio* methods.

6.2 Computational framework and preliminary results

The present work represents the “chain closure” of the complete multiscale framework developed during this PhD. As already described in detail in the previous chapters, the *ab-initio* approach

allowed acquiring a fundamental knowledge about the characteristics of the considered system, i.e. the quantum mechanics colloidal surface charge at sub-nanoscopic scale[11]. Through a coarse graining methodology, a Monte Carlo based code was developed to simulate the fouling formation. The schematic of such a methodology is shown in Fig.33.

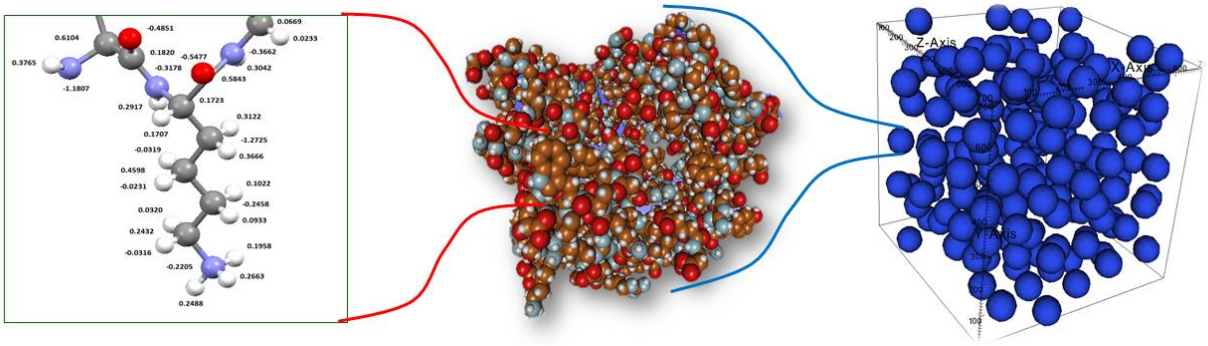

Figure 33: Developed multiscale-framework from sub-nanoscale to nano/microscale level. Point charges on external amino acid atoms (on the left) were coarse grained in total colloid charge of overall macromolecule (in the middle). Moreover, on nano/microscopic scale the MC simulations were performed (on the right).

A volume fraction range was preliminarily necessary to perform the MC simulation tests. For this purpose, a concentration-polarization profile, defined in previous work[11], was used as reference to exploit the input concentrations. A deriving volume fraction starting from 0.05 up to 0.35 resulted in good agreement with most of values of BSA concentrations usually developing in the CP layer, as reported in the literature[4,14]. It is worthwhile remarking that the pre-defined concentration range (or volume fractions) is to be considered as an input to the proposed procedure and can be varied to perform all the simulations that are required to characterize the UF system behavior.

An MC set of simulations was performed in the defined concentration range in order to obtain different representative colloids boxes. The size of the MC box was large enough as compared to the dimension of the colloids but small enough as compared to the dimensions of the physical domain of interest. For a very large simulation box, the size of the corresponding CFD model (actually representing a finite element mesh) could have gone beyond both the memory and computational power of available high-performance computers by many orders of magnitude. For this reason, a

balanced number of particles was fixed to 200 macromolecules. Specifically, the characteristic dimension of resulted box for the analyzed concentration $\phi = 0.2$ was equal to $71nm$ that is large enough on the basis of REV (Representative Element Volume) analysis considerations.

In this way, the corresponding microfluidic complexity across the porous-like structure, was reduced to a few hours of calculation on a standard workstation equipped with two Intel Xeon CPU E5-2609 v2 processors.

To develop the fluid-dynamic analysis of the fouling cake, a method aimed at importing into the CFD computational tool the porous box structures, as obtained from the Monte Carlo simulations, was formulated. The obtained geometry was implemented in Comsol® Multiphysics 5.2 thanks to the modification of the code through Matlab® scripts. The resulting geometry of the randomly displaced macromolecules consisted of the complementary part of the microfluidic field that was represented, in turn, by the external space through the colloid particles. The so defined micro-CFD simulations domain was meshed by the ad-hoc section of the aforementioned CFD tool. The 3D Navier-Stokes problem was computed through the defined mesh geometry after the definition of both the boundary and the initial conditions. The boundary conditions were as follows: no flux through the lateral walls of the box, parallel to the main flux direction (z-axis); a fixed value of flux, J, through the inlet section (x-y plane at z=0) and a zero pressure P_{out}=0 at the box outlet plane (x-y plane at z=L_{box}). A null initial velocity field was imposed as the initial condition too.

As an example, a schematic of MC/CFD procedure was reported in Fig.34.

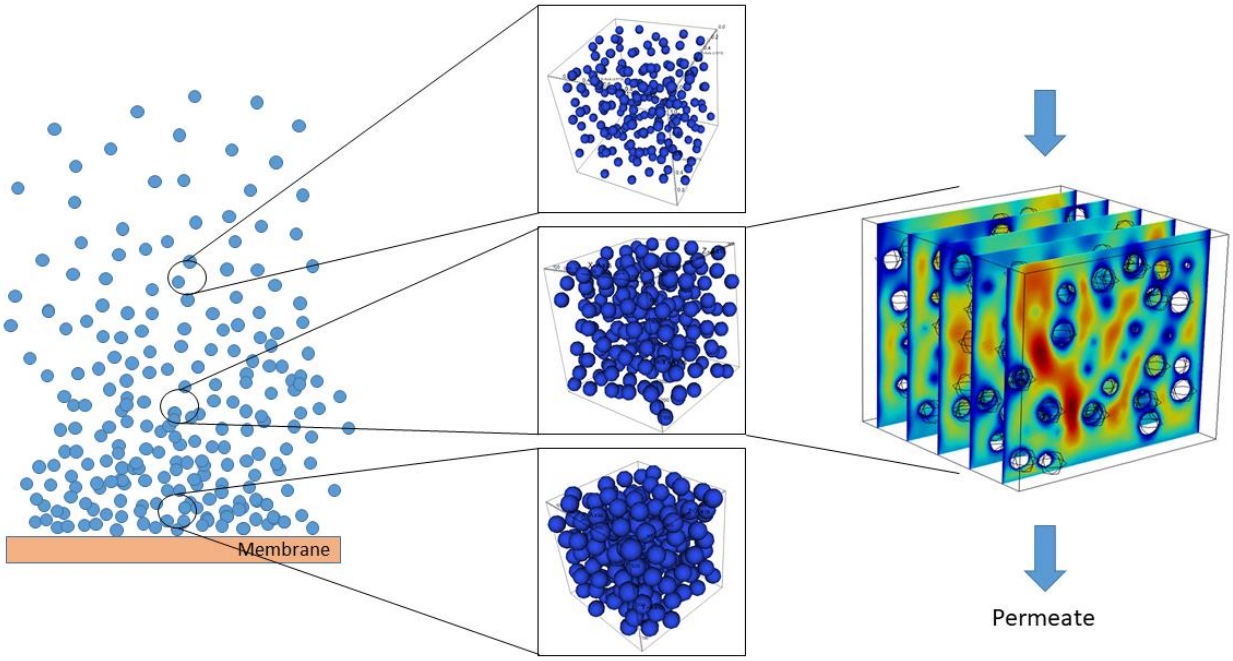

Figure 34: micro-CFD approach to develop a complete fluid dynamic study on the deposited cake layers during membrane filtration. The number of MC-CFD simulations depends on the computational resources.

A set of micro-CFD simulations of pure water flux through the interstitial channels developing within the colloid box was carried out. The velocity and pressure field were, therefore, obtained having chosen the simulation inputs as: number of BSA colloids, N = 200, volume fraction, $\phi = 0.2$, equivalent colloid radius, $a = 32\ \dot{A}$, operating temperature, $T = 300\ K$, permeate flux through the membrane, $J = 5 \cdot 10^{-6}\ m/s$. Considering an inlet x-y plane, chosen as close as possible to z=0, but not coinciding with it in order to avoid the edge effects, an integral average was performed and the pressure drop $\Delta P = 78\ Pa$ across the simulation box, was obtained.

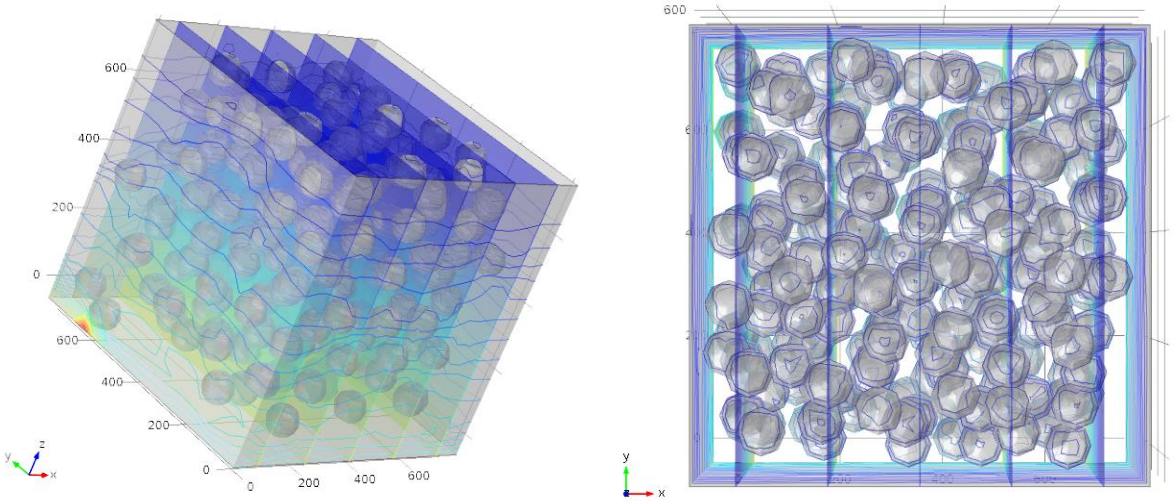

Figure 35:micro-CFD simulation on the MC derived structure. On the left a 3D plot with 5 section planes and 40 constant pressure surfaces. On the right a top view across the simulation box was reported.
$\phi = 0.2\ a = 32\ A\ T = 300\ K\ J = 5 \cdot 10^{-6}\ m/s$

It is to be remarked that the resulted value of average pressure drop is related to the fact that the box had a length of $71nm$. A normalized pressure drop was so defined for a volume fraction of 0.2, $\Delta P_{norm} = 1.1\ Pa/nm$.

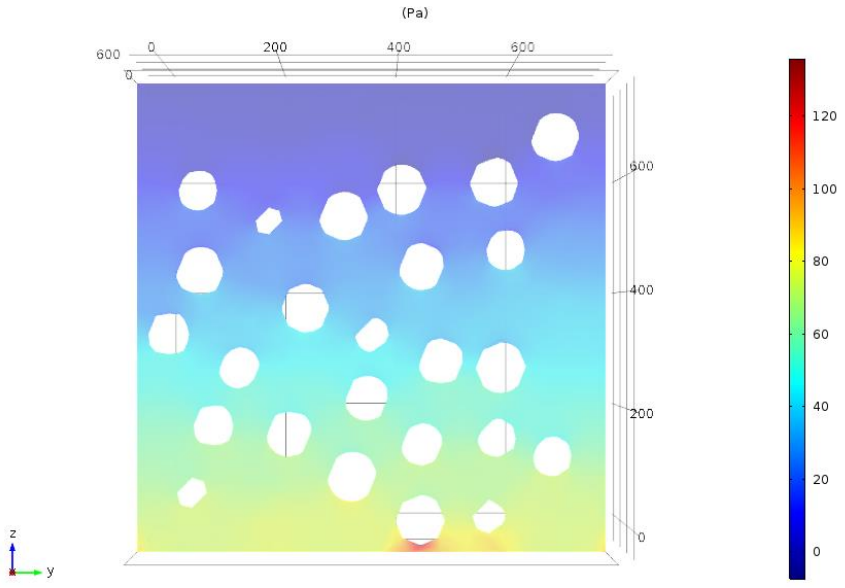

Figure 36: Pressure y-z plane at $x = 35nm$. Pressure color legend in Pa.
$\phi = 0.2\ a = 32\ A\ T = 300\ K\ J = 5 \cdot 10^{-6}\ m/s$

Assuming that the average volume fraction of the cake was equal to $\boldsymbol{\phi = 0.2}$, and estimating a cake thickness from some previously published works[11,15], a total pressure drop across the whole fouling

layers was calculated. In other terms, if the average volume fraction is known, the calculated pressure drop per unit length of the cake can be multiplied by the fouling thickness so to obtain a global pressure drop.

For a membrane Rejection equal to 0.9875 and a total pressure drop $\boldsymbol{TMP = 1.5 bar}$, taking into account the flux curve exploited from Fig.15 of these thesis (chapter 3)[11], a corresponding filtration time was equal to 5min at a permeate flux $J = 5 \cdot 10^{-6}\, m/s$. From this information an equivalent cake thickness of $\boldsymbol{d = 125\, \mu m}$ was estimated in agreement with the previous work[15]. A resulting total pressure drop from the presented model was $\boldsymbol{TMP = \Delta P_{norm} \cdot d = 1.4\, bar}$ with a relative error of 7% compared to original TMP of $\boldsymbol{1.5\, bar}$.

Finally, downstream of the obtained results, the additional resistance R_{add} was estimated on the basis of the well-known resistance-in-series model:

$$J(t) = \frac{TMP - \Delta\Pi}{\eta\,(R_m + R_{add}(t))} \qquad (6.1)$$

Where η was the permeate viscosity and the difference of osmotic pressure, $\Delta\Pi = 22\text{kPa}$, is equal to the quantity calculated on the basis of the analysis performed at mesoscopic scale and shown in Chapter 5. It is worthwhile remarking that the present multiscale model makes use of a series of important fundamental parameters calculated at each of the scales (from nanoscopic to microscopic) that are relevant for the analyzed system. Defining $R_m = 1.57 \cdot 10^{13}\, m^{-1}$ for the polysulfone membrane[12], the additional resistance at time of 5min, $R_{add} = 1.1 \cdot 10^{13}\, m^{-1}$, was obtained. It is meaningful noticing how in a short UF time (5min) the additional resistance rapidly increase becoming quite the same of the membrane resistance. As a comparison, taking into account the fouling resistance curve exploited from Fig.16 of the present thesis (chapter3)[11], a corresponding additional resistance, at filtration time of 5min and membrane rejection of 0.9875, resulted equal to $1.49 \cdot 10^{13}\, m^{-1}$ and so overestimated due to the missing of osmotic pressure.

Compared to the procedure illustrated in chapter 3, here CFD simulation is an upgrade level calculation without resorting to any hypothesis on the elementary packing of the fouling structure. Monte Carlo provide a stochastic simulated box and, due to its randomness, no simple force balance could be implemented. The CFD tools provide the resolution of Navier-Stokes equation giving additional information compared to the balance procedure of chapter 3. Aggregation zones can be predicted for example and preferential paths phenomena could be observed.

6.3 Conclusions

In the present work, a combined Monte Carlo/micro-CFD model was implemented. The overall aim was the calculation of the additional resistance, $\boldsymbol{R_{add}}$, in the cake layers. These macroscopic quantities were calculated starting from the *ab-initio* surface charge obtained by Quantum Mechanic techniques. Moreover, the stochastic based structures were used at the microscopic scale to implement the illustrated procedure for Fluid Dynamic simulations. The pressure drop across the simulation box was calculated out and a normalized value of $\mathbf{1.1}\ \boldsymbol{Pa/nm}$, was obtained taking into account the actual box length. This approach, although very preliminary, proposes a combined micro/macroscale procedure for the detailed CFD simulation of any membrane process. It is worthwhile remarking that such a model showed very satisfactory pressure drop results in comparison to previously validated approaches.

References

(1) Gollub, J. RESEARCH IN FLUID DYNAMICS : Meeting National Needs. *Theor. Appl. Mech.* **2006**.

(2) Teng, J.; Chu, J.-C.; Liu, C.; Xu, T.; Lien, Y.-F.; Cheng, J.-H.; Huang, S.; Jin, S.; Dang, T.; Zhang, C.; et al. Fluid Dynamics in Microchannels. In *Fluid Dynamics, Computational Modeling and Applications*; 2012.

(3) Marcos, B.; Moresoli, C.; Skorepova, J.; Vaughan, B. CFD Modeling of a Transient Hollow Fiber Ultrafiltration System for Protein Concentration. *J. Memb. Sci.* **2009**, *337*, 136–144.

(4) Guo, W.; Ngo, H. H.; Li, J. A Mini-Review on Membrane Fouling. *Bioresour. Technol.* **2012**.

(5) Gov, N.; Zilman, A. G.; Safran, S. Hydrodynamics of Confined Membranes. *Phys. Rev. E - Stat. Physics, Plasmas, Fluids, Relat. Interdiscip. Top.* **2004**.

(6) Pak, A.; Mohammadi, T.; Hosseinalipour, S. M.; Allahdini, V. CFD Modeling of Porous Membranes. *Desalination* **2008**.

(7) Cui, Z. Protein Separation Using Ultrafiltration — an Example of Multi-Scale Complex Systems. *China Particuology* **2005**, *3*, 343–348.

(8) Jianxin, L.; Zhijun, L.; Xiaofei, X.; Wei, W.; Xiaojuan, W.; Fengxia, L. Numerical Investigation of the Membrane Fouling during Microfiltration of Semiconductor Wastewater. *Desalin. Water Treat.* **2016**, *57*, 4756–4768.

(9) Vinther, F.; Jönsson, A. S. Modelling of Optimal Back-Shock Frequency in Hollow Fibre Ultrafiltration Membranes I: Computational Fluid Dynamics. *J. Memb. Sci.* **2016**, *506*, 130–136.

(10) Doering, C. R. The 3D Navier-Stokes Problem. *Annu. Rev. Fluid Mech.* **2009**.

(11) Curcio, S.; Petrosino, F.; Morrone, M.; De Luca, G. Interactions between Proteins and the Membrane Surface in Multiscale Modeling of Organic Fouling. *J. Chem. Inf. Model.* **2018**, *58* (9), 1815–1827.

(12) De Luca, G.; Bisignano, F.; Paone, F.; Curcio, S. Multi-Scale Modeling of Protein Fouling in Ultrafiltration Process. *J. Memb. Sci.* **2014**, *452*, 400–414.

(13) Petrosino, F.; Curcio, S.; Chakraborty, S.; De Luca, G. Enzyme Immobilization on Polymer Membranes: A Quantum and Molecular Mechanics Study. *Computation* **2019**.

(14) Suki, A.; Fane, A. G.; Fell, C. J. D. Flux Decline in Protein Ultrafiltration. *J. Memb. Sci.* **1984**, *21*, 269–283.

(15) F. Petrosino; S. Curcio; G. De Luca. Modellazione Multiscala Dei Processi Di Separazione Di Proteine Mediante Tecnologie a Membrana, University of Calabria, 2015.

Conclusions and future perspectives

In the present PhD thesis, a multiscale paradigm reporting a detailed analysis of the interactions among macromolecules as well as between the macromolecules and the surface of a polymeric membrane was presented. All the objectives concerning this work were addressed by the complex management of different theories formulated and exploited at several scales of detail. Various fields ranging from bioengineering up to process engineering, passing through ICT, CFD and biochemistry areas were opportunely examined and all the related theories, from molecular modeling up to process simulation, were suitably mixed and merged achieving the prefixed goals. Quantum simulations by the well assessed DFT theory, were performed for a complete sub-nanoscopic modelling of macromolecules. The achieved *ab-initio* knowledge allowed coarse graining to a microscopic scale where a stochastic Monte Carlo approach was used to describe the colloids aggregation in the fouling layers of ultrafiltration process. The calculation of osmotic pressure and diffusion coefficient was so attained and different micro-CFD simulations providing an estimation of the additional resistance of proteins deposited on the membrane surface were performed.

Regarding the future perspectives of this work, it is worthwhile noting that an extended *ab-initio* investigation about the effects of different process conditions, like pH, on the fundamental

parameters/inputs controlling the particles interactions, is to be performed. In particular, some refinements on the proposed Quantum Mechanic approach should be also considered, e.g. the calculation of surface total charge in presence of charged external ions. At nano-/microscopic scale, a combined Brownian Dynamics/Monte Carlo approach could be implemented so to describe more accurately the colloids aggregation. Moreover, a biased Monte Carlo approach could be considered to improve the sampling performance thus allowing to describe higher proteins concentrations. The proposed twisted Monte Carlo/Micro-CFD tool could be used to attain a deeper understanding of deposited layers in different membrane process conditions and the previously proposed MC-derived Diffusion Coefficient could additionally be calculated by micro-CFD scale analysis. A fully dynamic coupling of microscale and macroscale simulation models could be implemented to predict the changes in the fouling with time.

The present work points towards a much broader views providing, as compared to the papers available in the literature, a stronger and more versatile approach that can be exploited to investigate different fields of interest for science and technology. Moreover, to bring this multiscale modeling more widespread in engineering application, a complete modeling tool could be developed on the basis of the implemented codes. A user-friendly interface could also make it attractive in industrial processes applications. The illustrated approach allowed for a multiphysics description of many scientific and technological areas, such as material science, chemistry, fluid dynamics, biology and engineering.

Figures index

Figure 1 Characteristics lengths and times of a multiscale methodologies 6
Figure 2 Multiscale framework of the present work 14
Figure 3. Results of radiation-scattering experiments for the radial distribution function of liquid argon near the triple point [27]. 31
Figure 4 Structure of BSA at pH=7 showing valleys and flat regions (right side) and its 2D contact surface (left side) as coming out from the bespoke algorithm. 46
Figure 5 RMSD as function of simulation time (18 ns) at P=1 atm, T =300 K and step 1 fs. 48
Figure 6 BSA-polysulfone (ball-stick) model, tetz, tetx and d variables used to minimize the potential energy 51
Figure 7 Second protein assembled to the first one adsorbed on the surface model (ball-stick). Variables used in the minimization of the potential energy of interaction. 52
Figure 8 Schematic grid representing the three initial positions (red crosses) of a protein belonging to the second layer. Light blue circles represent proteins of the first layer. 54
Figure 9: Schematic representation of the formulated multi-scale model. 57
Figure 10 BSA solution Z-potential measurements performed at three pH and two NaCl concentrations. 60
Figure 11 Schematic grid to represent the optimized positions of one protein belonging to the second layer of the compact deposit on the polymer surface (red crosses: Opt_near initial height = 100 Å Opt_far initial = 400 Å). Proteins of the first layer in blue 61
Figure 12 Center-to-center equilibrium distance (dotted arrow) obtained by MM optimizations, equivalent radius (continuous arrow) obtained from the protein contact surface and $h_{min,}$ (lower bound) calculated from the difference between equilibrium distance and equivalent diameter. 62

Figure 13 Protein-protein distance vs number of layers a) for different transmembrane pressures, Rej=0.9875, t=15s; b) for different filtration times, Rej = 0.9875, TMP = 1.5 bar; c) for the old and new models at different filtration times, Rej = 0.9875, TMP = 2 bar, t = 30, 300, 900 s. 65

Figure 14 Comparison between simulated and experimental permeate flux decay using Rej = 0.9875. Details of the measurements can be found in ref.[12]. 66

Figure 15 Permeate flux vs simulation time at = 1.5 bar for different membrane rejections. 67

Figure 16 Additional resistance vs simulation time at TMP = 1.5 bar for different membrane rejections. 67

Figure 17 Permeate flux vs simulation time using Rej=0.9875 and the considered TMP. 68

Figure 18 Decays of the permeate fluxes as obtained by the new and previous work: a) Rej= 0.985 and TMP= 2 bar; b) Rej 0.99, TMP =1.5 bar. 69

Figure 19 PTE on polysulfone surface, d= protein-surface distance, tetz and tetx protein rotations around Z and X axis, respectively, used for the calculation of the interaction energy. 83

Figure 20 Enzyme-PSU interaction energy, U_{tot}, versus enzyme-surface distance obtained by QM/MM calculations 84

Figure 21 Adsorbed PTE on the PSU model surface in the global minimum (-107.96 Kcal/mol at 30 Å). (a) and (b) side and top view of the contact surface, respectively; (c) and (d) side and top view of full enzyme in the same orientation, respectively. Zinc atoms were shown in fuchsia. 86

Figure 22 Adsorbed PTE on the PSU surface at d=30 Å but rotated by 90 degrees around the X axis. (a) and (b) top and side view of the contact surface. Zinc atoms were shown in fuchsia. .. 87

Figure 23 Adsorbed PTE on the PSU model in the local minima. (a) and (b) side and top view of the PTE-PSU structure corresponding to minimum with interaction energies of -97.57 Kcal/mol at 27 Å., respectively; (c) and (d) side and top view of the PTE-PSU structure corresponding to minimum with interaction energies of -82.44 Kcal/mol at 35 Å, respectively. Zinc atoms were shown in fuchsia 88

Figure 24: First random configuration of an MC box. 101

Figure 25:Concentration-polarization profile discretization for a volume fraction set choice. BSA ultrafiltration on polysulfone membrane TMP=1.5bar, membrane Rejection Rej=0.9875, for a filtration time of 3200s (considered curve)[15] 106

Figure 26: Total energy profile as function of MC iterations for different volume fractions. 107

Figure 27 Hard-Sphere potential RDFs validations. + is the MC simulation points, lines the HNC theory results. r/a is the normalized distance with colloids radius a. Z=15.82, I=0.15M, pH=7, a=32 Å, σ=64 Å, T=300 K.....108
Figure 28 Yukawa potential RDFs validations. + is the MC simulation points, lines the HNC theory results. r/a is the normalized distance with colloids radius a. Z=15.82, I=0.15M, pH=7, a=32 Å, σ=64 Å, T=300 K.....108
Figure 29 Total energy as function of volume fraction for Yukawa potential total energy. 109
Figure 30 Osmotic pressure comparison as function as colloid concentration between the presented model Monte Carlo results (black dots), HNC theory results (red line) and experimental data. Ionic Strength 0.15M, pH=7. Concentration in g/L in agreement with literature[11].....110
Figure 31 Model predicted osmotic Pressure of the fouling cake as function of volume fraction during ultrafiltration process for Yukawa potential formulation. Total osmotic pressure in continuous line and the three different contributions basing on Eq.4. Z=15.82, I=0.15M, pH=7, a=32 Å, σ=64 Å, T=300 K.....111
Figure 32 Model predicted diffusion coefficient, D_c/D_0, of the fouling cake as function of volume fraction during ultrafiltration process for Yukawa potential formulation. D_0=7.7 10^{-11} m^2/s 112
Figure 33: Developed multiscale-framework from sub-nanoscale to nano/microscale level. Point charges on external amino acid atoms (on the left) were coarse grained in total colloid charge of overall macromolecule (in the middle). Moreover, on nano/microscopic scale the MC simulations were performed (on the right). 124
Figure 34: micro-CFD approach to develop a complete fluid dynamic study on the deposited cake layers during membrane filtration. The number of MC-CFD simulations depends on the computational resources. 126
Figure 35:micro-CFD simulation on the MC derived structure. On the left a 3D plot with 5 section planes and 40 constant pressure surfaces. On the right a top view across the simulation box was reported.....127
Figure 36: Pressure y-z plane at $x = 35nm$. Pressure color legend in Pa.....127
Figure 37 Permeate flux vs simulation time at TMP= 2 bar.....138
Figure 38 Permeate flux vs simulation time at TMP= 2.5 bar.....138
Figure 39 Permeate flux vs simulation time at TMP= 3 bar.....139
Figure 40 Additional resistance vs simulation time at TMP = 2 bar. 139
Figure 41 Additional resistance vs simulation time at TMP = 2.5 bar 140

Figure 42 Additional resistance vs simulation time at TMP = 3 bar 140
Figure 43 Permeate flux vs simulation time at Rej= 0.9825. 141
Figure 44 Permeate flux vs simulation time at Rej= 0.985. 141
Figure 45 Permeate flux vs simulation time at Rej= 0.99. 142
Figure 46. Radial distribution functions for a set of monte carlo simulations parametric in volume fraction. 150
Figure 47 Model predicted osmotic Pressure of the fouling cake as function of volume fraction during ultrafiltration process for Yukawa potential formulation. Total osmotic pressure in continuous line and the three different contributions. $Z = 15.82$, $I = 0.15M$, $pH = 7$, $T = 300\ K$. 151
Figure 48 Model predicted osmotic Pressure of the fouling cake as function of volume fraction during ultrafiltration process for Yukawa potential formulation. Total osmotic pressure in continuous line and the three different contributions. $Z = 20.07$, $I = 0.15M$, $pH = 7$, $a = 32$ Å, $T = 300\ K$ 152
Figure 49 Model predicted osmotic Pressure of the fouling cake as function of volume fraction during ultrafiltration process for Yukawa potential formulation. Total osmotic pressure in continuous line and the three different contributions. $Z = 15.82$, $I = 0.001M$, $pH = 7$, $a = 32$ Å, $T = 300\ K$ 153
Figure 50 Model predicted osmotic Pressure of the fouling cake as function of volume fraction during ultrafiltration process for Yukawa potential formulation. Total osmotic pressure in continuous line and the three different contributions. $Z = 15.82$, $I = 0.001M$, $pH = 7$, $a = 32$ Å, $T = 300\ K$ 154

Appendix A

In these part of appendix supplementary results about chapter 3 were reported.

Permeate fluxes, J(t), at different *Rej* were showed in the following Figs for TMP= 2 bar, 2.5 bar and 3 bar, respectively.

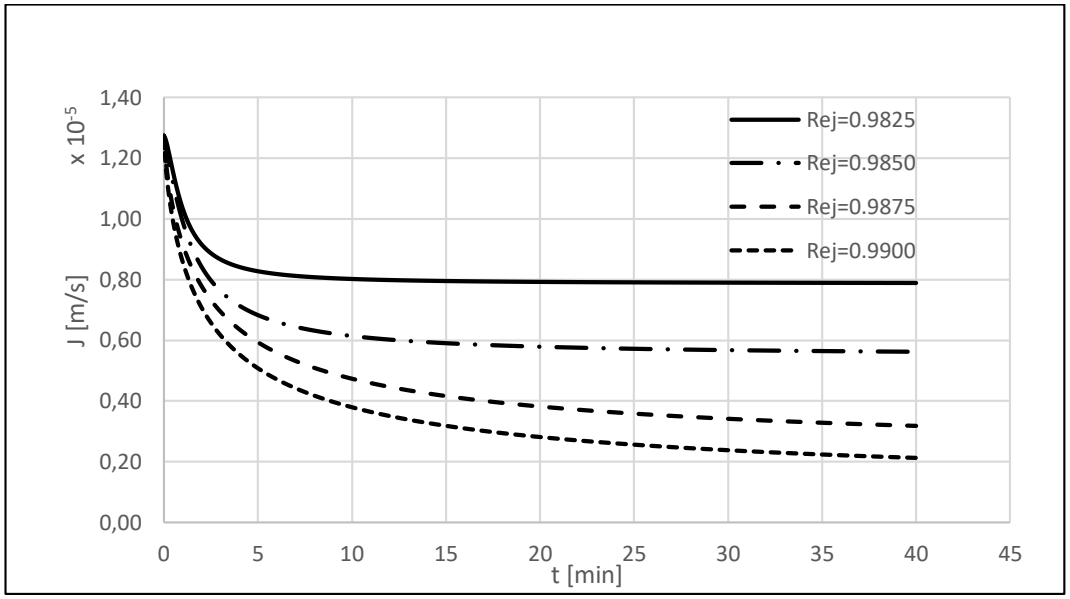

Figure 37 Permeate flux vs simulation time at TMP= 2 bar.

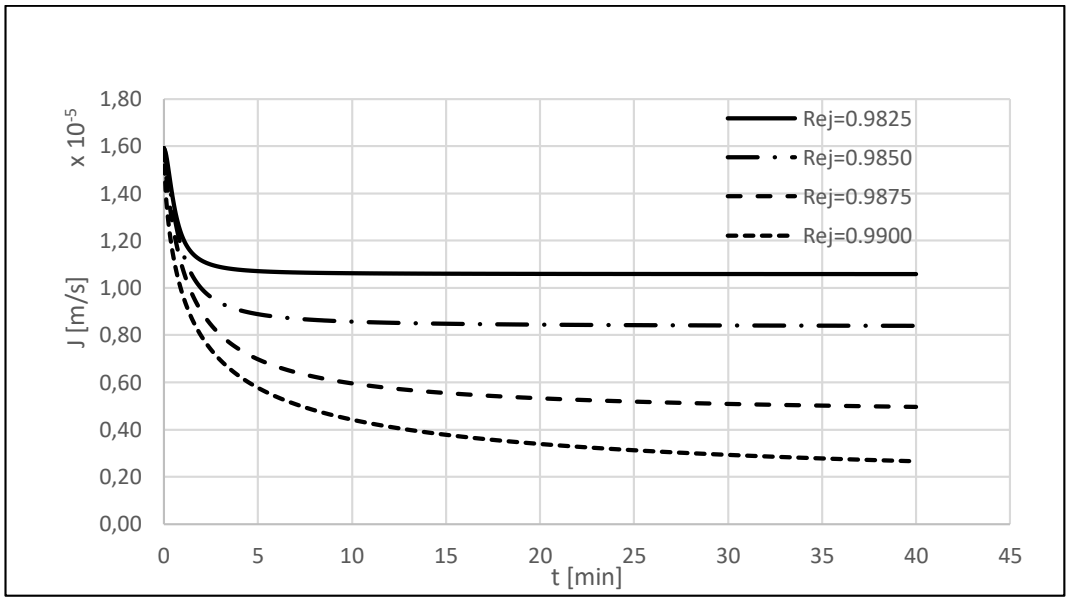

Figure 38 Permeate flux vs simulation time at TMP= 2.5 bar.

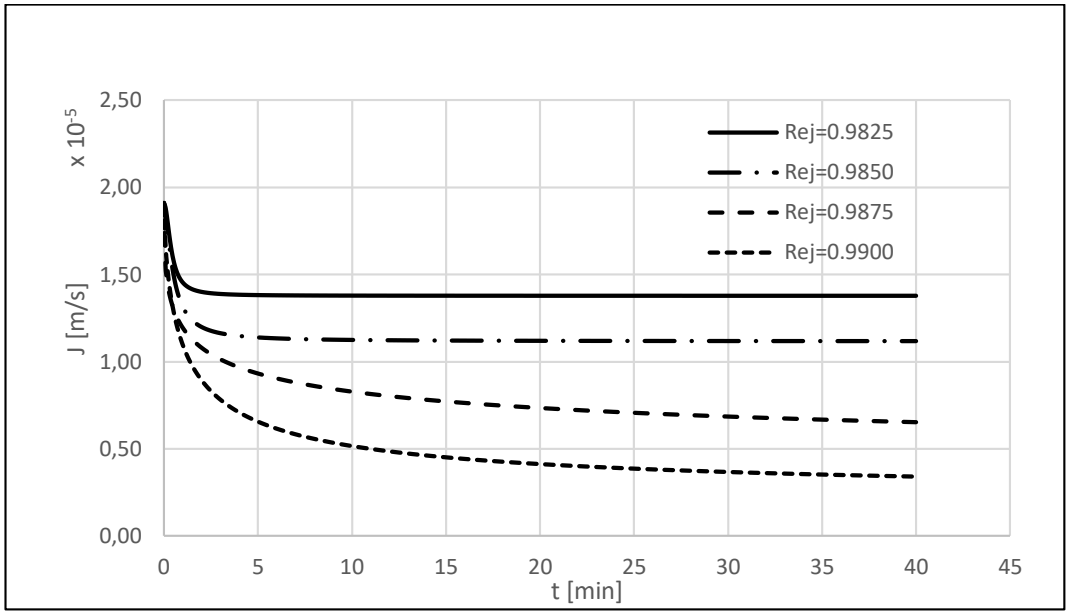

Figure 39 Permeate flux vs simulation time at TMP= 3 bar.

Moreover, additional resistances, R_{ad} (t), at different *Rej* were showed in the following Figures for TMP= 2 bar, 2.5 bar and 3 bar, respectively.

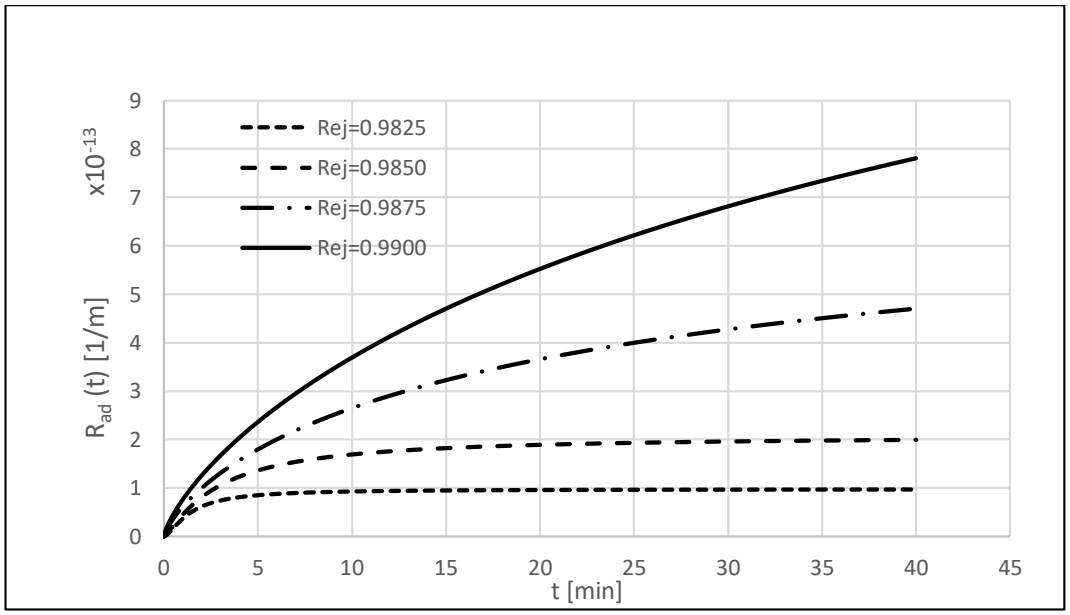

Figure 40 Additional resistance vs simulation time at TMP = 2 bar.

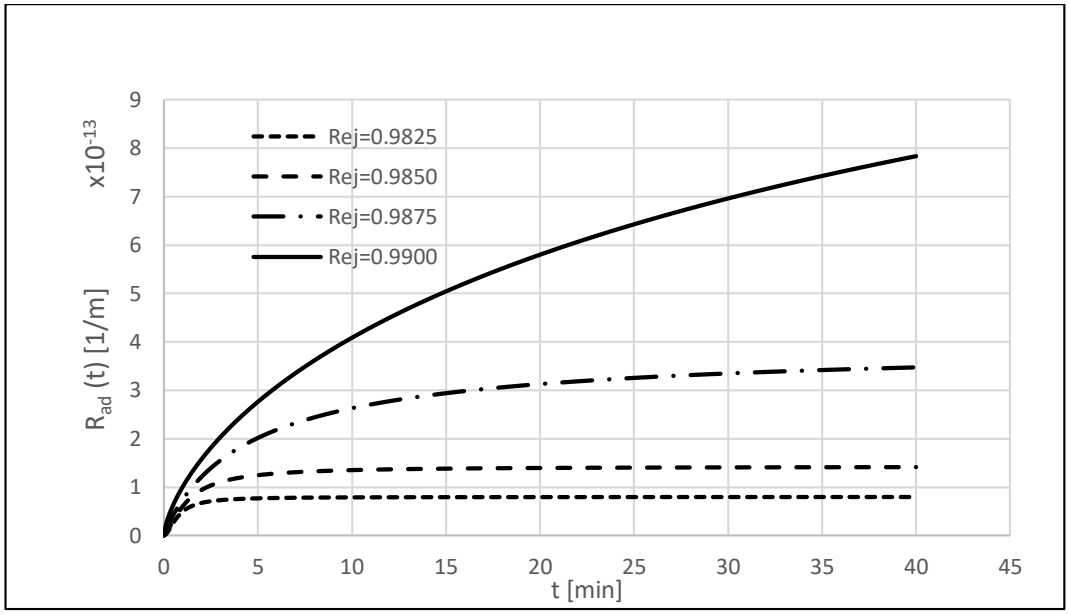

Figure 41 Additional resistance vs simulation time at TMP = 2.5 bar

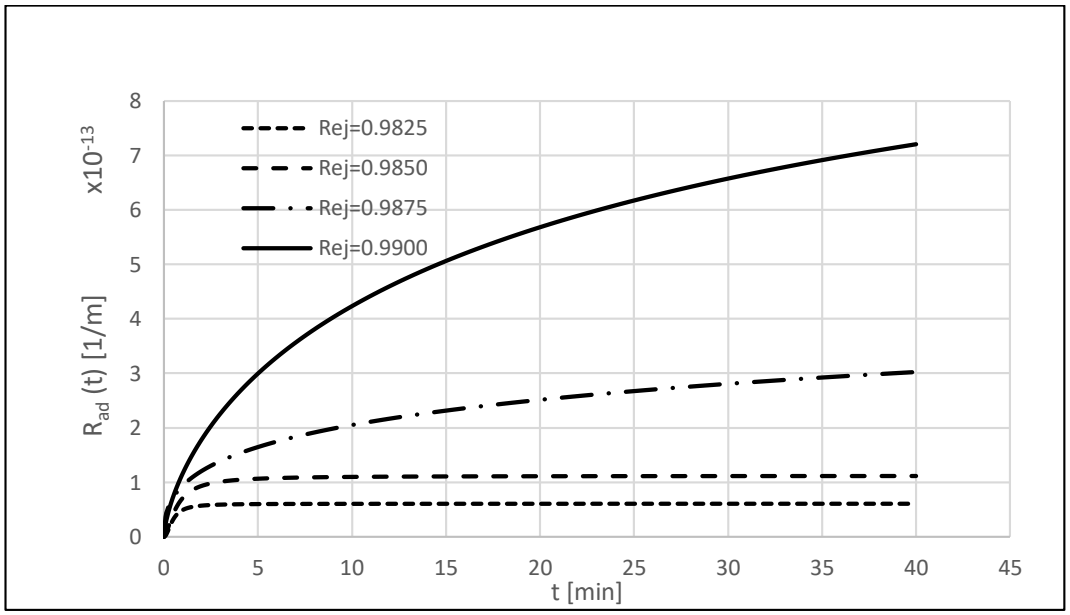

Figure 42 Additional resistance vs simulation time at TMP = 3 bar

Permeate fluxes decay for Rej= 0.9825, 0.985 and 0.99, respectively, were showed in the following Figures.

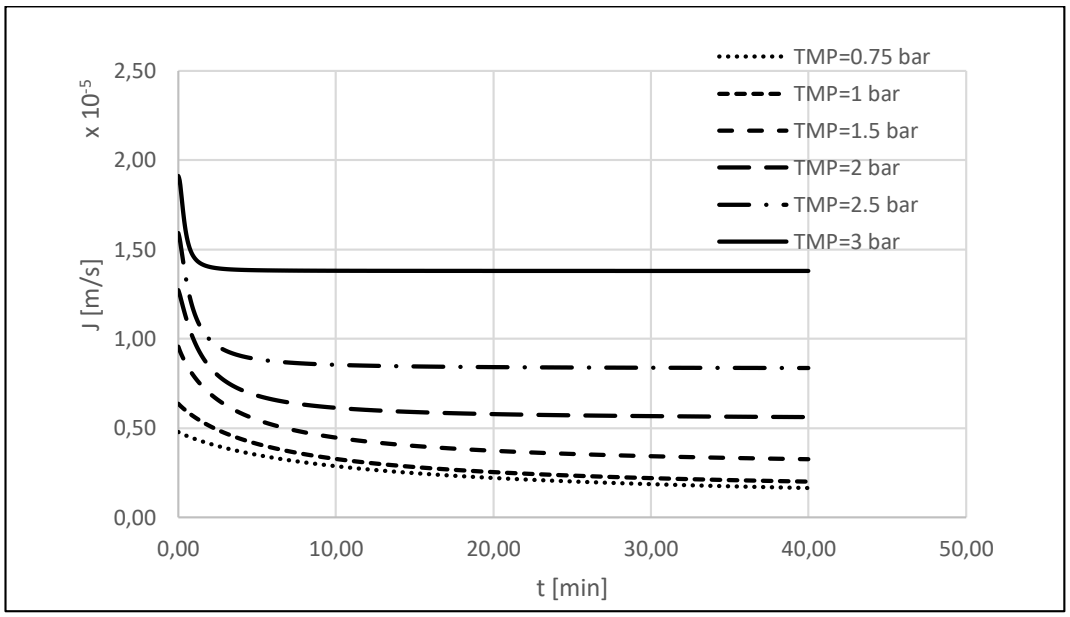

Figure 43 Permeate flux vs simulation time at Rej= 0.9825.

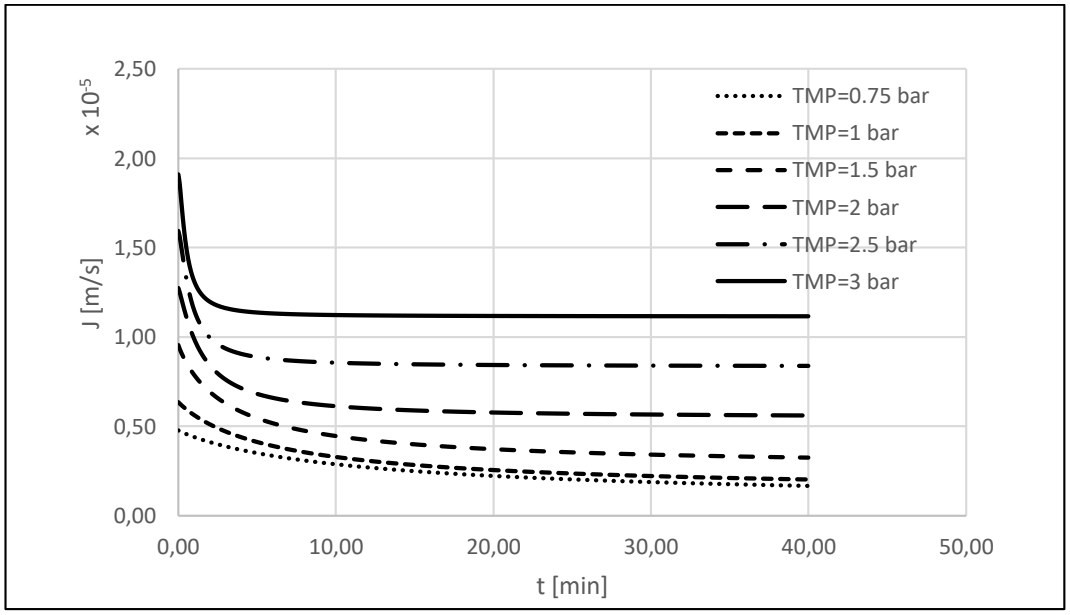

Figure 44 Permeate flux vs simulation time at Rej= 0.985.

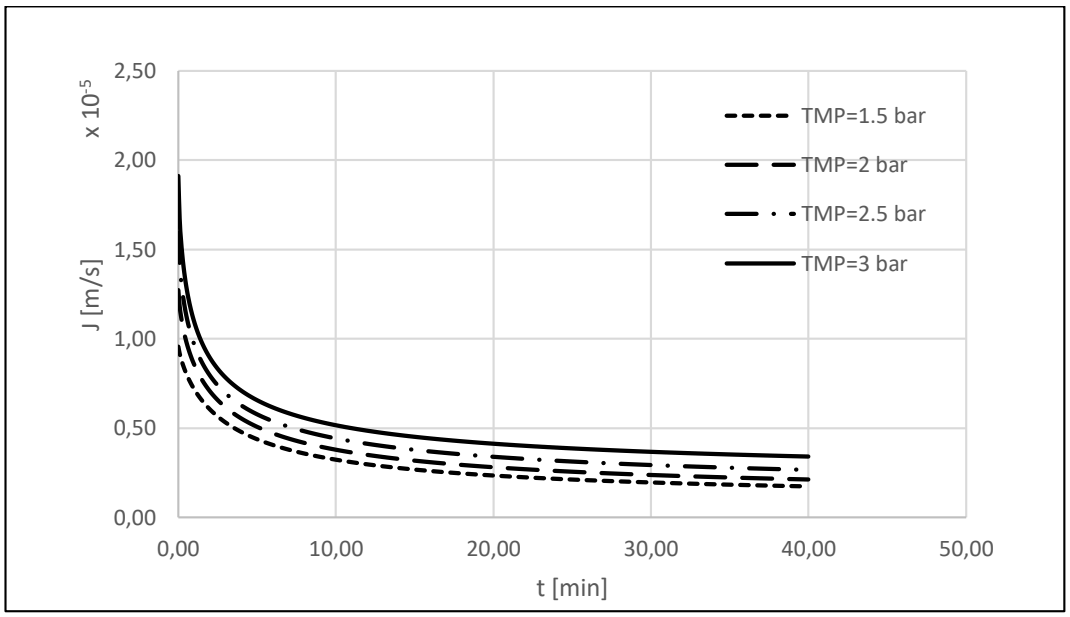

Figure 45 Permeate flux vs simulation time at Rej= 0.99.

Appendix B

In this part of appendix a few of the developed codes were reported.

Concerning the external amino-acid search on the macromolecules the main code was reported:

```
function skin_mod(delta,n_grid,str)

%% ############################################################################

%this function generates a .pdb file whit the external amino-acids of the
%macromolecule reading an input file "centered.pdb"

% INPUTS: -delta, skin depth
%         -n_grid, number of grid search
%         -centered.pdb macromolecule .pdb file
%         -'str' string of output file
% OUTPUT: -file skin.pdb with external aminoacids

%% ############################################################################

%% %INPUT%%%%%%%%%%%%%%%%%%%%%%%%%%%%%%%%%%%%%%
pdbstruct = pdbread('centrato.pdb');
%%%%%%%%%%%%%%%%%%%%%%%%%%%%%%%%%%%%%%%%%%%%%%%%%%%%%%%%%%%

%% %% N SEARCH %%%%%%%%%%%%%%%%%%

elc=[pdbstruct.Model.Atom.element]';
seq=[pdbstruct.Model.Atom.resSeq]';
xyzstruct=[pdbstruct.Model.Atom.X; pdbstruct.Model.Atom.Y;
pdbstruct.Model.Atom.Z]';
xyzmod=[xyzstruct,seq];
%.xyz file with N
s=1;
l=length(xyzmod(:,1));
for i=1:l
   if elc(i,1)=='N'
     xyzmod_N(s,:)=xyzmod(i,:);
     s=s+1;
   end
end

%% %% N SEARCH IN THE SKIN %%%%%%%%%%%%%%%%%%%%%%%%%%%%
Rmax=calc_Rmax(pdbstruct);
dteta=2*pi()/n_grid;
circonf=2*pi()*Rmax;
passo=circonf/n_grid;
ymax=passo/2;
ymin=-ymax;
zmax=ymax;
zmin=-zmax;
xyzmod_Nskin=xyzmod_N;
```

```
for i=0:n_grid
    xyzmod_Nskin=rotazione_mod(xyzmod_Nskin,'y',dteta);
    for j=0:n_grid
        xyzmod_Nskin=rotazione_mod(xyzmod_Nskin,'z',dteta);
        xyzmod_Nskin=skin_N(xyzmod_Nskin,ymax,ymin,zmax,zmin,delta);
    end
end

%% %% FILE .PDB WITH SKIN AMINOACIDS%%%%%%

%l=structure initial length
l_xyzmod_Nskin=length(xyzmod_Nskin);

%duplicates elimination of N%%%%
q=2;
while q<=l_xyzmod_Nskin
    if xyzmod_Nskin(q,4)==xyzmod_Nskin(q-1,4)
        xyzmod_Nskin(q,:)=[];
        q=q-1;
        l_xyzmod_Nskin=l_xyzmod_Nskin-1;
    end
    q=q+1;
end
%%%%%%%%%%%%%%%%%%%%%%%%%%%%%%%%%%%%%%%%%%%%%%%%%%%%%

finito=false;
i=1;
while ~finito
    trovato=false;
    for k=1:l_xyzmod_Nskin
        if pdbstruct.Model.Atom(i).resSeq==xyzmod_Nskin(k,4)
            trovato=true;
            break
        end
    end
    if ~trovato
        pdbstruct.Model.Atom(i)=[];
        i=i-1;
        l=l-1;
    end
    if i==l
        finito=true;
    end
    i=i+1;
end
pdbwrite(str, pdbstruct);

end
%########################################################################

function xyzmod_Nskin=skin_N(xyzmod_Nskin,ymax,ymin,zmax,zmin,delta)

%%% xmax e xmin search%%%%%%%%%%%%%%%%%%%%%%%%%%%%%%%%%%%%%%%%%%%%%%%%%%%%%
l=length(xyzmod_Nskin(:,1));
trovati=false;
xmax=0;
for i=1:l
    if xyzmod_Nskin(i,1)>0 ...
        && xyzmod_Nskin(i,2)>ymin && xyzmod_Nskin(i,2)<ymax...
```

```
        && xyzmod_Nskin(i,3)>zmin && xyzmod_Nskin(i,3)<zmax
        if xyzmod_Nskin(i,1)>xmax
            xmax=xyzmod_Nskin(i,1);
        end
        trovati=true;
    end
end

xmin=xmax-delta;

%%%%N deleting%%%%%%%%%%%%%%%%%%%%%%%%%%%%%%%%%%%%%%%%
l1=l;
if trovati
j=1;
while j<=l1
    if xyzmod_Nskin(j,1)>0 ...
        && xyzmod_Nskin(j,2)>ymin && xyzmod_Nskin(j,2)<ymax...
        && xyzmod_Nskin(j,3)>zmin && xyzmod_Nskin(j,3)<zmax...
        && xyzmod_Nskin(j,1)<xmin
        xyzmod_Nskin(j,:)=[];
        j=j-1;
        l1=l1-1;
    end
    j=j+1;
end
end
end

%%%%%%%%%%%%%%%%%%%%%%%%%%%%%%%%%%%%%%%%%%%%%%%%%%%%%%%%%%%%%%%%%%%%%%%%%%%%

function Rmax=calc_Rmax(pdbstruct)

Mol1=[pdbstruct.Model.Atom.element]';
l=length(Mol1);
Mol=ones(l,4);
for i=1:l
    if Mol1(i)=='H'
        Mol(i,1)=1.2;
    elseif Mol1(i)=='O'
        Mol(i,1)=1.4;
    elseif Mol1(i)=='C'
        Mol(i,1)=1.5;
    elseif Mol1(i)=='S'
        Mol(i,1)=1.75;
    elseif Mol1(i)=='N'
        Mol(i,1)=3;
    end
end
Mol(:,2)=[pdbstruct.Model.Atom.X]';
Mol(:,3)=[pdbstruct.Model.Atom.Y]';
Mol(:,4)=[pdbstruct.Model.Atom.Z]';

[~,a1,a2]=mcs_simply(Mol);

str=Mol(:,2:4);
r1=sqrt(sum((str(a1,:).^ 2)));
r2=sqrt(sum((str(a2,:).^ 2)));
Rmax=max(r1,r2);
end
```

The total energy function calculation with periodic boundary conditions used by Monte Carlo code is reported.

```
function Utot=total_energy(X,a,L_box,d_min,z,k,Kb,T,lB)
%%
%function calculates total DLVO energy [J] of data amount of macromolecules
%with same radius a and x,y and z positions data in matrix X (every line have
x,y and z in the 1th, 2th and 3th column)
%
% - X matrix xyz
% - a particle radius                                    [A]
% - L_box                                                [A]
% - d_min minimum centre to centre distance              [A]
% - z colloid charge number                              [-]
% - k 1/debye_lenght                                    [1/m]
% - Kb boltzmann constant                               [J/K]
% - T simulation temperature                             [K]
% - lB Bjerrum length                                    [m]

%% %%%%%%%%%%%%%%%%%%%% TOTAL ENERGY %%%%%%%%%%%%%%%%%%%%%%%%%%%%%%%%%%%%%%%%
Uelc = 0;    % double layer interactions
Uvdw = 0;    % van der waals interactions
Uborn= 0;    % born repulsion non-DLVO interactions
N_box = length(X(:,1));
for i=1:N_box
    for j=1:i-1
        for xx = -1:1                       % periodicity interactions
            for zz = -1:1                   % periodicity interactions
                for ll = -1:1               % periodicity interactions
                   hij = norm ( X(i,:) - ( [xx,zz,ll] * L_box + X(j,:) ) ); %[A]

                   %%%%%%%% Energy Calculation %%%%%%%%%%%%%%%%%%%%%%
%%                 % BORN COPENETRATION CRITERIA EXCLUSION
                   if hij < d_min %(2*a+d_min)
                       Utot=1E20;
                       return
%if there is an overlapping the command stop the calculations and function
return Utot = 1E20 J ;
                   end
%%                 % ELECTROSTATIC term
                   % Yukawa potential     Roa Nagele 2018 eq 10
                    Uelc = Uelc + (Kb*T) * lB * z^2 * (exp(k*a*1e-10)/(1+k*a*1e-
10))^2 * exp(-k*hij*1e-10) / (hij*1e-10);  %a and hij in [A]

%%                 % VAN DER WAALS term with Hamaker approach
                    %see Gerhard Nagele book
                   Uvdw = Uvdw - H/6 * ( ( 2*(a*1E-10)^2 / ((hij*1E-10)^2-
4*(a*1E-10)^2) ) + ( 2*(a*1E-10)^2 / (hij*1E-10)^2 ) + log(1 - 4*(a*1E-
10)^2/(hij*1E-10)^2) );  %a and hij in [A]
                   %%%%%%%%%%%%%%%%%%%%%%%%%%%%%%%%%%%%%%%%%%%%%%%%%%%%%%
                end
            end
        end
    end
end
Utot=(Uelc+Uvdw+Uborn); %[J]
end
```

The Monte Carlo code is reported here (without other auxiliary and post processing functions)

```
function [X_ads,Utot,Nm,tot_it,err]=MC_eff_par(seed,fi)
%% this function simulates adsorption whit Metropolis Monte Carlo NVT approach
in full space 3D
%
%  Note: to launch in an empty folder with imput_MC_par.m file
%%
%see plotsMC.m and input_MC.m
%
% INPUTS:  -input_MC_par.m
%          -random number generation seed
%          -fi volume fraction

% OUTPUTS: -X_ads = adsorbed matrix xyz;
%          -Utot  = Utot vector;
%          -Nm    = number of random movements that was performed
%          -err   = error vector of random movements
%
% OUTPUT FILES AND PLOT:  -plotsMC.m

close all; clc;

%% %%%%%%%%%%%%%%%% INPUTS %%%%%%%%%%%%%%%%%%%%%%%%%%%%%%%%%%%%%%%%%%%%%%%%

MC_inputs;
[ Zeff , keff ]=eff_par_calc(a,fi);  %effective parameter calculation
z=Zeff;
k=keff;
rng(seed);     %random number generation seed

%% %%%%%%%%%%%%%%%%%%%%%% void fraction control %%%%%%%%%%%%%%%%%%%%%%%%%%%%%

Vs = 4/3 * pi() * a^3 * N ;   %volume of all macromolecules
L_box = (Vs / fi)^(1/3) ;     %box  length
eps_max = 0.9 * 0.74048 ;     % 90% of the maximum packing factor (HCP packing)

if fi > eps_max
    disp('void fraction error --> number of macromolecules too high')
else

%% %%%%%%%%%%%%%%%% folder for all calculations %%%%%%%%%%%%%%%%%%%%%%%%%%%%%

str_fold=['BSA=',num2str(N),'_eps=',num2str(fi),'_Lbox=',num2str(L_box*1E-
1),'nm_T=',num2str(T),'K_seed=',num2str(seed)];
mkdir(str_fold);
cd(str_fold);
fold1 = 'Ads_xyz'  ; mkdir(fold1);
fold2 = 'gr'  ; mkdir(fold2);

%% %%%%%%%%%%%%%%%%%%%%%%%% MC_first_step %%%%%%%%%%%%%%%%%%%%%%%%%%%%%%%%%%

Tic
%%%%%%% first molecule sampling %%%%%%%%%%%%%%%%%%%%%%%%%%%%%%
X_ads = rand(1,3) * L_box ;

%%%%%% complete the first random sampling for all macromolecules %%%%%%
```

```
i=2;
while i<=N
    X_ads(i,:)=rand(1,3)*L_box;
    Utot=total_energy(X_ads,a,L_box,d_min,z,k,Kb,T,lB);    %TOTAL ENERGY
    if Utot<Utot_max
        i=i+1;
    end
end

%% %%%%%%%%%%%%%%%%%%%%%%%%%%%% MC random moves %%%%%%%%%%%%%%%%%%%%%%%%%%%%

err(1)=1;
Nm=0;             %number of right moves
Utot(1)=Utot;

tot_it=0; %total iterations

% for iter=1:Max_iter
while Nm<Max_iter

    tot_it=tot_it+1;

    %random molecule
    N_rand=randi(N,1);

    %new ads_mat
    X_ads_new=X_ads;
    X_ads_new(N_rand,:) = X_ads_new(N_rand,:) + (rand(1,3)-0.5) * a;
%L_box; %new random position for mol N_rand
    out = ( X_ads_new(N_rand,:)<0 | X_ads_new(N_rand,:)>L_box );
%logical array to check if molecule is out of the box
    while any(out)
%while molecule is out of the box repeate moves of N_rand molecule
        X_ads_new=X_ads;
        X_ads_new(N_rand,:) = X_ads_new(N_rand,:) + (rand(1,3)-0.5) * a;
        out = ( X_ads_new(N_rand,:)<0 | X_ads_new(N_rand,:)>L_box );
    end

    %new energy
    Utot_new=total_energy(X_ads_new,a,L_box,d_min,z,k,Kb,T,lB);

%TOTAL ENERGY CALCULATION

        Beta=1/(Kb*T);                          %MC factor
        dU=Utot_new-Utot(Nm+1);
        Pr(Nm+1)=exp(-Beta*dU);                 %MC probability

    if Utot_new<Utot(Nm+1)                      %if energy is decreasing
        X_ads=X_ads_new;
        Utot(Nm+2)=Utot_new;
        Nm=Nm+1;

    else                                       %if energy is increasing
        Rand=rand(1);
        if Rand<Pr(Nm+1)                       %if probability is high enough
            X_ads=X_ads_new;
            Utot(Nm+2)=Utot_new;
            Nm=Nm+1;
```

```
        end
    end


%%%%%%%%%% write and plots during iterations %%%%%%%%%%%%%%%%%%%%%%
    if mod(Nm,d_gr)==0 || Nm==0 || Nm==Max_iter
        plotsMC_par(lay_tick,L_box,X_ads,N,Nm,Utot,Pr,fold1,fold2);
    end
%%%%%%%%%%%%%%%%%%%%%%%%%%%%%%%%%%%%%%%%%%%%%%%%%%%%%%%%%%%%%%%%%%%%%%%
end
cd ..
if Nm>=Max_iter
    str=['for BSA=',num2str(N),'_eps=',num2str(fi),'_seed=',num2str(seed),' -->
Max_iter was reached'];
    disp(str);
end
toc
end
end
```

Appendix C

In this part of appendix different extra results concerning the chapter 5 are reported.

A comparison between radial distribution functions for two different ionic strengths $I = 0.15M$ and $I = 0.001M$ was firstly performed.

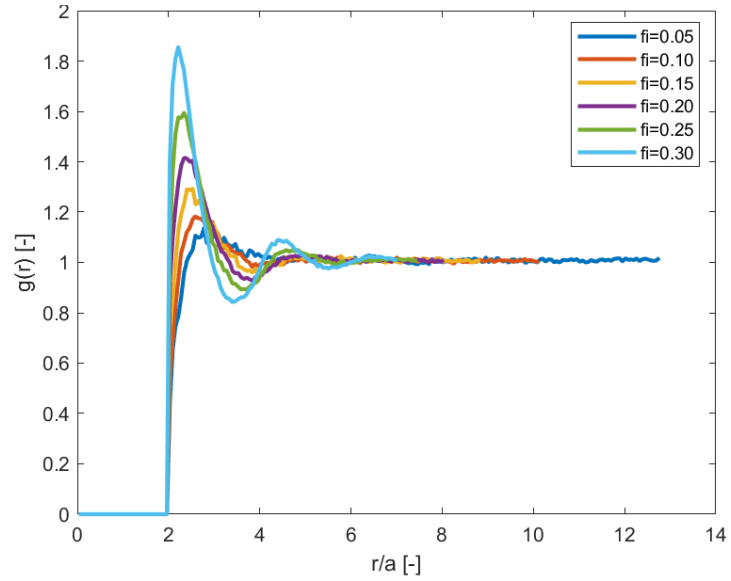

a) $I = 0.15M$

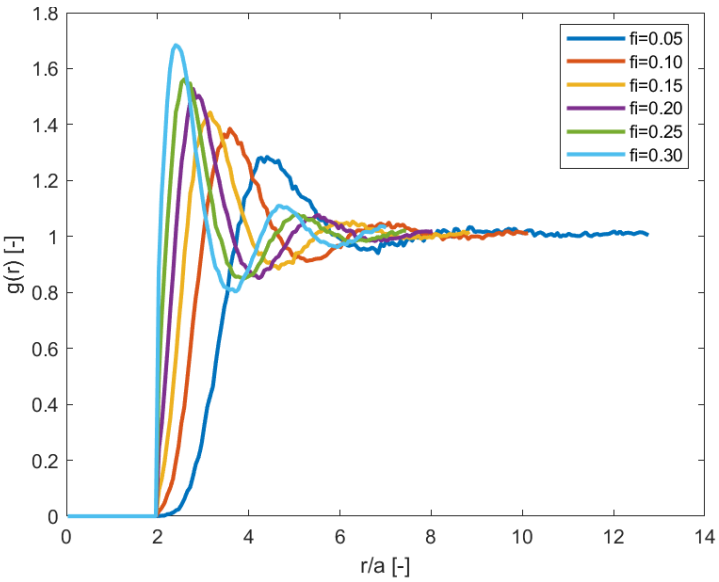

b) $I = 0.001M$

Figure 46. Radial distribution functions for a set of monte carlo simulations parametric in volume fraction. $Z = 15.82$, $pH = 7$, $a = 32$ Å, $T = 300$ K.

Different macromolecule equivalent radius approach was compared:

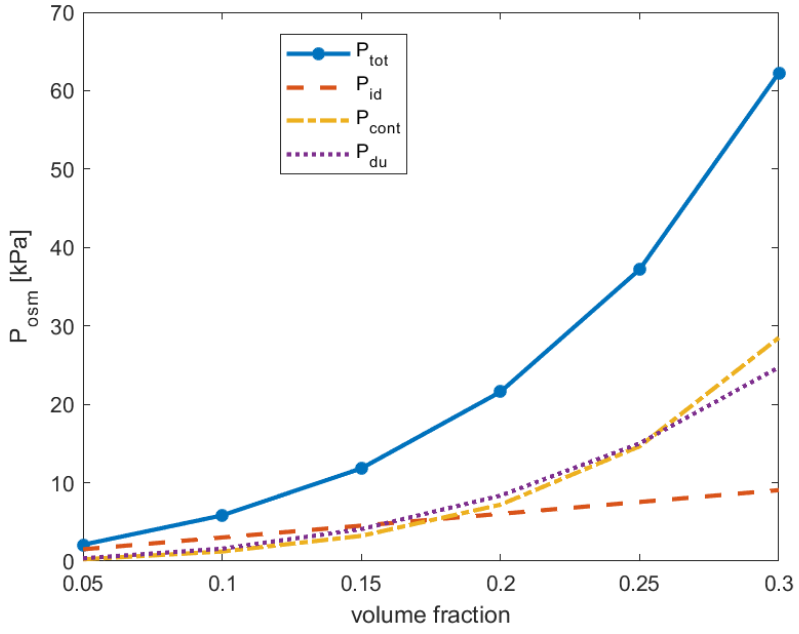

a) $a = 32$ Å

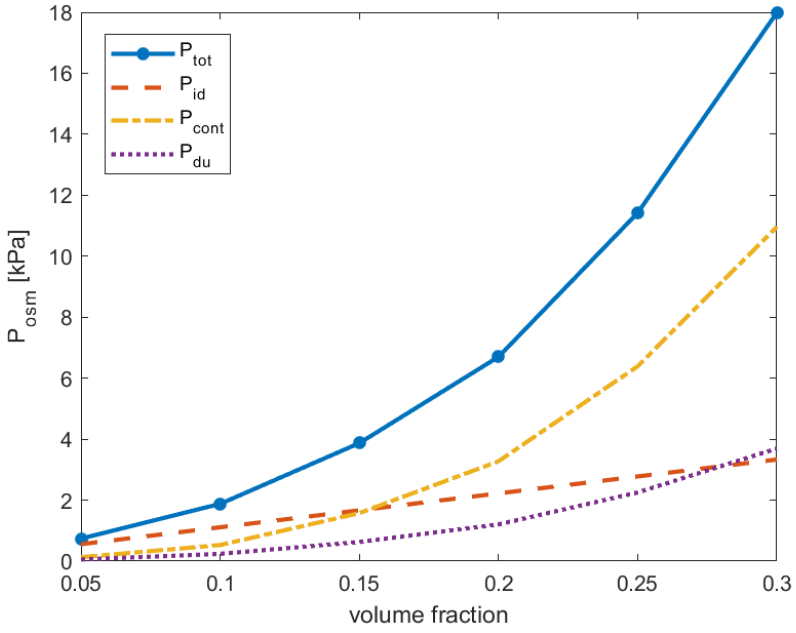

b) $a = 44.6$ Å

Figure 47 Model predicted osmotic Pressure of the fouling cake as function of volume fraction during ultrafiltration process for Yukawa potential formulation. Total osmotic pressure in continuous line and the three different contributions. $Z = 15.82, I = 0.15M, pH = 7, T = 300\ K$.
Process conditions: TMP=1.5bar, Rej=0.9875, t=3200s.

A strong dependence on macromolecule radius was observed both on the total osmotic pressure and on the contact term pressure percentage contribution.

Changing the total charge number, Z, a smooth variation was observed:

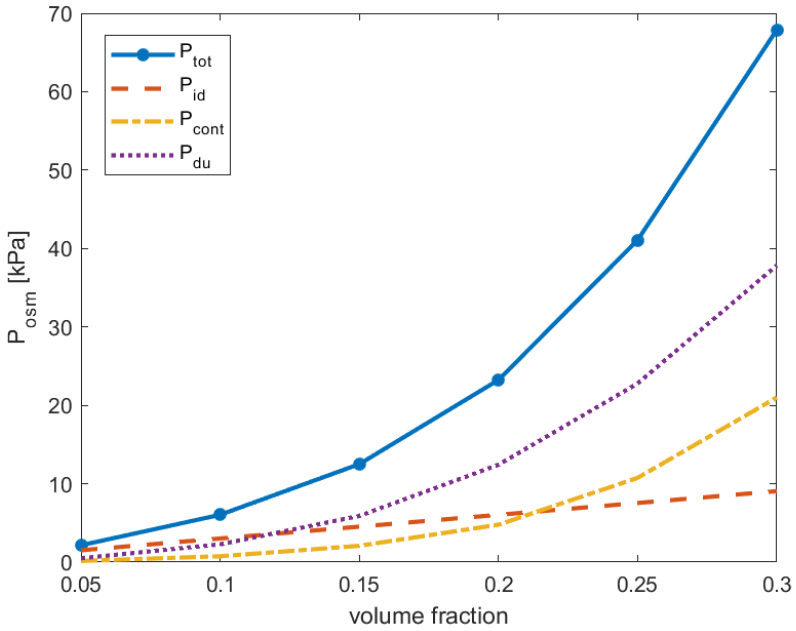

Figure 48 Model predicted osmotic Pressure of the fouling cake as function of volume fraction during ultrafiltration process for Yukawa potential formulation. Total osmotic pressure in continuous line and the three different contributions. $Z = 20.07$, $I = 0.15M$, $pH = 7$, $a = 32$ Å, $T = 300$ K.
Process conditions: TMP=1.5bar, Rej=0.9875, t=3200s.

However, comparing Figs.47a and 48, the total pressure is increased of low percentage but the contribution was differently weighted. The contact interaction pressure term is decreasing and the non-contact interaction increasing.

For very low ionic strength the renormalization theory was considered and the resulting pressure was compared to the non-renormalized one.

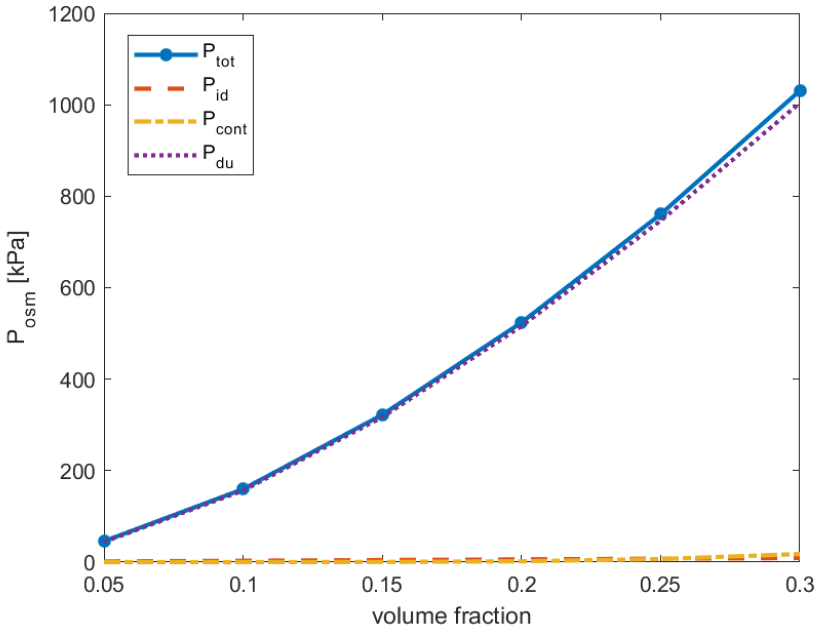

a) non-eff

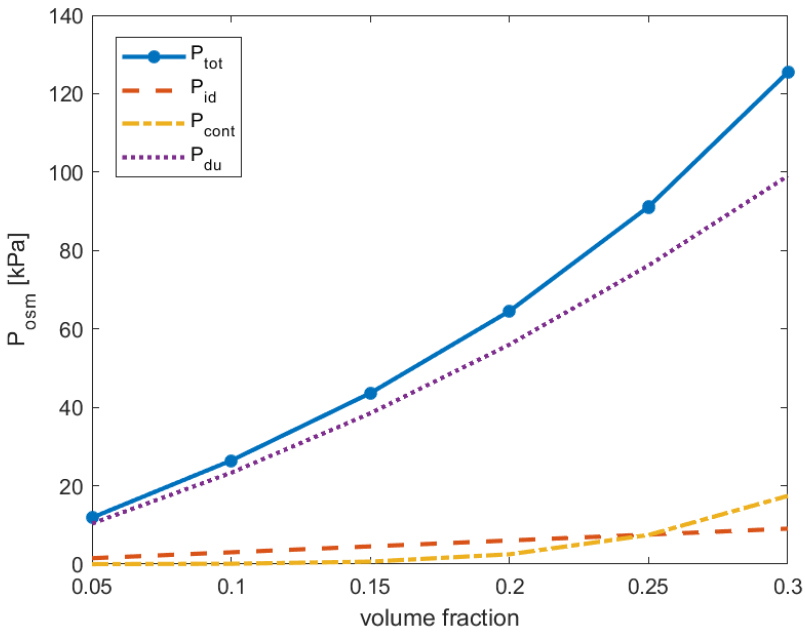

b) effective

Figure 49 Model predicted osmotic Pressure of the fouling cake as function of volume fraction during ultrafiltration process for Yukawa potential formulation. Total osmotic pressure in continuous line and the three different contributions. $Z = 15.82$, $I = 0.001M$, $pH = 7$, $a = 32$ Å, $T = 300$ K.
Process conditions: TMP=1.5bar, Rej=0.9875, t=3200s.

The renormalization is strong on these case and only *non-contact* pressure term is almost present

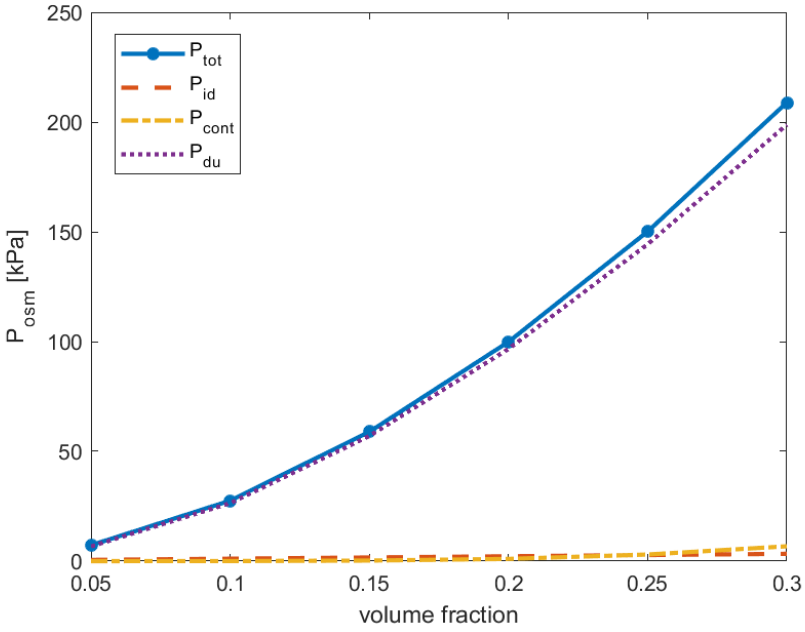

a) non-eff

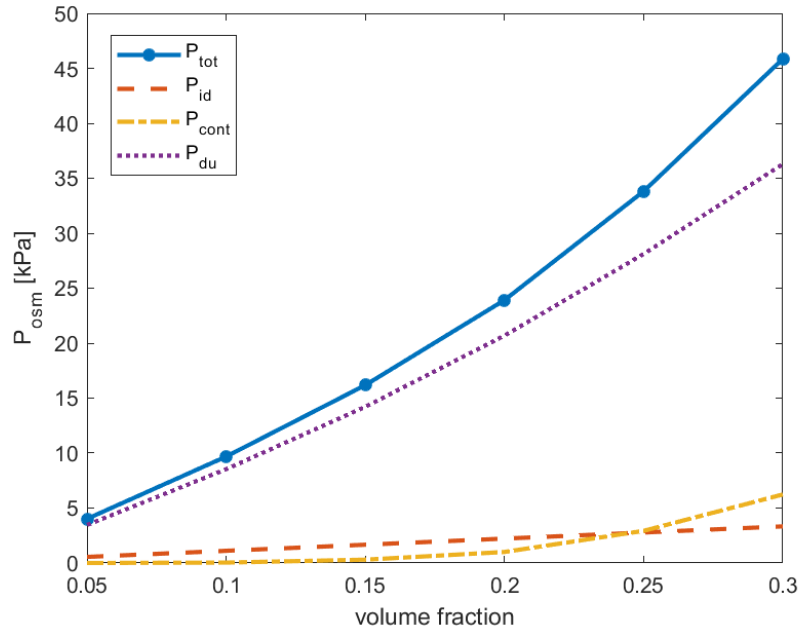

b) effective

Figure 50 Model predicted osmotic Pressure of the fouling cake as function of volume fraction during ultrafiltration process for Yukawa potential formulation. Total osmotic pressure in continuous line and the three different contributions. $Z = 15.82, I = 0.001M, pH = 7, a = 32$ Å, $T = 300\ K$.
Process conditions: TMP=1.5bar, Rej=0.9875, t=3200s.

Acknowledgments

Firstly, I wish to thank Prof. Stefano Curcio and Dott. Giorgio De Luca for their active participation to my PhD. The present thesis would not have been possible without their support.

I wish to thank Prof. Yannick Hallez for hosting me during my external research period in Toulouse and his participation to some parts of these thesis.

I wish to thank also my PhD coordinator and tutor Prof. Felice Crupi.

I would like to thank my fellow labmates in for the stimulating discussions and for all the fun we have had in the last four years.

Last but not the least, I would like to thank my family for supporting me spiritually throughout writing this thesis and my life in general.

Francesco Petrosino

Rende (CS), Italy

04/04/2020